Topics in semiclassics: Non-classical phenomena in integrable and non-integrable systems
Maitra, Neepa Tatyana
ProQuest Dissertations and Theses; 1998; ProQuest

INFORMATION TO USERS

This manuscript has been reproduced from the microfilm master. UMI films the text directly from the original or copy submitted. Thus, some thesis and dissertation copies are in typewriter face, while others may be from any type of computer printer.

The quality of this reproduction is dependent upon the quality of the copy submitted. Broken or indistinct print, colored or poor quality illustrations and photographs, print bleedthrough, substandard margins, and improper alignment can adversely affect reproduction.

In the unlikely event that the author did not send UMI a complete manuscript and there are missing pages, these will be noted. Also, if unauthorized copyright material had to be removed, a note will indicate the deletion.

Oversize materials (e.g., maps, drawings, charts) are reproduced by sectioning the original, beginning at the upper left-hand corner and continuing from left to right in equal sections with small overlaps. Each original is also photographed in one exposure and is included in reduced form at the back of the book.

Photographs included in the original manuscript have been reproduced xerographically in this copy. Higher quality 6" x 9" black and white photographic prints are available for any photographs or illustrations appearing in this copy for an additional charge. Contact UMI directly to order.

UMI

A Bell & Howell Information Company
300 North Zeeb Road, Ann Arbor MI 48106-1346 USA
313/761-4700 800/521-0600

Reproduced with permission of the copyright owner. Further reproduction prohibited without permission.

HARVARD UNIVERSITY
Graduate School of Arts and Sciences

THESIS ACCEPTANCE CERTIFICATE

The undersigned, appointed by the

Division

Department of Physics

Committee

have examined a thesis entitled "Topics in Semiclassics: Non-Classical Phenomena in Integrable and Non-Integrable Systems"

presented by Neepa Tatyana Maitra

candidate for the degree of Doctor of Philosophy and hereby certify that it is worthy of acceptance.

Signature Eric J Heller

Typed name Eric J. Heller, Chair

Signature Mara Prentiss

Typed name Mara Prentiss

Signature Dudley R. Herschbach

Typed name Dudley R. Herschbach

Date May 14, 1998

Topics in Semiclassics: non-classical phenomena in integrable and non-integrable systems.

A thesis presented
by

Neepa T. Maitra

to
The Department of Physics
in partial fulfillment of the requirements
for the degree of
Doctor of Philosophy
in the subject of

Physics

Harvard University
Cambridge, Massachusetts
June 1998

UMI Number: 9832441

UMI
300 North Zeeb Road
Ann Arbor, MI 48103

For my late father and my mother,
Priyatosh and Romola Maitra

Abstract

Semiclassical approaches can give us much insight into often perplexing quantum mechanical phenomena. More pragmatically perhaps, they may provide powerful approximation techniques for calculations where solving the full quantum mechanics could be daunting. In this thesis we discuss phenomena which appear in quantum systems but not in the corresponding classical systems. Each chapter explores an independent topic, and each is linked by a common semiclassical point of view.

The systems considered in the first half of the thesis are integrable. In chapter 1 we introduce a distorted-wave Born approximation based on semiclassical WKB wavefunctions and show how this may be used to compute non-classical processes such as barrier reflection and tunneling. Chapter 2 regards the uniformization of a "supercaustic": an especially harsh case of divergence of WKB where the energy manifold is asymptotic to the representation. In the third chapter we consider barrier crossing and reflection in the time as well as energy domains. We find classically forbidden tunneling and above barrier reflection are well defined and important processes in the time domain. They can overshadow classically allowed ones. We show that in general classically allowed trajectories in the time domain are insufficient to explain tunneling amplitudes in the energy domain. Chapter 4 is an example of how semiclassical techniques can reduce a problem of higher dimensionality to one involving only the variables of interest. This is demonstrated by an application of great interest in its own right, quantizing constrained systems.

In the second half we discuss the quantization of the whisker map, or separatrix map, a non-integrable system (Chapter 5). This map has particular significance in chaos: the separatrix is a ubiquitous structure in mixed phase-space systems and it is here where stochasticity is born. We show how semiclassical quantizations which initially may seem hopeless in fact work remarkably well. We study aspects of quantum localization inside the stochastic layer, arising from dynamical localization deep in the layer and at cantori and re-tunneling at cantori. Our conclusions regarding the quantum transport through near-critical cantori and the relation to classical scaling hold for generic cantori in any map.

Acknowledgements

First, I would like to thank my advisor, Professor Rick Heller, for his invaluable inspiration and guidance with my research throughout graduate school. I have learnt a tremendous amount from him and am indebted to him for this and also for his patience. I will always be very grateful for the opportunity I have had to hear his acutely intuitive and insightful explanations and views.

I also owe boundless thanks to Dr Lev Kaplan and Adam Lupu-Sax. Adam continually gave me crucial and valuable help with numerical work. Lev's perceptive suggestions with my research helped me incredibly. And they were great friends. Also to Alex Barnett, Bill Bies, Maurizio Carioli, Stella Chan, Jonathon Edwards, Mark Goldman, Michael Haggerty, Jesse Hersch, Kazuo Hirai, Sang-Wook Kim, Marcos da Luz, Areez Mody, Martin Narachewski, Tamar Schnerb, Alan Tameshtit, Steve Tomsovic: I have been lucky to be part of a vivacious and supportive research group over the last few years and I thank you all for your camaraderie and for sharing your ideas.

To my other dear friends Sheila Kannappan, Marko Kocic, Carol Livermore, Sasha Lyapin, Doug Mar, Ron Rubin, Rebecca Woodward, thank you for the fun times, the caring and the warmth, which have meant so much to me. I will treasure memories of my graduate school years and thank my whole grad school class for the great times and togetherness.

Thank you Carol Davis for always having what I needed at the last minutes before a presentation and for many calming conversations. Mary Lampros, for reminding me to file forms which prevented me from getting kicked out of grad school...

Professor Rob Ballagh, my undergraduate advisor at the University of Otago, thank you for introducing me to the world of quantum physics; Professor Andrew Lesniewski, for giving me a taste of mathematical physics.

I appreciate very much the kindness and caring that my "host parents" Professor Jim and Margaret Duesenberry have shown me.

Robert and Mary Woodward and family, thank you so much for your loving support and encouragement.

My deep gratitude goes to my wonderful husband, Chris Woodward, for so many joyful times and endless smiles ... and for keeping me sane!

No words are enough to express how grateful I am for my mother, Romola, my late father Priyatosh and my sister Rupa. Without their unwavering affection, support, refreshing cheer, this thesis would never have been.

Citations to Previously Published Work

Large portions of some chapters have been previously published:

Chapter 1 in *Physical Review A* **54**(6) 4763, (1996)
(N.T. Maitra and E.J. Heller)

Chapter 3 in *Physical Review Letters* **78** (16), 3035 (1997)
and in *Classical, Semiclassical and Quantum Dynamics in Atoms* Springer Lecture Notes in Physics, Eds. H. Friedrich and B. Eckhardt, Berlin (1997)
(N.T. Maitra and E.J. Heller)

Chapter 4 in *Physical Review A* **56** (4), 2592 (1997)
(L. Kaplan, N.T. Maitra and E.J. Heller)

Contents

List of Figures

Chapter 1

A Semiclassical Perturbation Approach to Quantum Reflection

In this first chapter, we discuss two approximation methods often used in quantum mechanics and we introduce a new method which combines ideas from each. We consider the problem of quantum "reflection above the barrier", introducing a distorted wave Born approximation based on the primitive semiclassical WKB wavefunction. The idea generalizes to the concept of an unperturbed Hamiltonian defined as the exact Hamiltonian plus small parts which "turn off" nonclassical processes such as barrier reflection and barrier tunneling. This work has been published in [1].

1.1 Introduction

The difficulty in exactly solving realistic quantum mechanical problems, and the quest for physical insight often drives us to consider approximation methods. Two of the most well-known are a perturbative approach, where the difference between the real problem and a solvable problem is in some sense "small", and a semiclassical approach, which takes advantage of the smallness of $\hbar$ relative to the actions in the problem. Clearly the two methods have different regions of validity and there are parameter ranges where neither works well. Here we introduce a technique which combines perturbation theory with semiclassics and in fact bridges a gap between the parameter domains where the individual approaches give good results. We consider the problem of "reflection above the barrier": scattering from a potential in one-dimension when the energy of the particle is greater than the potential maximum. In section 1.2, we briefly review the two standard approximations mentioned above and introduce our technique which combines ideas from both. Section 1.3 presents the results of the three techniques as applied to two types of potentials: a barrier and a ramp. In section 1.4 we discuss a fourth approximate method, the multiple scattering Bremmer result for above-barrier reflection. We discuss possible generalizations of our technique to calculate tunneling coefficients in section 1.5 and multidimensional cases in section 1.6. Finally, we conclude in section 1.7 and discuss some prospects for the ideas introduced in this chapter.

1.2 A semiclassically modified Born result

We address here the problem of scattering from a localized potential. Specifically, we consider the reflection coefficient in one-dimension of a particle of energy E incident from the left on an interaction region. In the typical perturbative (Born) approach to scattering theory [2], we start with a plane wave basis representing free particle motion: the effect of the potential is to induce transitions amongst these states. For transitions between two degenerate states in a continuum, Fermi's Golden Rule tells us the probability amplitude is proportional to the matrix element of the potential between the initial and final states. In our case, the initial(final) state is a plane wave moving to the right(left) with energy E : $e^{\pm ipx/\hbar}$ where $p = \sqrt{2mE}$. Choosing states normalized to unit flux, we obtain the reflection coefficient

$$\mathcal{R} = \frac{m^2}{\hbar^2 p^2} \left| \int_{-\infty}^{\infty} V(x) e^{\frac{2i}{\hbar}px} dx \right|^2 , \tag{1.1}$$

which is the Born scattering result [2]. This formula is valid under certain "smallness" conditions of the potential: we need

$$\left| \frac{V(x)a}{\hbar v} \right| << 1 \tag{1.2}$$

where $v = p\hbar/m$ is the classical velocity of the particle and a is the width of the potential, which essentially requires the scattering potential to be weak compared to the kinetic energy of the incoming particle [2]. For large potentials and for potentials which do not have a finite extent, (for example, step potentials rather than barriers), such a perturbative approach is expected to fail.

There are two well-known semiclassical methods, one based on the stationary phase approximation to Feynman's path integral [3], the other on WKB wavefunctions.

The equivalence of the two approaches is shown in [4]. Below we very briefly outline the methods: the reader is referred to the literature, for example, [4, 5, 6, 7, 9] for details. The probability amplitude that a state of positive momentum and definite energy evolves into a state of negative momentum, is obtained from the energy domain Green function in momentum representation:

$$G(-p,p,E) = \int G(-p,t;p,0)e^{iEt/\hbar}dt = \int \langle -p|e^{-iHt/\hbar}|p\rangle e^{iEt/\hbar}dt \tag{1.3}$$

$$= \int dt \int \mathcal{D}[p[\tau]]e^{i(S(p[\tau])+Et)/\hbar} \tag{1.4}$$

where $\mathcal{D}[p[\tau]]$ implies a summation over all paths in momentum space $p[\tau]$ which start with momentum p and end at time t with momentum $-p$ and $S(p[\tau])$ is the classical action $\int_0^t \mathcal{L}(p[\tau])d\tau$ along the (not necessarily classical) path $p[\tau]$, $\mathcal{L}$ being the Lagrangian. This latter expression is a Feynman path integral [3] in momentum space, the position space version of which is perhaps more familiar. In the limit $\hbar \to 0$, we may perform both the time integral and the path integral by stationary phase, which is justified as the integrand oscillates rapidly and cancels itself out everywhere except at stationary points of the integrand. This reduces the sum over all paths that begin with momentum p and end with $-p$ and have energy E, to a vastly smaller sum only over paths satisfying the classical equations of motion. However for energies greater than the maximum potential there are no such classical paths for real initial conditions and real time. We nonetheless find an approximation for the quantum reflection coefficient by looking in the the lower half complex time plane [4], picking up contributions from complex stationary phase points. (See also chapter 3 where this process is discussed in more detail and related to real stationary phase points from non-classical trajectories in the time domain). The uniformized semiclassical reflection coefficient derived in this way is:

$$\mathcal{R} = \frac{e^{-\frac{2}{\hbar}\mathrm{Im}\int_{-p_o}^{p_o} x(p')dp'}}{1+e^{-\frac{2}{\hbar}\mathrm{Im}\int_{-p_o}^{p_o} x(p')dp'}} \tag{1.5}$$

where p_o is the classical value for momentum at the center of the potential, $x(p)$ is the classical solution for the position in terms of momentum, and Im denotes the imaginary part. We note that this is a uniformized expression in the sense that 1.5 connects smoothly at $E = V_{max}$ to the reflection coefficient for energies just above the barrier top. The barrier penetration formula may be more familiar, which is of the form Eq. 1.5 with the exchange

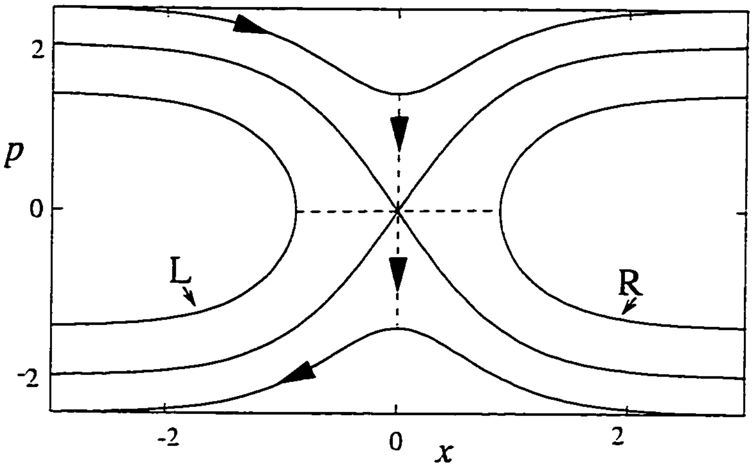

Figure 1.1: Classical phase space contours for a sech^2 barrier (solid line). The horizontal dashed line shows the classically forbidden quantum tunneling process from the left side of the barrier (L) to the right (R) at energy below the barrier. The vertical dashed line connecting contours at energy above the barrier, is what this chapter addresses, the classically forbidden quantum reflection process.

of the roles of position and momentum: the transmission probability at energy E is

$$\mathcal{T} = \frac{e^{-\frac{2}{\hbar}\mathrm{Im}\int_{-x_o}^{x_o} p(x')dx'}}{1 + e^{-\frac{2}{\hbar}\mathrm{Im}\int_{-x_o}^{x_o} p(x')dx'}} \tag{1.6}$$

where $\pm x_o$ are the classical turning points and $p(x') = \sqrt{2m(E - V(x))}$ (see also figure 1.1).

Formula 1.5 in fact gives the exact reflection coefficient for the inverse harmonic oscillator. This result may also be seen to arise from a semiclassical analysis by Zwaan which is based on WKB wavefunctions and Stokes line discontinuities in the complex plane (see [5] for many references and a review). We may also derive semiclassical reflection coefficients starting with the well-known Airy connection method for tunneling, which addresses the problem of barrier penetration and involves matching WKB solutions at turning points. The result may then be generalized to the problem of above-barrier reflection, either through extension to complex turning points or by working with analogous formulae in momentum space.

It is well known that the WKB formulae break down for energies near the top of the barrier. What is mentioned much less often is that they fail completely if the barrier is too low in a sense discussed below. However a low barrier is just the case that can be treated perturbatively, so one might imagine that most cases can be handled by one of the two methods. However, it can easily happen that the potential barrier is too high to be treated perturbatively, yet the action $\int^p x(p')dp'$ is too small compared to $\hbar$ for semiclassics to be reasonably applied. Bridging the gap between the regimes of validity of perturbative and semiclassical approaches is one of the main results of this chapter.

In the perturbative approach we consider a transition from a right-going plane wave to a left-going plane wave. For stronger potentials, this is clearly not an ideal choice for zeroth order states in perturbation theory. We should attempt to use states which incorporate some of the potential, as in the distorted wave Born approximation. This leads us to ask whether the WKB wavefunctions may play the role of the distorted wave basis, although it is not immediately obvious what Hamiltonian they solve exactly and therefore what perturbation to use. We investigate this next. Perhaps surprisingly, we shall find that the WKB wavefunctions are *exact* solutions to a well behaved, Hermitian Hamiltonian.

As is well known [2], semiclassical solutions to Schrödinger's equation for a potential $V(x)$ may be written as linear combinations of wavefunctions of the form

$$\psi^{\pm}_{WKB}(x) = \frac{1}{\sqrt{p(x)}} e^{\pm \frac{i}{\hbar}\int^x p(x)dx} \tag{1.7}$$

where $p(x) = \sqrt{2m(E - V(x))}$ is the classical momentum and $+(-)$ represents the right-(left-)going wave. As they satisfy Schrödinger's equation to first order in $\hbar$, we may expect that any "quantum" behavior shows up $O(\hbar^2)$ (or higher). Indeed, with $E = p(x)^2/2 + V(x)$, it is readily shown that $\psi^{\pm}_{WKB}(x)$ exactly solves the Schrödinger equation with an additional "potential" of order $\hbar^2$:

$$\left(-\frac{\hbar^2}{2m}\frac{d^2}{dx^2} + V(x) - E\right)\psi^{\pm}_{WKB}(x) = \hbar^2\left(\frac{-3p'(x)^2}{8mp(x)^2} + \frac{p''(x)}{4mp(x)}\right)\psi^{\pm}_{WKB}(x) \tag{1.8}$$

Casting the momentum derivatives onto potential derivatives and defining an effective potential for the WKB states as

$$V_{eff}(x,E) = V(x) - \hbar^2\left[\frac{5}{32m}\left(\frac{V'(x)}{E - V(x)}\right)^2 + \frac{V''(x)}{8m(E - V(x))}\right], \tag{1.9}$$

we have

$$\left(-\frac{\hbar^2}{2m}\frac{d^2}{dx^2} + V_{eff}(x,E) - E\right)\psi^{\pm}_{WKB}(x) \equiv (H_{WKB} - E)\,\psi^{\pm}_{WKB} = 0. \tag{1.10}$$

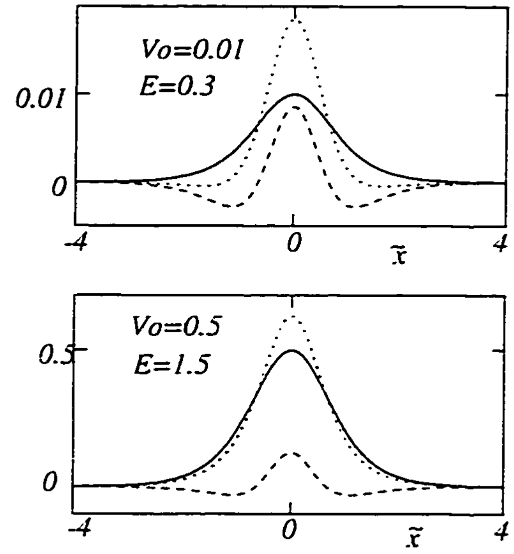

Figure 1.2: Effective potentials for the sech^2 barrier as a function of the dimensionless length $\tilde{x}$: the solid line represents $V(x)$, the dotted line $V_{eff}(x, E)$ and the dashed line $W(x, E)$.

Thus the WKB wavefuction exactly solves a quantum mechanical Hamiltonian problem with real potential which is smooth for energies above any potential maximum. We may think of the difference between the effective and exact potentials $W(x, E) = V_{eff}(x, E) - V(x)$ as a perturbation which "turns off" quantum reflection: a wave sent in from the left has no reflected component at energy E; it is perfectly "impedance matched". We note that $V_{eff}(x, E)$ is energy-dependent and blows up at classical turning points, as does the WKB wavefunction. At energies above the potential maximum both the WKB wavefunction and effective potential are well-behaved. In figure 1.2, we have plotted the potential $V(x)$, the effective potential $V_{eff}(x, E)$ and the difference potential $W(x, E)$ for a range of energies and potential heights for a typical barrier $V(x) = V_o \text{sech}^2(\alpha x)$. We scale x as $\tilde{x} = \alpha x$, then

$$W(\tilde{x}, E) = -\frac{\hbar^2\alpha^2}{m}\left[\frac{5}{32m}\left(\frac{V'(\tilde{x})}{E - V(\tilde{x})}\right)^2 + \frac{V''(\tilde{x})}{8m(E - V(\tilde{x}))}\right], \tag{1.11}$$

thus we choose as independent parameters V_o and E. In the figures we vary V_o and E and take $\frac{\hbar^2\alpha^2}{m}$ to be 1.

We observe that the effective perturbation has two valleys as well as a central peak, and this is what enables the quantum reflection of the semiclassical states to be turned off: loosely speaking, reflection from these valleys interferes destructively with the reflection from the original potential. At energies close to the barrier top, the difference potential is

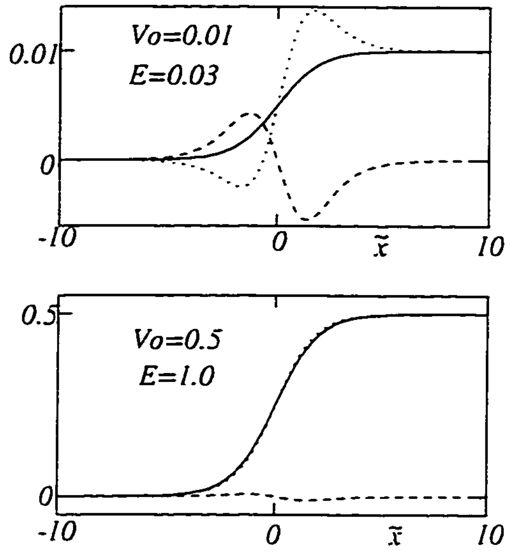

Figure 1.3: Effective potentials for the ramp: the solid line represents $V(x)$, the dotted line $V_{eff}(x, E)$ and the dashed line $W(x, E)$.

quite large. As we increase the energy, the effective potential approaches the original, and we expect that a perturbative approach using the correspondingly small difference potential would yield better results. The difference potential can be small even if the barrier is large.

Figure 1.3 shows $V(x)$, $V_{eff}(x, E)$, and $W(x, E)$ for the ramp $V(x) = V_o/(1 + e^{-\alpha x})$. We see that although the original potential had infinite extent in space, the effective perturbation is localized, and is thus now able to satisfy requirements for perturbation theory. Similar comments may be made for the unbounded inverse harmonic oscillator, where the effective potential is also localized and finite.

Some insight may be gained by considering a classical phase space picture for this problem. In figure 1.1, we showed typical phase space contours for a barrier. The quantum reflection process is indicated by the dashed line from the top curve to the bottom, forbidden in classical mechanics. Conventional perturbation theory based on plane waves used the horizontal p = constant asymptotes as contours to connect; in our modified perturbation approach using WKB wavefunctions, we take states associated with the curved, constant energy phase space contours.

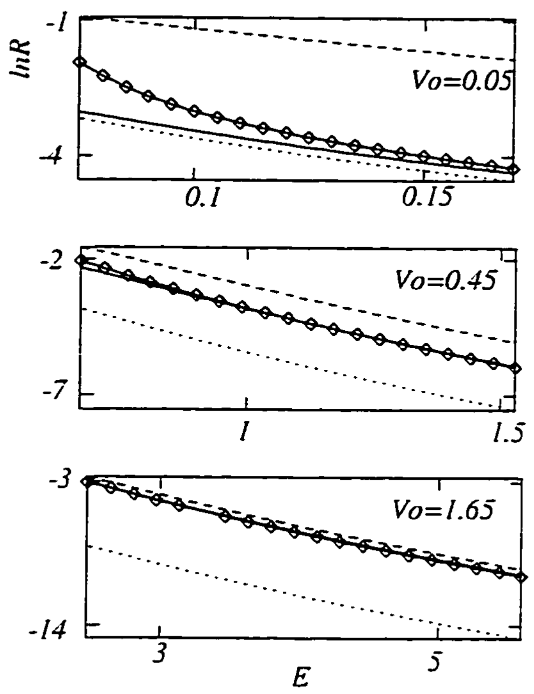

Figure 1.4: Reflection coefficients from the sech^2 barrier: solid line is the exact, dotted is the perturbative formula 1.1, dashed is the semiclassical formula 1.5 and the $\diamond$ line represents our semiclassical-perturbation formula 1.12.

1.3 Reflection coefficients

To calculate the reflection coefficient we use a perturbative approach with the WKB states as the unperturbed basis, and so calculate the matrix element of $-W = V - V_{eff}$ between the ψ^+ and ψ^-:

$$\mathcal{R} = \frac{m^2}{\hbar^2}\left|\int_{-\infty}^{\infty}(V(x) - V_{eff}(x))\,\frac{e^{\frac{2i}{\hbar}\int^x p(x')dx'}}{p(x)}dx\right|^2 \tag{1.12}$$

In figures 1.4 and 1.5 we graph the results of our combined semiclassical perturbation technique together with the known exact quantum reflection coefficient (see [2], for example), the semiclassical result, and the Born result (where applicable) for the two potentials: a sech^2 barrier $V(x) = V_o\text{sech}^2(\alpha x)$, and a ramp $V(x) = V_o/(1 + e^{-\alpha x})$, where $\alpha = 1$. Energy and potential are measured in units of $\frac{\hbar^2\alpha^2}{m}$.

For the sech^2 barrier, we see ordinary perturbation (Born) theory is only good for small potentials and high enough energies. Semiclassics is reasonable for large potentials and energy well away from the barrier top. Our combined approach works in the intermediate

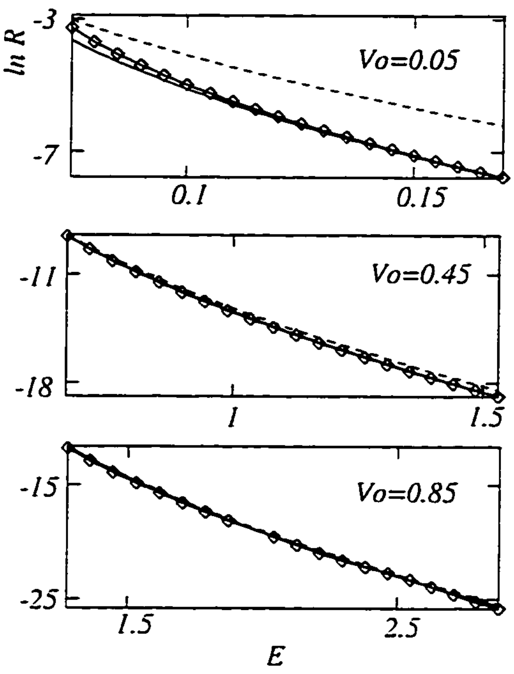

Figure 1.5: Reflection from the ramp potential:solid line is the exact, dashed is the semiclassical formula 1.5 and the ◇ line represents our semiclassical-perturbation formula 1.12.

parameter region, as we expected.

In the case of the ramp, where perturbation theory cannot be applied sensibly due to the infinite extent of the potential, we see our technique of combining semiclassics with perturbation theory still works well and is better than the semiclassical approximation, provided the energy is not too close to the potential top. In figure 1.6, the typical $\hbar$-dependence of the coefficients is plotted. We observe that for very small $\hbar$, the semiclassical result is a very good approximation as expected, whereas for large $\hbar$ perturbation theory does a better job. The combined semiclassical-perturbation method interpolates between. We notice that corrections to the semiclassical approach depend on $\hbar$ roughly as $e^{-O(\hbar)}$, indicating $\hbar^2$ (and higher) corrections to the action, as is expected in semiclassics.

1.4 The Bremmer method

We mention briefly another technique for computing quantum reflection coefficients, without which this study would be incomplete. The Bremmer method results from a multiple-scattering approach, where a smooth potential is approximated by a series of N

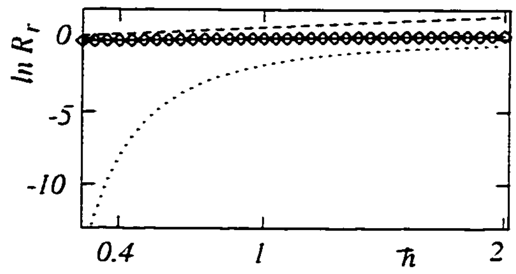

Figure 1.6: $\hbar$-dependence of the reflection coefficients, $R_r = \frac{R}{R_{exact}}$. Here we have taken the sech^2 barrier with $V_o = 0.5$ and $E = 1.0$: dotted is the perturbative result, dashed is semiclassical, and the $\diamond$ line is our semiclassical-perturbation theory.

sharp steps, N being large. The wavefunction at some position x can be expressed as

$$\frac{b_+(x)}{\sqrt{p(x)}} e^{\frac{i}{\hbar}\int^x p(x')dx'} + \frac{b_-(x)}{\sqrt{p(x)}} e^{-\frac{i}{\hbar}\int^x p(x')dx'} \tag{1.13}$$

where $b_\pm(x)$ are coefficients to be determined. An incoming wave partially reflects and partially transmits at each sharp step for which the fully quantum coefficients are known. Thus we calculate the wavefunction cumulatively and take the limit of a continuously varying potential. This gives two iterative equations for $b_\pm(x)$ and we take the first iteration to obtain:

$$\mathcal{R} = \int \frac{p'(x)}{2p(x)} e^{\frac{-2i}{\hbar}\int^x p(x')dx'} \tag{1.14}$$

The Bremmer approach is very much in the spirit of the semiclassical-perturbation results in that a semiclassical foundation is used to build quantum corrections. In the Bremmer case, the WKB wavefunction with no reflection results if the zeroth approximation is used, and equation 1.14 is the single scattering correction.

A numerical evaluation of Eq. 1.14 is in fact very close to the exact result as is shown in figure 1.7, providing in general a much better estimate than the three approaches discussed in the previous section. It is however challenging to apply the Bremmer approach to more general problems (see below).

Berry and Mount's discussion of the Bremmer approach [5] includes an analytic evaluation of the integral Eq. 1.14 by a contour integration. The semiclassics enters by including only the contribution from the pole involving the smallest imaginary action. Their explicit semiclassical calculation for the potential ramp results in a value for $\mathcal{R}$ which overshoots the standard semiclassical result by the factor of $\frac{\pi^2}{9}$. This 10% discrepancy,

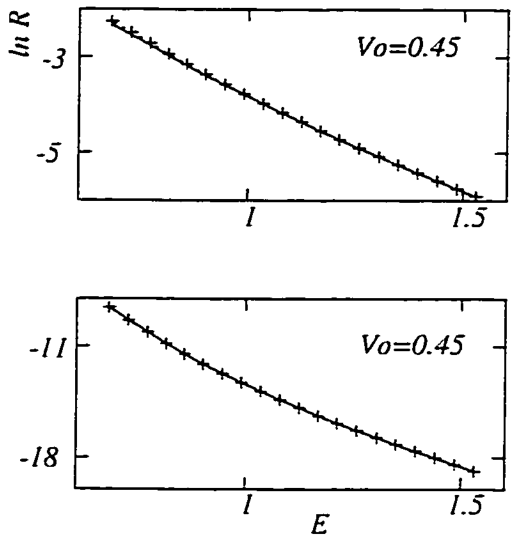

Figure 1.7: The Bremmer result (+ line) for the reflection coefficient for the sech^2 (top figure) and ramp (bottom figure) potentials is very close to the exact result (solid line).

very minor compared with the differences in the approaches of section 1.3 was attributed to taking only the first iteration in the multiple scattering coupled equations, that is, to formula Eq. 1.14 itself. Our numerical evaluation of Eq. 1.14 which indicates how very close it is to the exact result, together with Berry and Mount's semiclassical calculation, suggests that if all the singularities were included in the contour evaluation we would get an analytic result very close to the exact result. However this is not found to be correct. We can motivate why from the following observation: the exact reflection coefficient is $e^{-O(\hbar)}\mathcal{R}_{sc}$ (figure 1.6), yet summing the contributions from all the poles results in the addition of two geometric series (one stemming from complex turning points, the other from complex singularities) which cannot give such a dependence. This problem remains unsolved, but it is not the main point of our chapter.

1.5 Generalization to barrier penetration

We are now led to the question of whether the semiclassical-perturbation technique may be used in more general problems. The success in computing the nonclassical transitions between the positive and negative momentum branches in phase space for reflection from a barrier prompts us to ask whether can we compute the nonclassical transition probability between *any* two contours in classical phase space in a similar "semiclassically modified perturbation theory". In particular, we may be concerned with generalizing this to higher dimensions, where there is much interest in calculating couplings and energy splittings between classically degenerate tori[11].

We consider below the issue of tunneling across a potential barrier in one dimension, with energy below the barrier top. We need to find, for the unperturbed basis, wavefunctions which "live" on one side of the barrier only. We may attempt to construct appropriate combinations of the WKB wavefunctions Eq. 1.7 which do this. However at the turning point the wavefunction blows up (as does the effective potential). Uniformizations of WKB wavefunctions in position representation are well-studied [5]. It is however not clear how to uniformize at the turning points without inducing tunneling of the wavefunction to the other side of the barrier, which we want to avoid in order to follow our plan analogous to the above barrier case treated earlier. Consider the contours labelled L and R in the phase-space figure 1 again: at the turning points, the projection of the contour on to x is ill-defined; they are coordinate space caustics. We see the tunneling process connects curve L to curve R: the picture suggests momentum space is a more natural space to work in for this problem. If we work in coordinate space for barrier reflection (momentum tunneling) then we should expect to work in momentum space for barrier (position space) tunneling. The turning points then pose no problem, as can be seen by the projection on to the vertical axis. Performing a stationary phase Fourier transform of the x-space WKB wavefunctions living on the left(right) side of the barrier:

$$\psi^{+(-)}(x) - i\psi^{-(+)}(x) \tag{1.15}$$

we obtain the momentum-space wavefunction

$$\phi^{\pm}(p) = \frac{1}{\sqrt{-V'(x(p))}} e^{\mp\frac{i}{\hbar}\int^{p} x(p')dp'} \tag{1.16}$$

where $+(-)$ represents the wave on the left(right) of the barrier. We may calculate the behavior under Schrödinger's equation:

$$\left(\frac{p^2}{2m} + V(i\hbar\frac{d}{dp}) - E\right)\phi^{\pm}(p) = \hbar^2 h(p)\phi^{\pm}(p) + O(\hbar^3), \tag{1.17}$$

$$\begin{aligned} h(p) &= -\frac{x'(p)^2 V''''(x(p))}{8} - \frac{x''(p)V'''(x(p))}{6} - \frac{3V''(x(p))^3 x'(p)^2}{8V'(x(p))^2} \\ &\quad + \frac{V''(x(p))^2 x''(p)}{4V'(x(p))} + \frac{V''(x(p))V'''(x(p))x'(p)^2}{2V'(x(p))} \end{aligned} \tag{1.18}$$

where $V(i\hbar\frac{d}{dp})$ was calculated by an expansion-resummation technique, as follows: We consider the operation of the first few terms of a Taylor series expansion around zero for $V(i\hbar\frac{d}{dp})$ on $\phi^{\pm}(p)$, collect terms in orders of $\hbar$ and find that to each order in $\hbar$ we have a Taylor series which we then re-sum. This leads to the results above, where in a semiclassical vein, we write down explicitly the lowest order (i.e. $\hbar^2$) correction (see chapter 2 for more detail). Unfortunately the Hamiltonian is more complicated in its position dependence than in its momentum dependence ($V(x)$ as opposed to $p^2/2$) and the price we pay is a more complicated effective Hamiltonian. In addition, we observe from Eq. 1.16 and Eq. 1.17, that at the expense of eliminating the turning point caustic, we have introduced a new type of caustic, caused by the asymptotic constancy of the potential (see figure 1.1).

Before discussing this problem further, we present the results for the inverted harmonic oscillator, for which this new type of caustic is not a problem (in momentum-space, with $E > V_{max}$, the top of the barrier plays no role, as it is outside the relevant (i.e. real) domain for p). The analysis follows closely the case of above barrier reflection from this potential due to the symmetry of the harmonic oscillator Hamiltonian under the substitution $x \leftrightarrow p$. The series in $\hbar$ in Eq. 1.17 ends at $\hbar^2$ for this potential, so in fact $H - \hbar^2 h(p)$ is the effective Hamiltonian for which the WKB solutions Eq. 1.16 are exact eigenstates to any order in $\hbar$. The results are given in figure 1.8 and provide a good approximation to the exact result provided the energy is not too close to the barrier top.

For a generic barrier, which flattens out away from the interaction region, we encounter what we shall call a "supercaustic" (see chapter 2): as $p \to \pm\sqrt{2E}$, the WKB wavefunction blows up. The *exact* momentum-space solution *also* is singular for flat regions of potential, however the WKB behavior is still incorrect, as can be seen by the divergence of the effective perturbation in Eq. 1.17. Thus the WKB wavefunction is a poor approximation to the true wavefunction as $p \to \pm\sqrt{2E}$. It is possible however, to uniformize the supercaustic, and this process is described in chapter 2 for a barrier whose asymptotic behavior is exponential. This involves solving exactly the case of a potential which tends to the desired potential at large x, then adjusting by well-behaved WKB factors, to find a wavefunction $\phi_{unif}(p)$ which reduces to WKB in the $\hbar \to 0$ limit, and yet has the correct blow-up as $p \to \pm\sqrt{2E}$. Applying Schrödinger's equation in momentum space to the uniformized wavefunction we find that the difference between the Hamiltonian for which $\phi_{unif}(p)$ is an eigenstate and the original Hamiltonian does give a finite perturbation and we find this explicitly up to order $\hbar^2$. However the application of our semiclassical pertur-

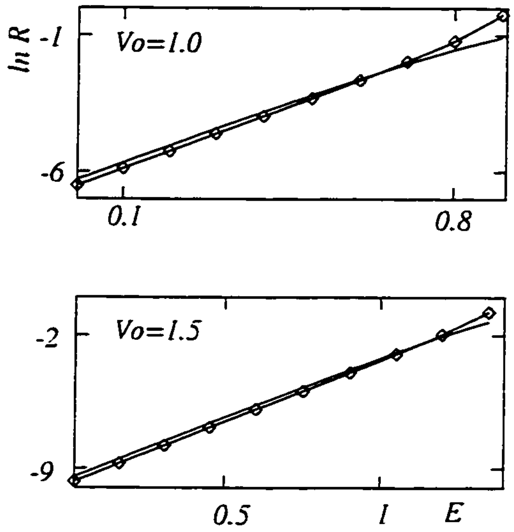

Figure 1.8: Transmission through the inverse harmonic oscillator $V(x) = Vo-\frac{1}{2}x^2$: the solid line represents the exact result, which in this case is also the semiclassical result formula 1.5, and the ◇ line is the result of our semiclassical-perturbative approach.

bation theory to calculate the tunneling probability from one side of the barrier to the other using the uniformized states as the zeroth order basis, has not been successful in yielding a good approximation, despite the effective perturbation being small and finite everywhere. Perhaps the neglect of the terms $O(\hbar^3)$ and higher may be partly responsible for this, but as yet this problem is unresolved.

1.6 Multidimensional cases

Of course the one dimensional problems addressed in this chapter are of limited utility. However, it is easy to see that as long as there are no position space turning points one can use the same methods in two, three, or more dimensions. For example, backscattering from a three dimensional potential which has no classical backscattering can be computed. We leave this for future work.

The situation we have discussed here is related to is an established technique used to estimate *dynamical tunneling*[10, 11] interactions in two or more degree of freedom bound state systems [12, 13, 14, 15]. Dynamical tunneling occurs when (1) there are good classical actions partitioning phase space, giving classical trajectories which fail to flow from one set of actions to another, even over infinite time and (2) tunneling (with associated tunnel splittings and mixing of wavefunctions otherwise localized to the vicinity of the tori) is observed quantum mechanically. It can be shown that classical resonance island chains which always can be found between the invariant tori control the tunneling between the states localized on the tori. This is most easily seen by analogy with the barrier reflection problem discussed in this chapter. In Fig. 1.9 we show the phase space plot for barrier reflection and for a mostly integrable two dimensional system (on a Poincaré surface of section). The two tori involved in the tunneling are indicated: note that between them sits a resonance island chain which has the right Fourier components to give a nonvanishing tunneling (perturbative) integral connecting the two tori. Locally, the resonance zone has exactly the structure of the barrier reflection problem, as indicated in the figure. In the very common case that the islands are narrow (as drawn) the problem can be handled in a manner similiar in spirit to this chapter. If a single pair of torus-localized levels is interacting, the resonant zone coupling two tori is removed from the Hamiltonian, thus turning off the tunneling. The tunnel splitting is then estimated by perturbation theory, using the WKB-like wavefunctions residing on the invariant tori. This program works very well in many cases. It generalization to stronger resonances and many interacting levels was given by Carioli, Møller, and Heller [16].

1.7 Prospects

We have shown that the WKB wavefunction for a scattering problem with no turning points solves a Hamiltonian problem close to the original problem. It can thus be used for perturbative calculations for reflection amplitudes. The resulting WKB-distorted wave Born approximation yields accurate results in parameter regions where neither WKB nor perturbation works alone.

The generalization of the coordinate space reflection problem to barrier tunneling was given. It is more complicated in form due to the need to work in momentum space and the relative functional complexity of $V(x)$ as opposed to $p^2/2$.

Further generalization leads us to the intriguing idea of finding a Hamiltonian which is very close to the exact one, but which is constructed to turn off certain nonclassical processes. Whenever such a Hamiltonian can be found and the perturbative matrix elements evaluated we may have a powerful tool. The reason is that the eigenstates of the unconventional Hamiltonian H_{WKB} can be constructed from classical mechanics, and the

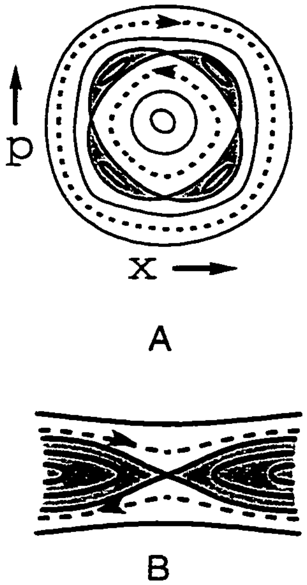

Figure 1.9: A. Poincaré surface of section plot for a typical interacting system of two degrees of freedom in the nearly integrable regime. Resonance zones which divide regions of phase space are evident. The contours on this (x, p_x) surface are of the same fixed energy E. Tunneling across the resonance zones is analogous to the barrier reflection: These resonance islands are to be compared to the phase space plot for the barrier, B, which shows the similarity of the tunneling across the separatrix in the two cases.

remaining quantum effects calculated by perturbation theory. We actually accomplished all the desired features of this plan, including simplicity of the integrals, in the case of reflection above a barrier top or a ramp. We described the analogous situation governing dynamical tunneling between invariant tori. Whether "turning off the tunneling", as it might be termed, will prove practicable in wider circumstances remains to be seen, but the idea is appealing.

Chapter 2

Uniformization of a Supercaustic: momentum-space semiclassics for an exponentially decreasing potential.

In the previous chapter we saw that in an attempt to apply our semiclassical-perturbation theory to tunneling across a generic barrier we ran into a new complication: the divergence of momentum-space WKB wavefunctions in the asymptotic region of the potential. It is well-known that semiclassics breaks down at caustics, where the Van-Vleck probability becomes singular. The projection of the WKB state onto the representation becomes tangential. This has been much studied in coordinate representation: one may construct uniformized semiclassical wavefunctions where the singular amplitude is replaced by a more accurate one. Uniformized wavefunctions do not display the caustic singularity. In momentum-space a new and more dramatic type of caustic may appear, where the divergence occurs over an infinite range of the energy manifold, rather than at a point: the energy manifold asymptotes to a momentum state. These "supercaustics" are the subject of this chapter. In particular, we uniformize the supercaustic associated with potentials which decrease exponentially at large x.

2.1 Introduction: The caustic problem

We begin with a discussion on caustics. To a manifold of constant energy in classical phase space one can associate a quantum wavefunction of the form $\sqrt{\rho}e^{\frac{iS}{\hbar}}$ where ρ is a classical probability density and S is the classical action for a particle travelling along the manifold. Such a semiclassical (or WKB) wavefunction provides a good approximation to the exact energy eigenfunction, solving Schrödinger's equation to order $\hbar$. Let us first consider the coordinate representation. Energy domain semiclassics breaks down at turning points, or caustics, in configuration space, which is reflected in the divergence of the WKB wavefunctions there. Near such points the classical probability is enhanced and we expect the quantum (and semiclassical) wavefunction to be more heavily weighted there. however the semiclassical wavefunction demonstrates this rather too enthusiastically, and blows up. Indeed, the operation of the Hamiltonian on a WKB state yields an error which blows up as we approach a turning point caustic:

$$\left(-\frac{\hbar^2}{2m}\frac{d^2}{dx^2}+V(x)-E\right)\psi^{\pm}_{wkb}(x)=\hbar^2\left(\frac{-3p'(x)^2}{8mp(x)^2}+\frac{p''(x)}{4mp(x)}\right)\psi^{\pm}_{wkb}(x), \tag{2.1}$$

where $\psi^{\pm}_{wkb}(x) = \frac{1}{\sqrt{p(x)}}e^{\pm\frac{i}{\hbar}\int^{x}p(x')dx'}$, $p(x') = \sqrt{2m(E-V(x'))}$, and one dimension has been, and will hereafter be, assumed for simplicity.

Considering this in classical phase space gives some insight. The caustic is a tangency of the energy manifold with a manifold of constant coordinate: as shown in figure 2.1, the projection onto the x-state becomes parallel. (This is at the turning point $p = 0$ which follows from considering the relation $p(x) = \pm\sqrt{2m(E-V(x))}$ describing the energy contours).

Now, turning points pose no problem in momentum space; indeed the p—state intersects the contour perpendicularly there. However momentum space comes armed with its own divergence problems: not only may we have the type of caustic above, where the projection of the energy contour onto the momentum axis is parallel (figure 2.1), but we may encounter a contour which slowly *asymptotes* to a p-state (figure 2.2) and remains almost parallel for an infinite extent along the contour. We shall call this more severe type of caustic a "supercaustic".

The WKB wavefunction in p-space, obtained either by a stationary phase Fourier transform of the position space wavefunction to momentum space or by solving Schrödinger's equation to order $\hbar$ directly in momentum space, is

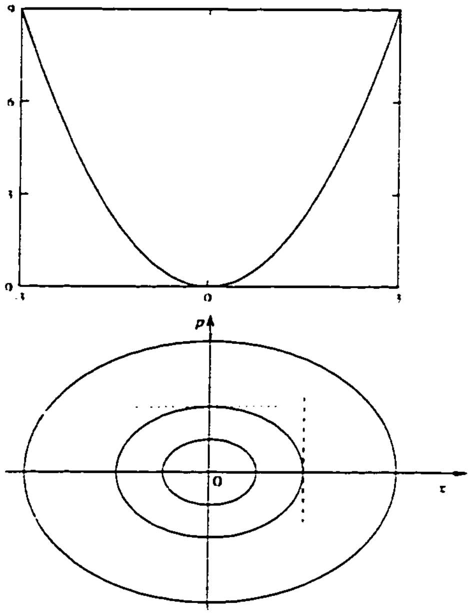

Figure 2.1: Harmonic oscillator potential $V(x) = x^2$(above) and associated phase space (below). Caustics in coordinate space are at the turning points of the motion (dashed line), and this is where the energy contour projects onto an x-state. There are also caustics in momentum space (dotted line), at the center of the well, and this is where the energy contour projects onto a p-state.

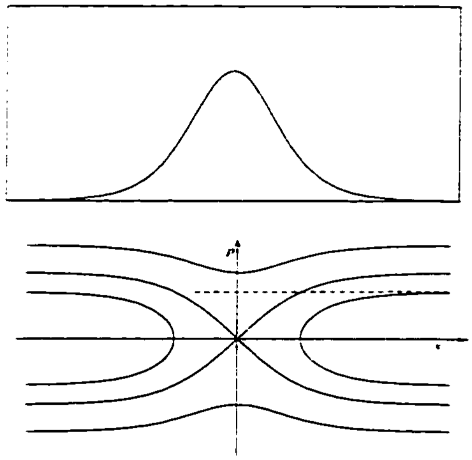

Figure 2.2: Eckart barrier $V(x) = \text{sech}^2 x$ (above) and associated phase space (below). Where the potential flattens out, there is a "supercaustic", and the energy contour asymptotes to a p-state.

$$\phi_{wkb}(p) = \frac{1}{\sqrt{-V'(x(p))}} e^{\frac{i}{\hbar}\int^{p} x(p')dp'} \tag{2.2}$$

where

$$x(p') = V^{-1}(E - p'^2/2m) \tag{2.3}$$

(We note that V^{-1} is in general a multivalued function; the branch chosen in (2.3) is determined by the branch that the classical contour corresponding to the semiclassical state we are describing belongs to. For example, for a potential barrier centered at $x = 0$ and energy below the barrier top, the positive(negative) branch choice of $x(p)$ gives a semiclassical state which lives on the right(left) side of the barrier. Please see figure 2.2 and also section 2.2.2.) Caustics in momentum-space, of the ordinary or super type, arise when the potential flattens out and the denominator in (2.2) respectively is, or tends to, zero. Indeed, the delta function in momentum, which is the exact solution for a flat potential, does indicate that the exact eigenfunction for a "flattening out" potential does blow up. However as we shall see in more detail shortly, the manner of the blow up of the WKB solution is quite incorrect.

Caustics of the simpler type have been well-studied in position space. The potential may be approximated linearly near the turning point and there the solution found exactly; the WKB solution, valid further away may then be "glued" smoothly to the exact solution near the turning point. Hence a wavefunction valid everywhere may be formed. More elaborately, there are uniformization techniques which involve a modification of the form of the WKB solution motivated by the exact solution near the turning point. In fact such methods give "connection formulae" between classically allowed and forbidden regions. The reader is referred to the review by Berry and Mount for details of this [5] and references therein. The resulting uniformized wavefunction satisfies Schrödinger's equation to order $\hbar$, yet does not have the divergence problems of the WKB solution, i.e. it is *uniformly* valid in x.

The main result of this chapter is the uniformization of the supercaustic associated with potentials which exponentially decrease asymptotically. In section 2.2 we first introduce the potentials and demonstrate the incorrect divergence of the p-space WKB wavefunction at the supercaustic by calculating to order $\hbar^2$ the difference between the true Hamiltonian and the Hamiltonian for which ϕ_{wkb} is an exact eigenfunction. This is followed by the construction of a uniform semiclassical wavefunction (section 2.2.1). In section 2.2.2

we show for the Eckart barrier how close our uniformization is to the exact eigenfunction, by calculating explicitly to order $\hbar^2$ the difference between the Hamiltonian for which the uniformized wavefunction is exact and the original wavefunction. This difference may be interpreted as an effective perturbation which "turns off tunneling" to order $\hbar^2$: the uniformization gives us a semiclassical solution to the barrier which lives only on either the right or the left side of the barrier and is an eigenstate up to order $\hbar$ of the original Hamiltonian plus this perturbation.

2.2 The Supercaustic of an exponentially decreasing potential

In this chapter, we uniformize a commonly occurring supercaustic in momentum-space. Potentials of the form:

$$V(x) = V_o\left(1 - \left(\frac{1-e^{-\alpha x}}{1+ce^{-\alpha x}}\right)^2\right) \tag{2.4}$$

where $0 \leq c \leq 1$, of which the Morse ($c = 0$) and Eckart ($c = 1$) are special cases (figure 2.3), possess supercaustics at $p \to \pm\sqrt{2mE}$. We point out that for $E > V_o$, the simpler type of caustic also exists: at $p = \pm\sqrt{2m(E - V_o)}$, $V'(x(p)) = 0$ and the energy contour projects tangentially onto the p-axis. Classically the particle with this momentum is at $x = 0$, the top of the potential. We are however interested in the supercaustic (which exists at any energy) when $p \to \pm\sqrt{2E}$. We shall see that this is due to the exponentially decreasing behavior of the potential and its derivatives at large x.

We shall first examine the supercaustic in more detail, by investigating how much the WKB solution in momentum-space misses being an exact eigenfunction. We need to compute the action of the Hamiltonian on wavefunction (2.2):

$$\left(\frac{p^2}{2} + V\left(i\hbar\frac{d}{dp}\right) - E\right)\phi_{wkb}(p).$$

where we shall henceforth take mass 1. In momentum-space it is the kinetic term that is trivial at the expense of the potential term which is now a differential operator (rather than simply a multiplicative term which it is in coordinate space). We evaluate the action of the potential term on the WKB wavefunction order by order in $\hbar$ in the following way. We first

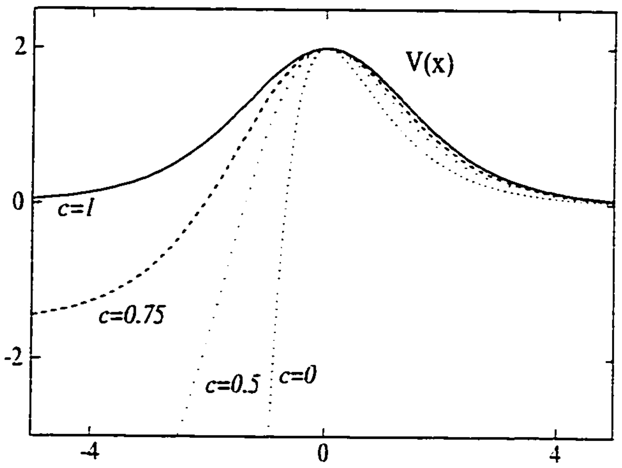

Figure 2.3: The potentials with $Vo = 2$ and $\alpha = 1$, equation 2.4. Uniformizing the p-space semiclassical wavefunction at the exponential tail ($x \to \infty$) is the subject of this paper.

expand $V(i\hbar\frac{d}{dp})$ in a Taylor series of the form

$$V(0) + i\hbar V'(0)\frac{d}{dp} - \hbar^2\frac{V''(0)}{2}\frac{d^2}{dp^2} - i\hbar^3\frac{V'''(0)}{6}\frac{d^3}{dp^3} + \hbar^4\frac{V''''(0)}{24}\frac{d^4}{dp^4}\cdots, \tag{2.5}$$

and operate with the series truncated say to 4 or 5 terms on 2.2. Terms of the same order in $\hbar$ are collected; of course, typically each differential contributes to every order. To each order we find we have the first few terms of a Taylor series of a different function; these functions are then taken to represent the result of $V(i\hbar\frac{d}{dp})\phi_{wkb}(p)$ to the respective order in $\hbar$. With the help of mathematica to calculate the derivatives and collect terms in order of $\hbar$, we find

$$V\left(i\hbar\frac{d}{dp}\right)\phi_{wkb}(p) = \left(V(x(p)) + \hbar^2 h(p) + O(\hbar^3)\right)\phi_{wkb}(p) \tag{2.6}$$

where

$$\begin{aligned} h(p) &= -\frac{x'(p)^2V''''(x(p))}{8} - \frac{x''(p)V'''(x(p))}{6} - \frac{3V''(x(p))^3x'(p)^2}{8V'(x(p))^2} \\ &+\frac{V''(x(p))^2x''(p)}{4V'(x(p))} + \frac{V''(x(p))V'''(x(p))x'(p)^2}{2V'(x(p))}, \end{aligned} \tag{2.7}$$

$x(p)$ is as in 2.3, $V(x(p)) = E - p^2/2$, and prime indicates differentiation with respect to the argument. Then, with $H = p^2/2 + V(i\hbar d/dp)$, we have

$$(H - E)\phi_{wkb}(p) = \hbar^2 h(p)\phi_{wkb}(p) + O(\hbar^3)$$

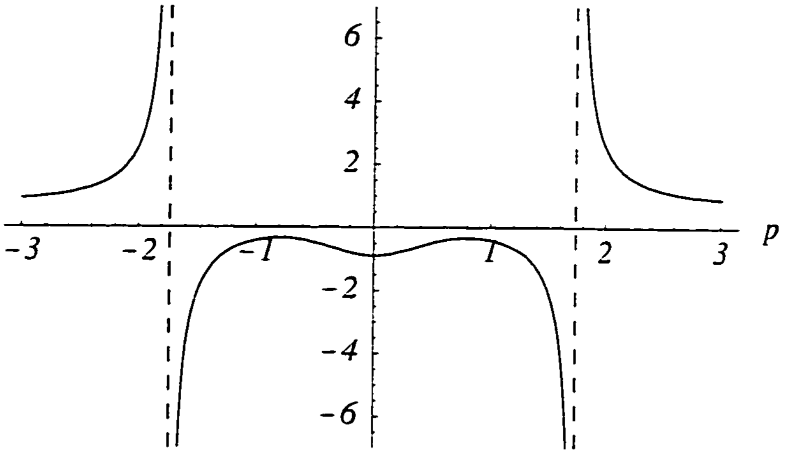

Figure 2.4: The WKB wavefunction in p-space misses being an eigenfunction of the Hamiltonian by $\hbar^2 h(p) + O(\hbar^3)$. Here is a plot of $h(p)$ for the Eckart barrier, $V(x) = 2\mathrm{sech}^2 x$, for $\phi_{wkb}(p)$ at energy $E = 1.5$. The dashed lines indicate the $p = \pm\sqrt{2E}$ asymptotes. This corresponds to the dashed line in figure 2.2 and is where the potential becomes flat.

$h(p)$ is thus, to lowest order in $\hbar$, how much the WKB solution misses being an energy eigenfunction.

Let us consider this function for potentials which, at large x, go like $W_o e^{-\alpha x}$ (e.g. for potentials (2.4) $W_o = 2V_o(c+1)$). Then, as $p \to \pm\sqrt{2E}$, $h(p)$ becomes very large. This is the momentum which a classical particle has asympotically, that is, in the region where the potential becomes flat (and zero). The exact p-space wavefunction does indeed approach delta-function behavior here; although the WKB wavefunction also blows up, it very poorly represents this divergence as is manifest in the blow-up of the difference Hamiltonian $h(p)$. In classical phase space this is where the constant energy manifold asymptotes to a p—eigenstate and this is what we refer to as a supercaustic. In figure 2.4 we plot $h(p)$ for the Eckart barrier.

2.2.1 Uniformization

We saw above that momentum-space WKB fails in the asymptotic region of the potential, when the potential flattens out. The first step in uniformization is to find the exact energy eigenfunction in momentum representation of the Hamiltonian in this region. The asymptotic form for potentials 2.4 is $H = p^2/2 + W_o e^{-\alpha x}$. We shall first find its exact eigenstates in configuration space and then calculate its exact Fourier transform to momentum space. Performing the change of variable $z = \frac{i2\sqrt{2W_o}}{\hbar a}e^{-\alpha x/2}$ in Schrödinger's equation

$$\left(-\frac{\hbar^2}{2}\frac{d^2}{dx^2} + W_o e^{-\alpha x} - E\right)\psi(x) = 0$$

yields Bessel's equation of order $\nu = \frac{i2\sqrt{2E}}{\hbar\alpha}$:

$$\left(\frac{d^2}{dz^2} + \frac{1}{z}\frac{d}{dz} + (1 - \frac{\nu^2}{z^2})\right)\bar{\psi}(z) = 0$$

with solution

$$\psi^{W_o e^{-\alpha x}}(x) = \mathcal{N} K_{\frac{i}{\hbar}\frac{2}{\alpha}\sqrt{2E}}\left(\frac{2\sqrt{2W_o}}{\hbar\alpha}e^{-\alpha x/2}\right) \tag{2.8}$$

which has the correct exponentially decaying behavior for $x \to -\infty$. $K_\nu(z)$ is MacDonald's function of order ν [17]. $\mathcal{N}$ is a normalization constant; choosing

$$\mathcal{N} = \frac{2}{\pi}\left(\frac{1}{2E}\right)^{\frac{1}{4}} \sinh\left(\frac{2\sqrt{2E}\pi}{\alpha\hbar}\right)\Gamma\left(1 + \frac{i}{\hbar}\frac{2\sqrt{2E}}{\alpha}\right) \tag{2.9}$$

gives unit incoming flux from the right; that is,

$$\psi^{W_o e^{-\alpha x}}(x \to \infty) \to \left(\frac{1}{2E}\right)^{\frac{1}{4}}(e^{-i\sqrt{2E}x/\hbar} + re^{i\sqrt{2E}x/\hbar})$$

where $|r| = 1$. This can be readily verified by the property (see [17])

$$K_\nu(z) \overset{small z}{\longrightarrow} \frac{\pi}{2}\left(\left(\frac{z}{2}\right)^{-\nu}\frac{1}{\Gamma(1-\nu)} + \left(\frac{z}{2}\right)^{\nu}\frac{1}{\Gamma(1+\nu)}\right)$$

$\Gamma(z)$ is the gamma function. The Fourier transform then gives the solution in momentum space:

$$\phi^{W_o e^{-\alpha x}}(p) = \frac{1}{\sqrt{2\pi\hbar}}\int_{-\infty}^{\infty} e^{-ipx/\hbar}\psi^{W_o e^{-\alpha x}}(x)dx.$$

With the help of the integral expression (see [17])

$$K_\nu(z) = \frac{1}{2}\left(\frac{z}{2}\right)^{\nu}\int_0^\infty e^{-t-z^2/4t}t^{-\nu-1}dt,$$

for $|\arg(z)| < \frac{\pi}{4}$, we may compute the Fourier transform exactly, obtaining

$$\phi^{W_o e^{-\alpha x}}(p) = \frac{\mathcal{N}}{4\sqrt{2\pi\hbar}}e^{\frac{-ip}{\hbar\alpha}ln(\frac{2W_o}{\alpha^2\hbar^2})}\Gamma\left(\frac{i}{\hbar\alpha}(p + \sqrt{2E})\right)\Gamma\left(\frac{i}{\hbar\alpha}(p - \sqrt{2E})\right) \tag{2.10}$$

This is the exact momentum space eigenfunction for the Hamiltonian $p^2/2 + W_o e^{-\alpha x}$. The semiclassical limit of the exact solution 2.10 yields the p-space WKB solution, which is as it should be: noting that ([17])

$$\Gamma(z \to \infty) \longrightarrow e^{zlnz - z - \frac{1}{2}lnz + \frac{1}{2}ln2\pi},$$

we find that as $\hbar \to 0$,

$$\phi^{W_o e^{-\alpha x}}(p) \longrightarrow \frac{\mathcal{N}\alpha}{4}\sqrt{\pi\alpha\hbar}\, e^{\frac{-\pi\sqrt{2E}}{\hbar\alpha}}\, \phi^{W_o e^{-\alpha x}}_{wkb}(p), \tag{2.11}$$

where

$$\begin{aligned} \phi^{W_o e^{-\alpha x}}_{wkb}(p) &= \frac{1}{\sqrt{-V'(x(p))}} \exp\left(\frac{-i}{\hbar}\int_0^p x(p')dp'\right) \\ &= \sqrt{\frac{1}{\alpha(E-p^2/2)}} \exp\left(\frac{-2i}{\hbar\alpha}\left(p - \sqrt{\frac{E}{2}} \ln\left(\frac{p+\sqrt{2E}}{p-\sqrt{2E}}\right)\right.\right. \\ &\quad \left.\left. + \sqrt{\frac{E}{2}}\pi i - \frac{p}{2}\ln(\frac{E-p^2/2}{W_o})\right)\right) \end{aligned} \tag{2.12}$$

We now have an exact solution for the region where the WKB for potentials of the form 2.4 diverges. This exact solution for the exponentially decreasing potential is what we need for the uniformization of the supercaustic of these potentials. We would like our uniform semiclassical wavefunction to satisfy Schrödinger's equation to $O(\hbar)$ and have the correct blow-up behavior near $p = \pm\sqrt{2E}$, so that the deficit in being an exact energy eigenfunction is everywhere finite and of order $\hbar^2$ (and higher). This is achieved by multiplying 2.10 by well-behaved WKB factors corresponding to the "non-flattening out" part of the potential, accounting for the behavior away from the supercaustic. We hope the following will clarify what we mean.

The general potential 2.4 has the exponential asymptotic behavior:

$$V(x \to \infty) \to 2V_o(c+1)e^{-\alpha x} := V_{asymp}(x). \tag{2.13}$$

We first observe that the classical position for the exponentially decaying potential $V_{asymp}(x)$ may be written

$$x^{V_{asymp}(x)}(p) = -\frac{1}{\alpha}\ln\left(\frac{E-p^2/2}{2V_o(c+1)}\right)$$

and, for this potential,

$$V'(x(p)) = -\alpha(E-p^2/2)$$

The classical position as a function of momentum for the general potential (2.4), is

$$
\begin{aligned}
x(p) &= -\tfrac{1}{\alpha}\ln\left(\tfrac{E-p^2/2}{2V_o(c+1)}\right) - \tfrac{1}{\alpha}\ln\left(\frac{2(c+1)\left(1-c\sqrt{1-\frac{E-p^2/2}{V_o}}\right)}{\left(1-c^2\left(1-\frac{E-p^2/2}{V_o}\right)\right)\left(1+\sqrt{1-\frac{E-p^2/2}{V_o}}\right)}\right) \qquad (2.14)\\
&= x^{V_{asymp}}(p) + xextra(p)
\end{aligned}
$$

and the derivative of the potential is

$$
\begin{aligned}
V'(x(p)) &= -\alpha\,(E-p^2/2)\left(\frac{2(c+1)\left(1-c\sqrt{1-\frac{E-p^2/2}{V_o}}\right)}{\left(1-c^2\left(1-\frac{E-p^2/2}{V_o}\right)\right)\left(1+\sqrt{1-\frac{E-p^2/2}{V_o}}\right)\left(\frac{1-e^{-\alpha x(p)}}{1+ce^{-\alpha x(p)}}\right)}\right) \qquad (2.15)\\
&= V'_{asymp}(x(p)) \times Vextra'(p)
\end{aligned}
$$

The factorization and sum properties in equations 2.15 and 2.14 respectively enable us to write the p-space WKB wavefunction for the general potential as the product,

$$
\phi_{wkb}(p) = \phi_{wkb}^{2V_o(c+1)e^{-\alpha x}}(p) \times \frac{1}{\sqrt{Vextra'(p)}}e^{-\frac{i}{\hbar}\int^p xextra(p')dp'} \qquad (2.16)
$$

We are now motivated to assert the uniformization for potentials of form (2.4) as

$$
\begin{aligned}
\phi_{unif}(p) &= \mathcal{N}' e^{\frac{-ip}{\hbar\alpha}\ln(\frac{2V_o}{\alpha^2\hbar^2})}\Gamma(\frac{i}{\alpha\hbar}(p+\sqrt{2E}))\Gamma(\frac{i}{\alpha\hbar}(p-\sqrt{2E})) \qquad (2.17)\\
&\times \frac{1}{\sqrt{Vextra'(p)}}e^{-\frac{i}{\hbar}\int^p xextra(p')dp'}
\end{aligned}
$$

where we have replaced the WKB solution for the exponential part with the exact solution for the exponential potential from (2.10). This wavefunction has the correct blow up behavior as $p \to \pm\sqrt{2E}$ (the extra WKB factors tend to 1 (up to a a phase) in this limit) and, as $\hbar \to 0$, this reduces, by construction, to the WKB wavefunction. The extra WKB factors are well-behaved semiclassical objects: the divergent part of the semiclassics has been extracted and replaced by an exact solution, which we then modify by the benign WKB factors accounting for the difference between the true potential and the exponential.

The final check, of course, is to calculate the deficit of ϕ_{unif} as an eigenfunction (as in (2.6)). That it is now finite is clear, from the above comments. We shall demonstrate this explicitly for the symmetric Eckart barrier, $V(x) = V_o\text{sech}^2(x)$.

2.2.2 The Sech^2 barrier.

For $V(x) = V_o\text{sech}^2(x)$, equation (2.18) gives

$$
\phi^R_{unif}(p) = e^{\frac{-ip}{2\hbar}\ln(\frac{V_o}{2\hbar^2})}\Gamma\left(\frac{i}{2\hbar}(p+\sqrt{2E})\right)\Gamma\left(\frac{i}{2\hbar}(p-\sqrt{2E})\right) \qquad (2.18)
$$

$$\times \quad \left(\frac{1}{1-\frac{E-p^2/2}{V_o}}\right)^{\frac{1}{4}} e^{-\frac{i}{\hbar}\int_0^p \ln\left(1+\sqrt{1-\frac{E-p'^2/2}{V_o}}\right)dp'}$$

where the R superscript denotes the state at energy E that lives on the right-hand side of the barrier, corresponding to the positive branch of the V^{-1} function (see also figure 2.2). The state on the left, is given by the complex conjugate:

$$\phi^L_{unif}(p) = \overline{\phi^R_{unif}(p)}$$

(stemming from uniformization based on the $e^{\mp ax}$ potential). To calculate the action of the Hamiltonian on (2.19), we proceed as in (2.5). It is easiest however to perform the differentiation operations on the $\Gamma-$functions within the integral expression for the $\Gamma-$function:

$$\Gamma\left(\frac{i}{2\hbar}(p \pm \sqrt{2E})\right) = \int_0^\infty e^{-t} t^{\frac{i}{2\hbar}(p\pm\sqrt{2E})-1} dt. \tag{2.19}$$

and then integrate the result at the final stage. In particular,

$$(i\hbar)^n \frac{d^n}{dp^n}\Gamma\left(\frac{i}{2\hbar}(p \pm \sqrt{2E})\right) = \int_0^\infty (-\frac{1}{2}\ln t)^n e^{-t} t^{\frac{i}{2\hbar}(p\pm\sqrt{2E})-1} dt$$

We use mathematica to operate with the first few terms of (2.5) on ϕ_{unif}, but with the $\Gamma\left(\frac{i}{2\hbar}(p+\sqrt{2E})\right)\Gamma\left(\frac{i}{2\hbar}(p-\sqrt{2E})\right)$ replaced by $t^{\frac{i}{2\hbar}(p+\sqrt{2E})}\tilde{t}^{\frac{i}{2\hbar}(p-\sqrt{2E})}$. At the expense of simplifying the differentiation operations we have complicated the re-summing at each order in $\hbar$. We obtain, after much algebra:

$$V(i\hbar\frac{d}{dp})\phi_{unif}(p) = \left(V(x(p) + \hbar^2 h_{unif}(p) + O(\hbar^3))\right)\phi_{unif}(p) \tag{2.20}$$

where $h_{unif}(p)$ is a very long expression (a sum of about 50 terms) depending on V_o, E, and p. $\hbar^2 h_{unif}(p)$ is the perturbation which turns off the quantum effect of barrier tunneling (to order $\hbar^2$): the semiclassical wavefunction $\phi^{R(L)}_{unif}$, which lives only on the right(left) side of the barrier is an eigenstate of $H - \hbar^2 h_{unif}$ to order $\hbar^2$ so in this sense the effect of h_{unif} is to suppress tunneling to the left(right). We note that a complementary concept of turning off above-barrier reflection has been discussed in chapter 1.

In figure 2.5 we plot $h_{unif}(p)$ for energy $E = 1.5$ in the Eckart barrier $2\text{sech}^2 x$ (*c.f.* the corresponding quantity for the WKB function, figure 2.4).

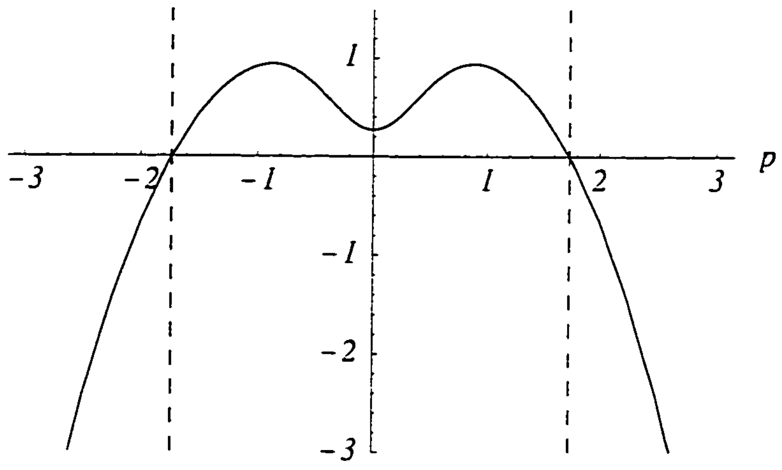

Figure 2.5: This plot of $h_{unif}(p)$ shows how much the uniformized semiclassical wavefunction at energy $E = 1.5$ for the Eckart barrier $2\text{sech}^2 x$ misses being an energy eigenfunction to order $\hbar^2$. Notice that the function is finite and "small" in the physical domain $|p| \leq \sqrt{2E}$, unlike the case for the WKB wavefunction (fig 2.4).

Chapter 3

Barrier Tunneling and Reflection in the Time and Energy Domains: The Battle of the Exponentials

In this chapter we turn from the WKB wavefunctions of the previous sections to more general semiclassical objects, semiclassical propagators. We will again be considering the description of classically forbidden processes (specifically, quantum barrier crossing and reflection), however this time in the time domain as well as the energy domain. We shall find classically forbidden barrier tunneling and above barrier reflection are well defined and important processes in the time domain. In fact classically forbidden processes can overshadow allowed ones when both are present. We shall find that the classically allowed trajectories in the time domain are not in general sufficient to explain tunneling amplitudes in the energy domain: They do not correctly account for tunneling below the barrier when the time-energy Fourier transform is done, nor for quantum reflection above the barrier. Another important result of this chapter concerns the stationary phase Fourier transform (WKB result): this cannot be thought of as an approximation to the Fourier integral because of a branch cut in the complex-time plane. Rather, it is the tunneling trajectories in the time domain that give the WKB result under stationary phase Fourier transform. We also make clear the essential distinction of barriers which flatten out at large distance and those which do not. Parts of this work have been published in [8] and in [9].

3.1 Introduction

Tunneling through (or reflection from) a barrier at fixed energy E is well understood from a semiclassical (WKB) perspective. WKB theory involves the use of complex trajectories which travel partly in imaginary time in order to penetrate the barrier. The same barrier problems in the time domain have received much less scrutiny, and have caused confusion at times, due to some subtleties which we expose here. For example: *is* there any tunneling in the time domain across a barrier, since classically trajectories can always be found which connect two positions, one on each side of the barrier? The probability amplitude for a particle initially at x_1 to be found at x_2 after time T is given semiclassically by the propagator

$$G^{sc}(x_2,T;x_1,0) = \sum_{\substack{classical\\paths}} \frac{1}{\sqrt{2\pi i\hbar}} \left|\frac{\partial^2 S_{cl}(x_2,x_1,T)}{\partial x_2 \partial x_1}\right|^{\frac{1}{2}} e^{iS_{cl}(x_2,x_1,T)/\hbar - i\nu\pi/2} \tag{3.1}$$

which is the classical limit of Feynman's path integral [3, 4, 6, 18]. The sum goes over all classical paths linking x_1 to x_2 in time T and $S_{cl}(x_2,x_1,T)$ is the action along that path. ν is the Maslov index. Consider a transmission problem where x_1 and x_2 are on the left and right sides respectively of a barrier in an otherwise constant potential. Since to be at position x_1 with certainty at time 0 is to have completely uncertain momentum and therefore completely uncertain energy, there is always a supply of classical paths surmounting the barrier in just such a way as to arrive at x_2 at time T. At long times the energy of the arriving trajectories approaches the top of the barrier, since the slowing down near the barrier top is needed to effect the time delay necessary to arrange arrival at x_2 at long times. At any real time T there is exactly one classical path with $E_{cl} > V_{max}$ which contributes in (3.1).

So the barrier problem in the time domain seemingly does not involve "tunneling" or classically forbidden paths and the semiclassical Green function 3.1 can apparently be constructed with ordinary "over the barrier" trajectories. In order to obtain the semiclassical energy domain Green function, one performs the Fourier transform by stationary phase:

$$G^{sc}(x_2,x_1;E) = \frac{1}{i\hbar}\int_{sp} e^{iET/\hbar} G^{sc}(x_2,T;x_1,0)\, dT \tag{3.2}$$

The kernel of the stationary phase Fourier transform is the time domain semiclassical propagator, which is always non-vanishing because of the "over the barrier" trajectories. However for energies below the barrier top, no real time stationary phase point is found, forcing a search in the complex time plane for a saddle point. The search is rewarded with the well known classically forbidden imaginary time tunneling trajectories, which asymptotically give the correct WKB fixed energy tunneling amplitudes (transmission $\sim e^{-\int_{a_1}^{a_2} |p_{cl}| dx/\hbar}$, where $a_{1,2}$ are the classical turning points at energy E). Suppose the semiclassical time domain Green function is very accurate. Then a correspondingly accurate energy domain result would follow from *numerical* Fourier transform and would be different numerically from stationary phase evaluation. It is thus tempting to think that if the original (real time) Fourier transform over the semiclassical propagator were performed *numerically* (rather than by stationary phase) one would get an even better result. Strangely, such a result would be given only in terms of classically allowed over-the-barrier trajectories (since $G^{sc}(x_2, T; x_1, 0)$ is). The smallness of the tunneling amplitude in this view would be due to the rapid oscillation of the integrand. This method was considered in recent work [19]. It is reinforced by analogy with certain *uniformizations* in semiclassical theory, in which troublesome semiclassical amplitudes are replaced by more accurate, "uniform" ones, which can come from an integral expression. The foundation of such an idea was however called into doubt in [20], and the situation remained cloudy. Here, we show that the numerical time-energy Fourier integral, using above barrier information, is indeed inadequate. We find the time integral, normally approximated by saddle point integration, for energies below the barrier top cannot generally give an improved transmission coefficient under exact (numerical) evaluation. In fact, below-barrier tunneling trajectories are needed *even in the time domain* in certain regimes, where for finite $\hbar$ they *dominate* the classically allowed result. Moreover they dominate the Fourier transform at below barrier energies. Conventional semiclassics (above-barrier trajectories) breaks down at long times (for the transmission problem) but this is where our correction works well. The corrected time domain semiclassical Green function could then be numerically Fourier transformed to give a good tunneling amplitude at fixed energy.

In section 3.2 we begin with a brief review of the semiclassical propagator in the time domain. Then we present a quasi-classical picture of barrier transmission which suggests that in the generic case the semiclassics based on classically allowed trajectories is incomplete. We indicate how a correction may be made. At long times and distant endpoints we obtain a close approximation to the exact propagator where the conventional semiclassical propagator completely fails. In Sect. 3.3, we investigate the tunneling problem in the energy domain and give numerical evidence for why using the conventional semiclassical propagator in a Fourier transform is inadequate. We show that it is the stationary phase Fourier transform of our time domain tunneling term that gives the WKB energy tunneling result. By discussing branch structure in the complex-time plane we show how in performing the Fourier transform of the conventional semiclassical propagator we miss the stationary phase contribution because of an intervening branch cut. Finally, in section 3.4, we analyze the case of quantum reflection above a barrier.

3.2 The Time Domain

Consider a particle of mass m in one dimension interacting under the Hamiltonian $H = \frac{p^2}{2m} + V$, p being the momentum and V a time-independent potential. The probability amplitude for the particle, initially at x_1, to be found at x_2 after time T, is given by the propagator

$$G(x_2, T; x_1, 0) = \langle x_2 | e^{-iHT/\hbar} | x_1 \rangle = \int \mathcal{D}[x(t)] e^{\frac{i}{\hbar} S[x(t)]} \tag{3.3}$$

where $\mathcal{D}[x(t)]$ implies a summation over all paths $x(t)$ linking x_1 to x_2 in time T and $S[x(t)]$ is the classical action $\int L dt$ for the (not necessarily classical) path $x(t)$ linking x_1 to x_2 in time T. The formula on the right-hand side, due to Feynman ([3]), provides a natural basis for a semiclassical evaluation of the propagator, the exact evaluation of which is, in general, very difficult. (See [21] for a recent review of some exactly solvable path integrals.) The reader is referred to the existing literature [4, 18, 6] for details of the derivation of the semiclassical propagator. The essence of the technique lies in stationary phase evaluation of the path integral, and reduces the formidable sum over all paths to the sum over only classical paths in equation 3.1. We may write equation 3.1 as:

$$G^{sc}(x_2, T; x_1, 0) = \sum_{\substack{classical \\ paths}} \left| \frac{1}{2\pi i\hbar p_{cl}(x_1) p_{cl}(x_2) \int_{x_1}^{x_2} \frac{dx}{p_{cl}(x)^3}} \right|^{1/2} e^{i\int_{x_1}^{x_2} p_{cl}(x)dx/\hbar - iE_{cl}T/\hbar - i\nu\pi/2} \tag{3.4}$$

where $p_{cl} = \sqrt{2m(E_{cl} - V(x))}$ is the classical momentum at x of a particle with energy E_{cl}, and E_{cl} is determined by the classical relation

$$T = \int_{x_1}^{x_2} \frac{dx}{\sqrt{2m(E_{cl} - V(x))}}. \tag{3.5}$$

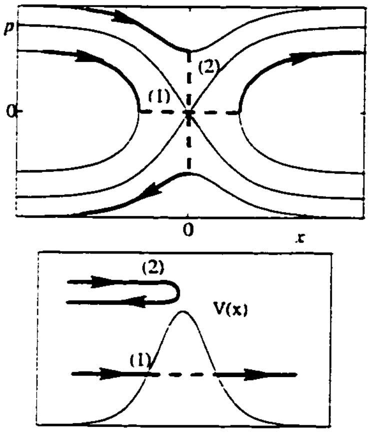

Figure 3.1: Whether the semiclassical propagator, which involves classical paths only, can describe classically forbidden processes such as tunneling through a barrier (1) and above-barrier reflection (2), is the subject of this chapter. The lower figure shows schematically the processes and the potential and the upper figure is the associated phase space.

ν is the Maslov index, counting the number of conjugate points the trajectory encounters. In the special case of a harmonic or linear potential, which generates a quadratic action, this gives the exact propagator, due to the exactness of the stationary phase method for quadratic exponents. The contour taken for the integral in 3.5 is the same as for the action integral, and reflects the behavior of the associated classical trajectory.

The question now arises: what role if any do tunneling paths play in this semiclassical approach? As this semiclassical recipe calls only for ordinary real time classical paths linking x_1 to x_2 in time T, the issue arises whether classically forbidden phenomena such as tunneling through or quantum reflection above a barrier (see Fig. 3.1) are somehow encoded in the classical trajectories, in the sense mentioned above: i.e. does *explicit* real time Fourier transform over the "classically allowed" Green function into the energy domain give good results?

For definiteness, we consider a quasi-classical phase space view of propagation across a symmetric Eckart barrier $V_0\mathrm{sech}^2x$ and take mass 1. A state $|x\rangle$ may be represented by a vertical line through x corresponding to momentum being completely unspecified when the position is exactly known. For our propagation problem we thus consider each point on a line at x_1 as an initial condition, and the overlap of the phase space distribution obtained after evolving these under the classical equations of motion for time T with a vertical line at x_2 corresponds to the classical analog of the quantum propagator. Since

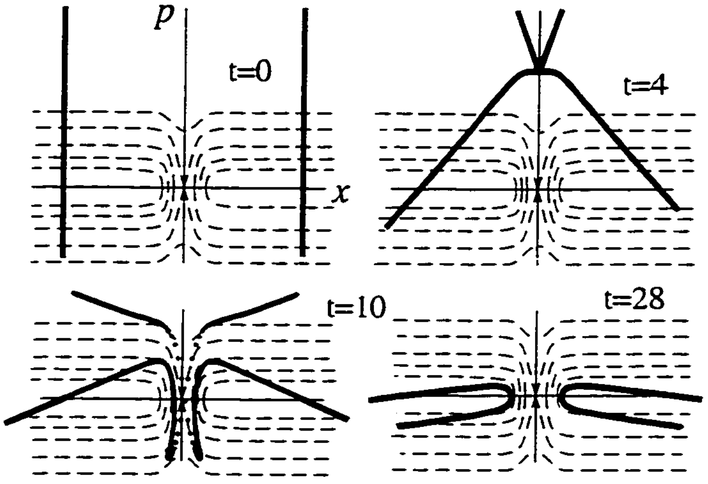

Figure 3.2: A quasi-classical view of the propagator $G(10, T; -10, 0)$ in phase space ($t = T/2$) (see text). As time evolves the density dies exponentially; only at very dense seeding of initial conditions will the thin manifold be seen. "Tunneling loops" develop. Phase space contours are overlayed.

$\langle x_2|x_1(t)\rangle = \langle x_2|e^{-iHt/\hbar}|x_1\rangle = \langle x_2|(e^{iHt/2\hbar})^{\dagger}e^{-iHt/2\hbar}|x_1\rangle = \langle x_2(-t/2)|x_1(t/2)\rangle$, we may represent the propagator by the overlap of the phase space distribution from a vertical line at x_1 evolved for time $T/2$ with that of a vertical line at x_2 evolved backward in time for $T/2$. In Fig. 3.2 we focus on the case $x_1 = -x_2 < 0$ and $V_0 = 1$. We have shown the phase space distribution at four successive times. At first this distribution simply shears, as it would for free particle motion. Only very high energy trajectories reach the interaction region. As time evolves, lower energy trajectories arrive near the barrier. The classical overlap of the forward and backward propagated distributions is proportional to the Van Vleck determinant. Because of the separatrix and the concomitant exponential instability, the density of trajectories at the intersection $x = 0$ (classically allowed above-barrier trajectories) falls away exponentially rapidly. In the plots we have propagated a finite uniform density of several hundred trajectories along the initial line; after some time ($t = 10$) the density at the separatrix is so low that the manifold is not seen at $x = 0$. We call this contribution to the time Green function the A term (classically allowed, over the barrier). At the same time however, we see a below barrier loop structure developing with a healthy density. At time $t = 10$ for example, trajectories of a certain energy (below V_0) have just reached the barrier and are beginning to turn around. The loops are strongly suggestive of a tunneling contribution to the propagator, since they are very similar to the fixed energy manifolds(Fig. 3.1) which tunnel across the barrier in the energy domain. The loops from x_1 and x_2 make no contribution in the primitive semiclassical limit as they do not overlap. However if we include ***tunneling*** between these loops we have a second contribution to the time Green function, term B. For finite, fixed $\hbar$, a "battle of the exponentials" ensues. The classical term A Van Vleck prefactor, which dies exponentially in time, is pitted against the tunneling term B, which is a factor bounded by a fixed exponential multiplied by an algebraically decaying prefactor. Thus the battle is always lost by the classical term A at long times. For the Eckart barrier and endpoints far from the interaction region, tunneling overtakes the classical contribution when $e^{-\pi(\omega-2x/T)/\hbar}/\sqrt{T} > \sqrt{\omega/2}e^{x-\omega T/2}$. The right-hand side of this is the square-root of the long-time limit of the Van Vleck determinant (term A), which determines the magnitude of the semiclassical propagator and ω is the frequency of the (inverted) oscillator in the harmonic approximation to the barrier top. The left-hand side is the tunneling contribution (term B) at long times and far endpoints. To evaluate this, we observe that in this limit, the loops approach energy contours and so the issue of getting across the barrier region becomes identical to the energy tunneling problem. The energy of trajectories arriving at the barrier changes only slowly with time. Moreover as time increases the trajectories arriving from the distant points are of lower and lower energy, so the loop "falls through" successively lower energies as time increases. The tunneling part of the amplitude at a given time then follows from the usual energy tunneling at the energy of the arriving trajectories, suitably weighted by their number density. We use expression 3.1 but substitute the (time-dependent) energy of the loop for the classical energy. This gives the left-hand side of the above inequality: the density on the loops falls off as $1/T$, much slower than the exponential fall-off of the classical contribution. A simple way to see this is as follows: For x_1 far from the interaction region and long times, where the loops resemble below-barrier energy contours, the density on the loop is proportional to $\sim p_{turn}/x_1$, where p_{turn} is the initial momentum that the trajectory which has just hit the barrier and is beginning to turn around had. This may be seen by considering the top half of the loop which we approximate as a horizontal line from x_1 to the turning point at the barrier. As time increases, the energy needed to reach the barrier decreases and p_{turn} falls roughly as x_1/t, with $t = T/2$ (free-particle motion). Hence the density on the loops falls as $1/T$, much slower than the exponential fall-off at the direct overlap. Once we have reached the cross-over time ***tunneling dominates the classically allowed contribution.*** Indeed the conventional semiclassical propagator using only above barrier trajectories becomes a

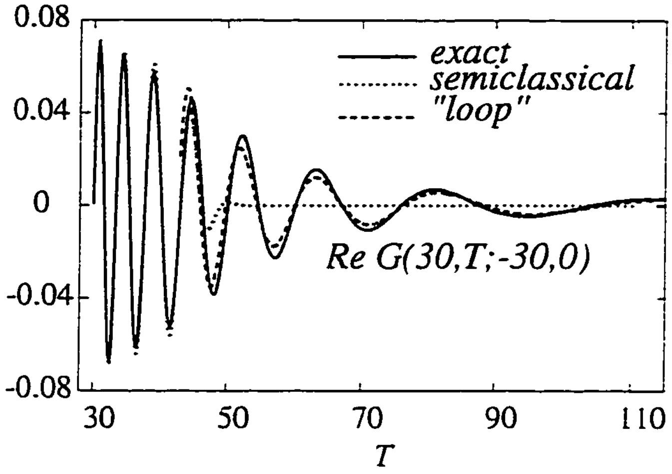

Figure 3.3: Transmission through $V = \text{sech}^2 x$:$G(30, T; -30, 0)$.

much worse approximation at longer times. This is seen in Fig. 3.3, which shows the exact Green function and the "primitive" semiclassical result, which collapses around $T = 50$. Also shown is the "loop" contribution, which does an excellent job representing the full Green function at such long times. The exact propagator was obtained by numerical Fourier transform of the exact energy Green function for the Eckart barrier; the latter was calculated in [22]). In Figs. 3.3 and 3.10, $\hbar = 1$.

3.2.1 Inverted Harmonic Oscillator

In [24], Wigner functions are used to show that tunneling at energies below the inverted harmonic oscillator arises through real trajectories with above-barrier energies. However an essential physical aspect of the barrier problem is that it asymptotes to a flat potential, a property which the inverse harmonic potential does not share. This has profound analytic consequences, introducing branch structure of trajectories in the complex plane (see section 3.3). In the inverted harmonic case, no tunneling loops develop, since a vertical line at $x = x_1$ representing the initial phase space density always only shears because the dynamics is linear (figure 3.4).

The conventional semiclassical propagator (which picks up the classically allowed intersection of the forward and backward propagated pieces) is exact in this case. No tunneling trajectories exist to compete with the classically allowed ones. The tunneling loops are also suppressed even for the Eckart-type barriers if $|x_1|, |x_2|$ are near the barrier,

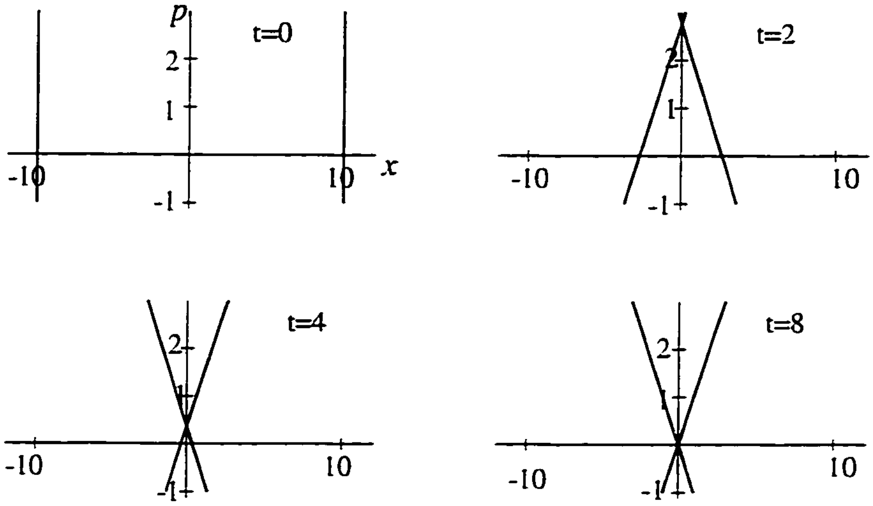

Figure 3.4: Phase space evolution through the inverse harmonic oscillator $V(x) = 1 - x^2$, the harmonic approximation to the top of the sech^2 barrier in the previous picture. Here the initial vertical line simply shears. The density variation is *not* shown in this picture - the manifold becomes very thin very rapidly at the intersection just like the sech^2 case. No loops develop.

where the problem begins to look harmonic. In this limit one might hope the contribution to the semiclassical propagator from the classical "over the barrier" overlap would give reasonable results. This was already successfully exploited in [19] and may be of practical significance.

3.3 The Energy Domain

We address now the probability of going from x_1 to x_2 at energy E. This is given by the energy Green function, which may be written as the Fourier transform

$$G(x_2, x_1; E) = (i\hbar)^{-1} \int_0^\infty e^{\frac{i}{\hbar}ET} G(x_2, T; x_1, 0)\, dT \qquad (3.6)$$

In particular, consider the tunneling case, when $E < V_o$. Consider the idea that the classically allowed term is sufficient to use in the numerical transform. The thinking is as follows: The complex time stationary phase integral (leading to standard WKB results) is an approximation to the Fourier transform over the (primitive) semiclassical propagator (term A); therefore, doing the Fourier transform numerically should yield a better result. However the first phrase is incorrect: the integral through the complex saddle point is *not*

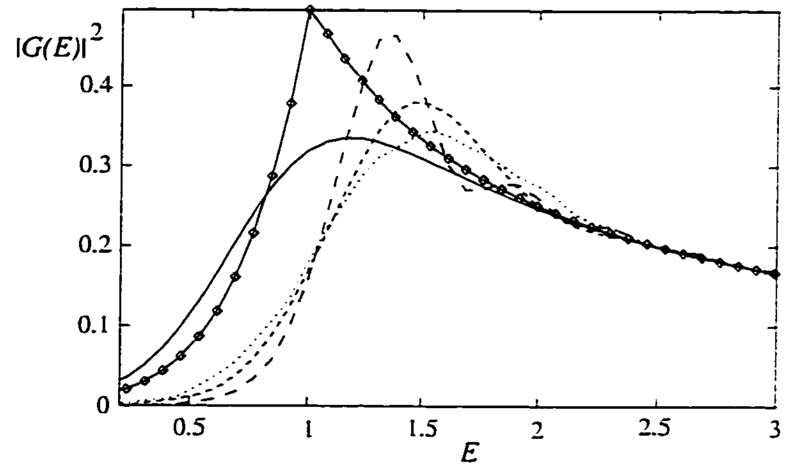

Figure 3.5: Modulus-squared of the energy Green function $G(-x_2, x_2; E)$ for $V(x) = \text{sech}^2 x$ (barrier top at 1). The solid line is the exact, the -◇-line is the WKB result (stationary phase contribution of the Fourier transform of G^{sc}), the dotted, small-dashed and larger-dashed lines are the numerical FFT's of G^{sc} with endpoints $x_2 = 5, x_2 = 10, x_2 = 30$ respectively. The exact and WKB results are independent of the endpoint, as required.

the same integral as the real-time integral. For general endpoints and barrier potentials a branch cut in the complex-time plane makes the integral along the complex contour distinct from that along the real-time contour. We shall come back to this shortly, but first see what happens if we perform the numerical FFT of the semiclassical propagator (term A).

In figure 3.5, we plot the numerical FFT of the semiclassical propagator for the sech^2 barrier (the dotted, small-dashed and large-dashed lines). The endpoints are taken to be on either side of the hump, well away from the interaction region: we take $x_1 = -x_2$ and consider the three cases $x_2 = 5, 10$, and 30.

We first note that well above the barrier the magnitude of the Fourier transform falls as $1/\sqrt{2mE_{cl}}$ and in this domain, there is good agreement with the exact energy Green function. However, below the barrier, not only does this method fall below the exact result, but $\left|(i\hbar)^{-1}\int G(x_2, T; x_1, 0)e^{iET/\hbar}dT\right|^2$ *decreases* as the endpoints are moved away. This is a non-physical effect since the endpoints are well beyond the barrier range, where the motion is essentially free-particle: there is no loss of amplitude before the barrier region is reached, nor after. As the endpoints move out, the exact Fourier transform of the uncorrected semiclassical propagator regresses towards the classical transmission coefficient of 0 for $E < V_o$ and this decay appears to depend approximately exponentially on the endpoint. Further, for energies above but close to the top of the barrier, the exact Fourier

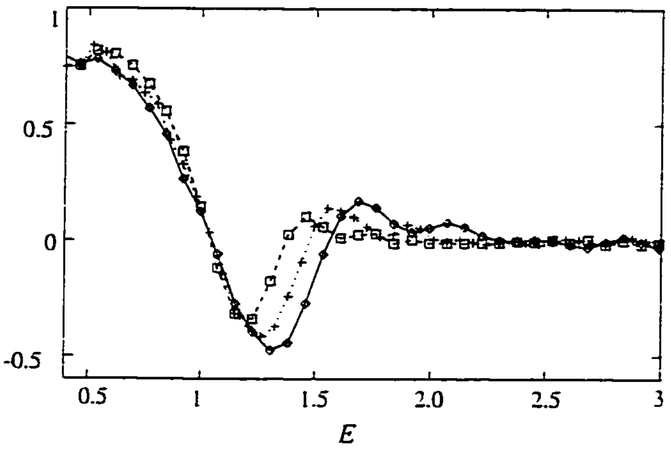

Figure 3.6: $(|G(30,-30;E)|^2 - |G(5,-5;E)|^2)/|G(5,-5;E)|^2$ (which is zero for the exact Green function), for $\hbar = 1$ (–◇–), 0.75 (–+–),0.5 (–□–). Above the barrier top (at 1), the endpoint dependence vanishes as $\hbar \longrightarrow 0$, in accordance with the stationary phase evaluation at energies above V_o being independent of $x_{1,2}$. However below the barrier top the endpoint dependence persists.

transform of the uncorrected semiclassical propagator overshoots the exact result, and this effect increases as the endpoints are moved out. This effect was also observed in a recent paper ([20]), where the S-matrix for the Eckart barrier was computed, involving the Fourier transform of the correlation function between Gaussian wavepackets. We also note here that as $\hbar$ is decreased, the endpoint dependence persists at energies below the barrier but dies away for energies above (Fig. 3.6). We shall come back to this point in section 3.3.

In fact in a numerical FFT, *term B must be added to term A as separate contributions to the amplitude.* This is in tune with the essence of the semiclassical limit to Feynman's path integral, which requires a sum over distinct, stationary paths. The tunneling term B, dominant at long times, is resonant at below barrier energies, so also dominates the Fourier integral there. One may therefore eliminate the A term when calculating the tunneling, at least in the large $|x_1|, |x_2|$ limit.

The Fourier transform of the B term can be performed by stationary phase; in the large $|x_1|, |x_2|$ limit the result is the usual WKB below barrier tunneling amplitude which we now show. This is not a contour deformation on the A term; rather, both A and B exist as distinct contributions. When x_1 and x_2 are far from the barrier, the loops approach energy contours of energy $E(T)$, where $E(T) \sim 2x_1^2/T^2$ is the energy needed to arrive at the barrier in time $T/2$. The loop contribution then follows from Eqn. 3.1 where we substitute $E(T)$

in place of the classical energy E_{cl}. The stationary phase point in the time-energy Fourier transform of this at energy E_0 is given by:

$$\left.\frac{\partial E}{\partial T}\right|_{T^*}\int_{x_1}^{x_2}\frac{dx}{p_{E(T^*)}}-\left.\frac{\partial E}{\partial T}\right|_{T^*}T^*-E(T^*)+E_0=0 \tag{3.7}$$

Now, by definition, $T=2\int_{x_1}^{-x_T}dx/p_{E(T)}(x)$ where $-x_T$ is the(left-hand) turning point at energy $E(T)$. This means the first two terms of Eqn. 3.7 together give:

$$-i\int_{-x_T}^{x_{T^*}}\frac{dx}{|p_{E(T^*)}(x)|}\left.\frac{\partial E}{\partial T}\right|_{T^*}\sim i\pi\frac{\sqrt{2E}}{T^*}=\frac{i\pi E(T)}{|x_1|}$$

where the integral is calculated for the case of the Eckart barrier and we have used the large-x_1 approximation $E(T)\sim 2x_1^2/T^2$ to evaluate the partial derivative. In the large-x_1 limit, this term is ignorable compared to the other two terms of Eqn. 3.7 as it is suppressed by a factor of $1/|x_1|$. The stationary phase condition becomes $E(T^*)=E_0$. This (real) stationary phase point is the time at which a loop of energy E_0 (below the barrier) has formed at time $T/2$ i.e. particles of energy E_0 have just reached their (left-hand) turning point at the barrier in time $T/2$. The prefactor for the stationary phase integral is then calculated from the second derivative of the exponent and, under the large-x_1 approximation, gives $2\pi i\hbar\int_{x_1}^{x_2}dx/p_{E_0(T^*)}^3$. Gathering all factors, we find

$$\int_{sp}G_B e^{iE_0T/\hbar}dT=\frac{1}{i\hbar\sqrt{p(x_1)p(x_2)}}e^{\frac{i}{\hbar}\int_{x_1}^{-x_0}p\,dx+\frac{i}{\hbar}\int_{x_0}^{x_2}p\,dx-\frac{1}{\hbar}\int_{-x_0}^{x_0}|p|\,dx} \tag{3.8}$$

which is exactly the WKB result. p, x_0 etc are momentum and turning point at energy E_0. This is plotted as the -◇- line in figure 3.5; it is a better approximation than any of the numerical FFT's and there is no endpoint dependence.

We note that (3.8) is also the result of a stationary phase "FFT" of the *classical* term A but along the complex-time contour through the saddle point. We stress again that this is not the same integral as the real-time FFT of term A due to the branch cut and we shall now turn to a discussion of this.

Branch structure in the complex plane

We begin by reviewing the common lore leading to the WKB result for energy domain tunneling from the time domain. In the stationary phase Fourier transform of the semiclassical propagator 3.1, the critical point T_{sp} is determined by

$$-\left.\frac{\partial S_{cl}}{\partial T}\right|_{T_{sp}}=E_{cl}(x_2,x_1,T_{sp})=E \tag{3.9}$$

where E_{cl} is the classical energy function for the trajectory, determined by (3.5). For energies above any potential maximum between the endpoints, a real stationary phase point may be found and we obtain

$$G^{sc}(x_2, x_1; E) = \frac{1}{i\hbar\sqrt{p(x_2)p(x_1)}} e^{\frac{i}{\hbar}\int_{x_1}^{x_2} p(x)dx}. \tag{3.10}$$

where $p(x) = \sqrt{2m(E - V(x))}$. However if the transform variable E is less than any potential maximum between the endpoints, then there is no real stationary phase point satisfying (3.9) as there are no classical paths which can overcome the potential barrier. We may obtain a non-zero value for the transmission by extension into the complex-time plane, where there are many stationary phase points:

$$T_{sp,n} = \left(\int_{x_1}^{a_1} + \int_{a_2}^{x_2}\right) \frac{dx}{\sqrt{2m(E - V(x))}} - i(2n+1)\int_{a_1}^{a_2} \frac{dx}{\sqrt{2m(V(x) - E)}}$$

where $n = 0, 1, 2...$ and $a_{1,2} = V^{-1}(E)$ are the turning points. The resulting complex time stationary phase points are in accord with the idea that energy is fixed and therefore time is arbitrary, even complex. Each stationary phase point corresponds to analytically continuing a classical trajectory through the barrier where its momentum becomes imaginary. $T_{sp,n}$ can be thought of as representing a trajectory which bounces n times in imaginary time inside the inverted barrier before emerging out from the barrier.

It is not the aim of this paper to discuss the issue of the "multiple inside bounces" and the debate surrounding whether to sum the many stationary phase points; the reader is referred to the literature for this (see [5] and references therein). We note that the contributions become exponentially smaller as n increases. The stationary phase points with $n \neq 0$ make little difference to the dominant $n = 0$ contribution (except for near the barrier top, where semiclassics breaks down whether we include them or not).

Picking up the contribution from only the first stationary phase point gives

$$G^{sc}(x_2, x_1; E) = \frac{1}{i\hbar\sqrt{p(x_2)p(x_1)}} e^{\frac{i}{\hbar}\left(\int_{x_1}^{a_1} + \int_{a_2}^{x_2}\right)p(x)dx - \frac{1}{\hbar}\int_{a_1}^{a_2}|p(x)|dx} \tag{3.11}$$

where $|p(x)| = \sqrt{2m(V(x) - E)}$ is the magnitude of the imaginary momentum at x between the turning points at energy E. This gives the standard semiclassical answer for the transmission amplitude across a barrier after multiplication by $i\hbar\sqrt{2E}$ and taking endpoints beyond the interaction region.

However as stated earlier, the integral through the complex stationary phase point is *not* an approximation to the Fourier integral (3.6) of the semiclassical propagator. (Rather, it is the stationary phase (real-time) Fourier transform of the tunneling term in the time domain, term B, as showed in the argument leading to 3.8). This is a subtle, but fundamental point. We cannot interpret evaluation of the complex stationary phase point as arising from a deformation of the real time contour, because of an intervening (and non-rotatable) branch cut singularity. In deforming the time contour to pick up a saddle "hiding" behind a branch cut, one is not performing the same integral as in the original real time contour.

Let us consider again the Eckart barrier, $V(x) = V_o\text{sech}^2(\alpha x)$, and investigate the analytic structure of the time domain propagator in more detail. Branch point structure of $G^{sc}(x_2, T; x_1, 0)$ in the complex time plane arises from that of the action $S_{cl}(x_2, x_1, T)$ which in turn arises from that of the classical energy function $E_{cl}(x_1, x_2, T)$ defined implicitly by (3.5). In the case of the Eckart barrier, we have

$$T = \frac{1}{\alpha\sqrt{2mE_{cl}}}\ln\left(\frac{\sinh(\alpha x_2) + \sqrt{\cosh^2(\alpha x_2) - V_o/E_{cl}}}{\sinh(\alpha x_1) + \sqrt{\cosh^2(\alpha x_1) - V_o/E_{cl}}}\right). \qquad (3.12)$$

As this expression does not lend itself easily to inversion we show there is a branch cut singularity as asserted above in a more indirect fashion. First we argue that the integral of $e^{iET/\hbar}G^{sc}$ along the contours C_1 (real-time) and C_2 (through the complex stationary phase point) shown in figure 3.7 are different, with the help of an observation made in Sect. 3.3. We assert that the non-physical endpoint-dependence of the exact integral along the real-time contour C_1 discussed earlier, which persists at $E < V_o$ as $\hbar$ becomes small (figure 3.6), is not present in the exact integral along contour C_2: it does not appear in the stationary phase evaluation along that contour which the exact integral along C_2 must tend towards as $\hbar$ becomes small. Thus the integrand cannot be analytic between C_1 and C_2. We note in contrast that the endpoint dependence for $E > V_o$ diminishes to zero as $\hbar \to 0$, in accordance with the fact that the evaluation by stationary phase (where, for such energies, the critical point lies on the real axis) is endpoint independent. Thus a singularity of the semiclassical propagator lies between the contours.

Next we deduce this singularity is a branch cut, by pointing out that $E_{cl}(t)$ (and therefore $G^{sc}(x_2, T; x_1, 0)$) is a multi-valued function of time. It is clear that time is a multi-valued function of energy in the classical time-energy relation for the sech^2 barrier

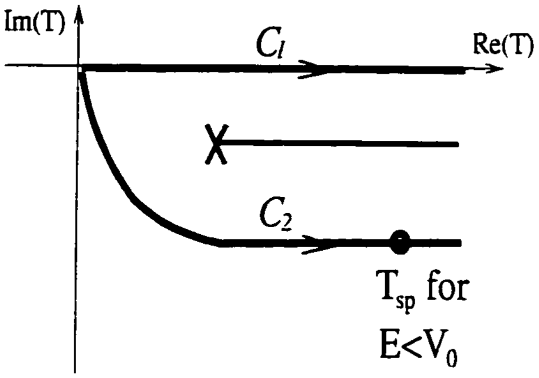

Figure 3.7: Integration contours for time-energy Fourier transform of the semiclassical propagator.

(3.12), with branches differing by $2\pi i/(\alpha\sqrt{2mE_{cl}})$, reflecting the behavior of the trajectory through (possibly complex) turning points. What is perhaps not so clear, is that the inverse function, energy as a function of time, is also multi-valued. To see this, due to the lack of a closed form for the inverse function, we must resort to a numerical search for the E_{cl} which solve (3.12) for a given T. This reveals in fact a countably infinite number of possible complex roots: for example, for real time, there is a unique real $E_{cl} > V_o$ representing the classically allowed path and the complex solutions represent trajectories with complex initial momentum leaving x_1, then bouncing between complex classical turning points before reaching x_2.

We emphasize that there are no such branch points in the case of the inverse harmonic oscillator. For the potential $V(x) = -\frac{1}{2}\omega^2x^2$ we may solve exactly for the action as a function of time:

$$S(x_2, x_1, T) = \sqrt{\frac{m\omega^2}{4}}\left((x_1^2 + x_2^2)\coth(\omega T/\sqrt{m}) - 2x_1x_2\text{cosech}(\omega T/\sqrt{m})\right)$$

As semiclassics in the time domain is exact for this potential, an exact Fourier transform of the semiclassical propagator gives the exact result. Also the stationary phase evaluation of 3.6 may be done and yields a good and legal approximation as there are no intervening branch points to prevent the deformation of contour into the complex plane.

The analytic structure of the trajectory of a particle of energy E gives us some insight into the different, but related, analytic structure of the action which we have been discussing above. Approaching the barrier from the left at energy $E < V_o$, there are two choices at the barrier: either to continue taking real time steps for total time T and turn

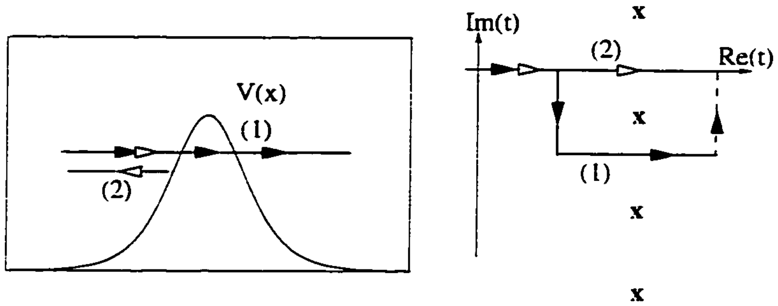

Figure 3.8: Trajectories of $E < V_o$ and branch structure of $x^E(t)$. $x^E(t)$ is multi-valued: shown explicitly are a tunneling path (1), complex-time, and a reflected path (2), real-time. (1) returns to the real time axis through the dashed line (see text).

around or take imaginary time steps and be transmitted through the barrier (figure 3.8). Once through to the other side, to return to the real time axis with the same total time T that the reflected path traveled for, we must take imaginary time steps to cancel the imaginary time gained from passage under the barrier (the dashed line in the figure). For barriers which flatten out, this results in a complex final endpoint and final momentum. We thus have two trajectories with the same initial conditions which in the same total time have different final conditions: one with real position and momentum which was reflected from the barrier and after time T is on the left side of the barrier, and the other with complex position and momentum "on" the right side of the barrier (that, is the real part of the position is at $x > 0$). This implies a branch point as shown. In fact, there is an infinite number of branch points stacked above each other, corresponding to the different paths which "bounce" a different number of times inside the inverted barrier, as mentioned earlier (see also [23]).

In the case of a harmonic barrier $-\frac{1}{2}\omega^2 x^2$, there is no branch point; the trajectory that has penetrated the barrier will in fact return to the left side of the barrier in imaginary time due to the non-zero slope of the potential: explicitly, the equation for the trajectory is $x(t) = x(0)\cosh(\omega t/\sqrt{m}) + (p(0)/m\omega)\sinh(\omega t/\sqrt{m})$, free of any singularities. This is quite in contrast to the solution for the Eckart barrier $V_o\text{sech}^2(\alpha x)$,

$$x(t) = -\sinh^{-1}\left(\sqrt{Vo/E - 1}\cosh(\sqrt{2mE}\alpha t\right)/\alpha + \sinh^{-1}\left(\sqrt{Vo/E - 1}\right)/\alpha + x(0),$$

which has branch points in the complex-time plane at times ($n = 0, 1, 2...$),

$$t = \pm\frac{1}{\alpha\sqrt{2mE}}\left(\tanh^{-1}\sqrt{\frac{E}{V_o}} + i\pi(2n + \frac{1}{2})\right).$$

Branch points of the trajectory in the complex-time plane arise from singularities of the potential in the complex x-plane, causing singular behavior in the trajectory of a particle which has approached this divergence after a particular series of complex time steps. Whether a certain potential gives branch structure may be deduced from the relation 3.5: if, at energy E, we can reach a final x_2 where $V(x_2)$ blows up, in a finite (complex) time, by taking a certain sequence of complex dt and dx, then the trajectory has branch structure. We see then for the sech^2, equation (3.12), we can have $x_2 = i\pi/2$ and a finite complex time, but for the inverse harmonic oscillator a particle cannot reach the blow up at $x = \infty$ except at infinite times. An interesting case is a Gaussian potential $V(x) = V_o e^{-x^2}$, which blows up at $x = \pm i\infty$: this point may in fact be reached in a finite time, which can be roughly seen by the relation 3.5: as $x \rightarrow \pm i\infty$, the integrand vanishes and the resulting time is finite.

We also suspect (although this is yet to be proven) that the larger $|x_1|, |x_2|$, the more "hidden" is T_A^* behind the branch cut, where T_A^* is the complex time satisfying the stationary phase condition at $E < V_o$ for term A. This happens because of the large real time propagation outside the barrier region. The contribution from T_A^* is equal to that from the saddle point from term B at the real time $Re(T_A^*)$, as shown above. This is independent of any real-time contribution from term A (e.g. from a numerical FFT) which vanishes in this limit of far endpoints. For small $|x_1|, |x_2|$, term B does not exist, and the problem looks harmonic. Indeed in this case the complex saddle point from term A is near the branch point and a permitted contour deformation could pick it up. The distinctness of the A term and integral through the complex saddle point is thus blurred in the small $|x_1|, |x_2|$ limit.

3.4 Barrier Reflection

A similar analysis may also be applied to quantum reflection above a barrier. Taking $x_2 = x_1$ to the left of the barrier in the propagator (3.1) involves summing over classical paths which have returned after reflection from the barrier as well as the fixed zero-energy trajectory. Clearly, these have energies below the barrier. Until a certain time, real trajectories have not had time to reach the barrier and turn around; only the zero energy, fixed classical path contributes to the semiclassical amplitude. Quantum above-barrier reflection (process (2) of figure 3.1) plays an important role in this time regime as quantum reflected amplitude interferes with the zero energy path. In figure 3.9, we show

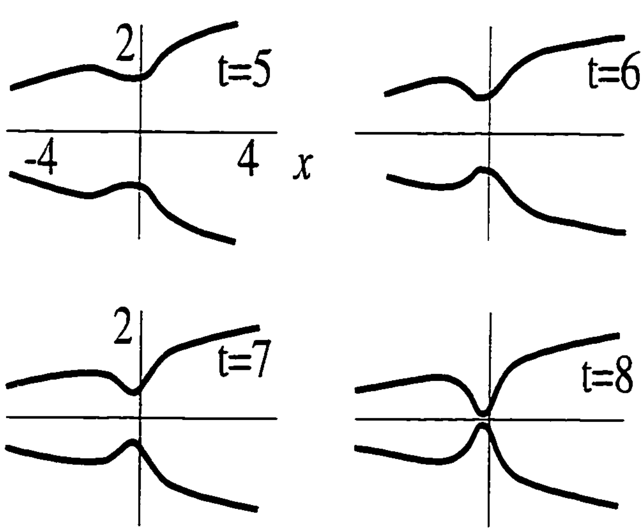

Figure 3.9: A quasi-classical view of the propagator $G(-10, T; -10, 0)$ in phase space ($t = T/2$, see text). In this intermediate time range, where there is nonclassical reflection, contours resembling above-barrier energy contours have formed, suggesting a quantum reflection contribution.

the quasi-classical picture for reflection where now we take the overlap of the $T/2$-evolved line from x_l with its mirror image through the x-axis. The latter represents $|x_l(-T/2)\rangle$. We see contours resembling energy contours above the separatrix (figure 3.1), classically disconnected, but across which quantum above-barrier reflection occurs. At longer times the classical reflection kicks in: it is at the shorter times that quantum reflection is significant. In analogy to the tunneling case, we may evaluate the quantum reflection contribution at time T, approximating the phase space distribution at an intermediate time by an energy contour at the energy of the trajectory which has reached $x = 0$ at time $T/2$. We then analytically continue the semiclassical reflection propagator to this above-barrier energy, just as in the tunneling loop case. We plot the result in Fig. 3.10 where our quantum reflection contribution (missing in the primitive semiclassical propagator) reproduces the oscillations at shorter times well.

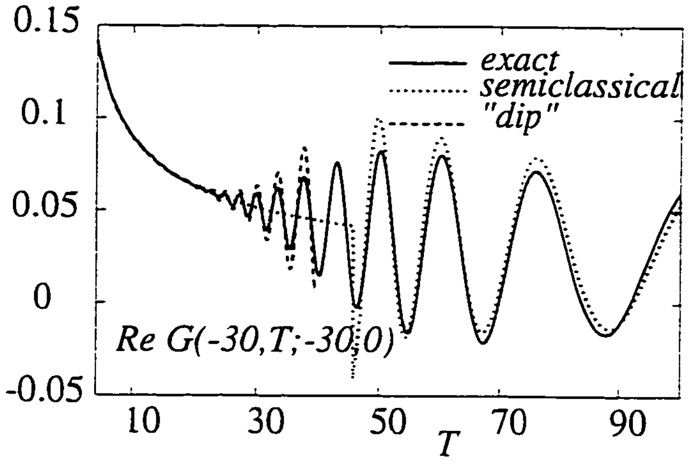

Figure 3.10: The reflection propagator $G(-30, T; -30, 0)$.

Chapter 4

Quantization of Constrained Systems as an Application of Semiclassically Reduced Path Integrals

We are often faced with the problem of having many degrees of freedom but only being interested in the dynamics of a few of them. The example of an open system jumps to mind, where a few degree-of-freedom system interacts with its environment which is an infinite degree of freedom system. Although we only care to know about the few degree-of-freedom system, the surroundings clearly affect its behavior and cannot be ignored. In the spirit of this thesis, we ask whether semiclassical methods can help us to reduce the very complicated description of everything to a simpler reduced description of just the system of interest. We shall however not look at open systems in this thesis. Rather, in this chapter we show how a semiclassical reduction of a larger system to a smaller one can be used in an analysis of the quantization of constrained systems [25]. This chapter is based on part of the work published in [25]. For completeness we provide a copy of the paper at the end of the thesis.

4.1 Introduction

There has been a long controversy over the proper way to quantize a constrained dynamical system [6, 26, 27]: ambiguities arise involving terms in the Hamiltonian of order $\hbar^2$ multiplying the Gaussian curvature. This work was originally motivated by an attempt to clarify these ambiguities by considering constraints to be the limits of large restoring forces as the constraint coordinates deviate from their constrained values. We find however additional ambiguous terms of order $\hbar^2$ arising from freedom in the constraining potentials [25]. This indicates that the classical constrained Hamiltonian or Lagrangian cannot uniquely specify the quantization: the ambiguity of directly quantizing a constrained system is inherently unresolvable. There is however no problem with any physical quantum system, which cannot have infinite constraint forces and always fluctuates around the mean constraint values. In [25], the issue is addressed from the perspectives of adiabatic approximations in quantum mechanics, Feynman path integrals, and semiclassically in terms of adiabatic actions. Here, as a demonstration of using semiclassics in this interesting problem, we present just the path integral approach. We refer the reader to [25] for more discussion.

4.2 Outline of the problem

There are operator ordering ambiguities in quantizing the kinetic term. Canonical quantization would give $K = -\frac{\hbar^2}{2m}\frac{1}{\sqrt{g}}\frac{\partial}{\partial q^i}(g^{ij}\sqrt{g}\frac{\partial}{\partial q^j})$ however it is not clear whether this is "correct": the kinetic term $g_{ij}\dot{q}^i\dot{q}^j/2 = g^{ij}p_ip_j/2 = \vec{p}\cdot\vec{p}/2$ is mixed in its coordinate and momentum dependence. These ambiguities, at order $\hbar^2$, are proportional to the local Gaussian curvature of the constraint surface, which is the only available coordinate-invariant quantity. So for constrained systems with flat constraints (*e.g.* the simple pendulum or a particle confined to a one-dimensional curve), the ambiguity does not arise; for systems with constant curvature (*e.g.* motion on a sphere) it leads only to a physically unobservable shift in the zero-point energy, but for the generic case of varying curvature, the ambiguities are very relevant.

In the path integral method, the ambiguity arises in choosing how to incorporate the metric into the kernel and in deciding at what point in the infinitesimal time interval to evaluate functions of the metric [6, 27]. Two commonly used kernels give answers that differ by an effective $R/6$ contribution to the Laplacian (and naturally enough both differ from the canonical quantization result). These issues are discussed at some length in Ali's recent paper [27].

We approach the problem in a different way by considering constrained systems as part of a larger system allowing the constrained dimensions to have freedom: the constraints arise from the limit of tightening the forces in their degrees of freedom. The principle governing our view is that arriving at a unique quantization is essential only in real, physical systems. For example, quantization of the usual rigidly constrained classical double pendulum is not a physical problem, because the requirement that the pendulum lengths remain exactly constant is not realizable. To make the problem as close as possible to physical, the constraints should be imposed through a limiting procedure, fluctuations remaining physically allowable along the way. This embodies the idea of classical constraints arising as the limit of ever larger restoring forces normal to the constraint surface, an idea discussed in Arnol'd, for example [28]. In this way the constraint coordinates appear as part of the full dynamical system in the usual Euclidean metric. As the constraint forces are increased, the constrained degrees of freedom acquire a very high frequency, and their actions remain adiabatically constant as the slow variables move. This however does not imply that the fast variables (which we here call the $r-$variables) are *energetically* decoupled from the slow ($\theta-$) variables. We shall find that different limiting constraint potentials give the *same* classical constrained motion but *different* quantum dynamics at order $\hbar^2$. The uncertainty principle requires that in any real physical system there will be quantum fluctuations around the surface of constraint. By examining the effects of these fluctuations in the limit of ever tighter constraints, we find unavoidable ambiguities in the quantum dynamics along the surface of constraint. In [25], the analysis was performed in three different ways: a Born-Oppenheimer type approach to deal with adiabatic processes, a Feynman path integral approach and a semiclassical one based on considering the adiabatic action invariant. Here, we discuss only the path integral method, as mentioned earlier, as an example of applying semiclassical techniques to reduce a larger degree of freedom problem to one in a smaller space.

4.3 Semiclassical Path Integral Reduction

A path integral analysis shows that quantization on the constrained surface is ambiguous at order $\hbar^2$.

The Lagrangian L on the full space is given by

$$L = \frac{1}{2} g_{ij} \dot{q}^i \dot{q}^j - V(q) - \tilde{V}_\lambda(q) \tag{4.1}$$

where g_{ij} is the flat metric for the full space and V is the potential. The additional potential $\tilde{V}_\lambda$ enforces the constraint in the limit $\lambda \to \infty$. Classically we require $\tilde{V}_\lambda$ to have the same value everywhere on the constraint surface S, for each λ. Now locally, near some region of the constraint surface S we may separate the coordinates q into "slow coordinates" θ parameterizing S and "fast coordinates" r orthogonal to the surface. We will be looking for an effective theory of the coordinates θ when the constraining potential $\tilde{V}_\lambda^\theta(r)$ allows only small fluctuations in r (small compared to the length scale associated with the physical potential V, the curvature scale of the constraint surface S, and the scale on which $\tilde{V}_\lambda^\theta$ varies as a function of θ). Our approach will be to use the full propagator corresponding to L to evolve an initial state of the full system and then to reduce the description on the full space to that of just the θ-coordinates using semiclassical techniques throughout. We take the initial density operator to be the "product" state $|\Psi_{\mathrm{GR}}^{(\theta)}\rangle \otimes |\phi\rangle$, where the initial state of the fast variables is the (purely real) ground state $\Psi_{\mathrm{GR}}^{(\theta)}(r)$, with θ regarded as a fixed parameter. $\Psi_{\mathrm{GR}}^{(\theta)}$ is the ground state of the fast Hamiltonian

$$H_r = -\frac{\hbar^2}{2} \frac{1}{\sqrt{g}} \frac{\partial}{\partial r^i} (g^{ij} \sqrt{g} \frac{\partial}{\partial r^j}) + \tilde{V}_\lambda^\theta(r) , \tag{4.2}$$

where i and j are summed over the fast variables only and the metric is evaluated at a fixed value of θ. Note that g here is the determinant of the full metric on the (r, θ) space.

In order for the quantum mechanics to have a sensible semiclassical limit, the energy of the ground state $E_{\mathrm{GR}}^{(\theta)}$, defined by

$$H_r \Psi_{\mathrm{GR}}^{(\theta)} = E_{\mathrm{GR}}^{(\theta)} \Psi_{\mathrm{GR}}^{(\theta)} , \tag{4.3}$$

must be θ—independent, for any λ, to avoid infinite torques acting on the slow variables. Also the energy of the first excited state must be well separated from it, with the separation growing with λ. One way to do this is to take $\tilde{V}_\lambda(q) = \lambda v(q)$, where v is a smooth function vanishing on the constraint surface and having its minimum there (but with a non-singular second derivative matrix with respect to the fast variables). Near the constraint surface, the constraining potential will have the harmonic oscillator form

$$\tilde{V}_\lambda^\theta(r) = r^i A_{ij}^{(\theta)} r^j + O(r^3) , \tag{4.4}$$

where the matrix function $A^{(\theta)}$ is smooth. The ground states $\Psi^{(\theta)}_{\mathrm{GR}}$ will to first approximation be harmonic oscillator ground states with spatial extent of order $\hbar^{1/2}/\lambda^{1/4}$ and energy E_{GR} of order $\hbar\lambda^{1/2}$. The matrices $A^{(\theta)}$ can easily be adjusted to satisfy this condition. In the case of more than one constraint variable, this still allows for much freedom in the function $A^{(\theta)}$ and the resulting eigenstates $\Psi^{(\theta)}_{\mathrm{GR}}$ (energy can flow from one fast degree of freedom to another as a function of θ, as long as the total energy remains constant). One may choose to adjust (some of) the an-harmonic parts of the potential as well but this is not really necessary or natural.

We begin with the propagator on the full coordinate space. Because the space is flat, this is given by the usual Feynman prescription $\int \mathcal{D}(q(\tau)) \exp(iS(q(\tau))/\hbar)$ where $S(q(\tau)) = \int L(q(\tau), \dot{q}(\tau), \tau) d\tau$. We extract the effective dynamics for the "slow" variables θ by performing a trace over the "fast" variables r in the adiabatic limit. Specifically, we calculate $\langle\theta_f|\rho(t)|\theta_o\rangle$ where $\rho(t) = \mathrm{Tr}_r(W(t))$ is the trace over the fast variables of the density operator W(t) on the full space. The time t is taken to be small on the time scales of θ-motion but r may undergo many oscillations during this time. Noting that the evolution of the full density operator is given by $W(t) = e^{-iHt/\hbar}W(0)e^{iHt/\hbar}$, and inserting identities in the form of complete sets of states, we have

$$\langle\theta_f|\rho(t)|\theta_o\rangle = \int dRdr'dr''d\theta'd\theta''\langle\theta_f R|e^{-iHt/\hbar}|\theta'r'\rangle\langle\theta'r'|W(0)|\theta''r''\rangle\langle\theta''r''|e^{iHt/\hbar}|\theta_o R\rangle\,. \tag{4.5}$$

Replacing the two propagators by path integrals, we then have

$$\langle\theta_f|\rho(t)|\theta_o\rangle = \int d\theta'd\theta'' \int_{\theta(0)=\theta'}^{\theta(t)=\theta_f} \mathcal{D}\theta(\tau) \int_{\tilde{\theta}(0)=\theta''}^{\tilde{\theta}(t)=\theta_o} \mathcal{D}\tilde{\theta}(\tau)\phi(\theta')\phi^*(\theta'')\mathcal{F}\left(\theta(\tau), \tilde{\theta}(\tau)\right)\,, \tag{4.6}$$

where

$$\begin{aligned} \mathcal{F}\left(\theta(\tau), \tilde{\theta}(\tau)\right) &= \int dRdr'dr'' \\ &\times \int_{r(0)=r'}^{r(t)=R} \mathcal{D}r(\tau) \int_{\tilde{r}(0)=r''}^{\tilde{r}(t)=R} \mathcal{D}\tilde{r}(\tau)e^{iS^{(1)}/\hbar - iS^{(2)}/\hbar}\Psi^{(\theta'')}_{\mathrm{GR}}(r'')\Psi^{(\theta')}_{\mathrm{GR}}(r')\,. \end{aligned} \tag{4.7}$$

$S^{(1)} = S(r(\tau);\theta(\tau))$ and $S^{(2)} = S(\tilde{r}(\tau);\tilde{\theta}(\tau))$ are the actions along the respective paths. In performing the path integrals over the fast variables, $\theta(\tau)$ ($\tilde{\theta}(\tau)$) is to be treated as an external forcing function with the property $\theta(0) = \theta'$, $\theta(t) = \theta_f$ (resp. $\tilde{\theta}(0) = \theta''$, $\tilde{\theta}(t) = \theta_o$).

We evaluate $\mathcal{F}$ using stationary phase with respect to $\hbar$ on the path integrals, trace, and the integrals over the intermediate fast variables. In fact the stationary phase approximation becomes exact in the adiabatic limit: we shall now show that the errors due to stationary phase evaluation are of order $\hbar^{1/2}/\lambda^{1/4}$, so they vanish as $\lambda \to \infty$. Recall that

$$\int g(x)e^{if(x)/\hbar}dx \approx_{\mathrm{sp}} \sum \sqrt{\frac{2\pi i\hbar}{f''(x_n)}}g(x_n)e^{if(x_n)/\hbar}\left(1+O(\hbar^{1/2}\frac{f'''(x_n)}{f''(x_n)^{3/2}})\right), \tag{4.8}$$

where the sum is over stationary phase points x_n satisfying $f'(x_n) = 0$. Stationary phase evaluation of path integrals, although different in the details, scales in the same way. $f(x)$ corresponds to the action S. The stationary paths are the classical paths and we now argue that $S_{\mathrm{cl}} \sim O(\lambda^{1/2})$ to leading order in λ. The leading behavior of the action in the fast variables arises from the kinetic term in r and the constraint potential: $L_r \sim g_{ij}\dot{r}^i\dot{r}^j/2 - \tilde{V}^{\theta}_{\lambda}(r)$, where the sum is over fast variables only. This Lagrangian corresponds to the fast Hamiltonian of Eq. 4.2 which gives harmonic motion for r at least throughout the range of the fast variable ground state. Because the initial fast state is this ground state, the leading behavior of $e^{iS/\hbar}$ gives

$$\int dr' \int \mathcal{D}r(\tau)e^{iS^{(1)}/\hbar}\Psi^{(\theta')}_{\mathrm{GR}}(r') \sim e^{-iE_{GR}t/\hbar}\Psi^{(\theta')}_{\mathrm{GR}}(r), \tag{4.9}$$

where we note again that $E_{\mathrm{GR}} \sim O(\hbar\sqrt{\lambda})$ is required to be θ-independent. This shows the leading behavior of the action on the ground state is simply to multiply it by an evolving phase. The fast variable $r(t)$ remains in the domain of harmonic approximation to the constraint potential. Sub-leading terms are a factor of $1/\sqrt{\lambda}$ smaller. Thus the dominant behavior of the action and its derivatives is simply that of a harmonic potential of frequency $O(\sqrt{\lambda})$. The errors in the stationary phase evaluation of the path integrals are of order $\hbar^{1/2}/\lambda^{1/4}$, vanishing in the adiabatic limit. The errors in using stationary phase to compute the trace and integrals over the intermediate variables r' and r'' scale in the same way. In the harmonic approximation to the action and the ground state it is readily seen that the stationary phase points are $R = r' = r'' = 0$, the constrained value of the fast variable. Corrections to this approximation due to sub-leading terms vanish in the adiabatic limit, $\lambda \to \infty$.

We have then,

$$\begin{aligned}\mathcal{F}(\theta(\tau),\bar{\theta}(\tau)) &= \left(\frac{\partial^2 \ln \Psi^{(\theta')}_{\mathrm{GR}}}{\partial r'^2}\right)^{-1/2}\left(\frac{\partial^2 \ln \Psi^{(\theta'')}_{\mathrm{GR}}}{\partial r''^2}\right)^{-1/2} \\ &\times \left|\frac{\partial^2 S^{(1)}_{\mathrm{cl}}}{\partial R\partial r'}\right|^{1/2}\left|\frac{\partial^2 S^{(2)}_{\mathrm{cl}}}{\partial R\partial r''}\right|^{1/2} e^{iS^{(1)}_{\mathrm{cl}}/\hbar - iS^{(2)}_{\mathrm{cl}}/\hbar},\end{aligned} \tag{4.10}$$

where the derivatives are evaluated at $R = r' = r'' = 0$. $S_{\rm cl}^{(1)}$(resp. $S_{\rm cl}^{(2)}$) is the action along the classical path starting and ending at the constraint value $r = 0$ subject to the Lagrangian of Eq. 4.1 with $\theta(\tau)$ (resp. $\tilde{\theta}(\tau)$) treated as an undetermined forcing function. In the adiabatic limit, we shall now show that the action exponent is just the action for the reduced slow variable system on the constraint surface, *i.e.* the action we would have written down had we begun in the reduced space. The kinetic term in r together with the constraint potential give a θ-independent term in the exponent as discussed above. This, being a constant energy shift as far as θ is concerned, can be neglected. The mixed kinetic term goes to zero: we may expand $g_{ij}(r,\theta)$ about $r = 0$ and take functions of θ out of the time-integral as they are slowly varying functions of time:

$$\begin{aligned} \int g_{ij}(r,\theta)\dot{r}^i\dot{\theta}^j dt &= g_{ij}(0,\theta)\dot{\theta}^j \int_0^t \dot{r}^i dt + \frac{\partial g_{ij}}{\partial r^p}\dot{\theta}^j \int_0^t \dot{r}^i r^p dt \\ &+ O(\hbar^{3/2}/\lambda^{1/4}), \end{aligned} \tag{4.11}$$

where the derivatives of the metric are evaluated at $r = 0$. The first term on the right-hand side is zero, since the integral gives $r^i(t) - r^i(0) = 0$ due to the stationary phase condition on the endpoints. For $p = i$, the integral in the second term is zero for the same reason (the integrand is $d(r^{i2})/dt$). For $p \neq i$ the integral averages to zero, because different directions of the fast variables generically oscillate at different frequencies. The higher order terms in the expansion vanish in the adiabatic limit (they involve at least two powers of r but only one power of $\dot{r}$ so scale at least as $(\hbar/\lambda^{1/2})(\hbar^{1/2}\lambda^{1/4})$). We are thus left with the kinetic term in the slow variables only, with the metric evaluated at the constraint value for r.

Inserting $\mathcal{F}(\theta(\tau),\tilde{\theta}(\tau))$ into Eq. 4.6 gives the reduced density matrix at time t. This factorizes into a part involving (θ, θ_f, and $\theta(\tau)$) and a part involving (θ', θ_o, and $\tilde{\theta}(\tau)$). This implies that the reduced density matrix factorizes: $\langle\theta_f|\rho(t)|\theta_o\rangle = \langle\theta_f|\theta(t)\rangle\langle\theta(t)|\theta_o\rangle$, *i.e.* the final θ-state is pure and so we may describe it in terms of a wavefunction. Adiabaticity has thus uncoupled the fast and slow degrees of freedom. We have

$$\phi(\theta_f,t) = \int d\theta \int \mathcal{D}\theta(\tau) A(\theta(\tau)) e^{iS/\hbar}\phi(\theta,0)\,, \tag{4.12}$$

where

$$A(\theta(\tau)) = \left(\frac{\partial^2 \ln\Psi_{\rm GR}^{(\theta)}}{\partial r^2}\Big|_{r=0} \right)^{-1/2} \left| \frac{\partial^2 S_{\rm cl}^{(1)}}{\partial R \partial r}\Big|_{R=r=0} \right|^{1/2}. \tag{4.13}$$

$S = S_{\rm cl}^{(1)}$ is the action function for the θ variable on the constrained surface: $S = \int L dt$

where the Lagrangian is $L = \frac{1}{2}g_{ij}\dot{\theta}^i\dot{\theta}^j - V(\theta)$, with g_{ij} now the metric on the curved space defined by the constraint surface and the sum is over the slow (θ-)variables only.

We may compare this to the expressions discussed in Ali, where one works in the reduced space from the start. Different Feynman kernels are postulated to attempt to account for the curvature of the constrained surface [6, 27, 3]. There, for infinitesimal time t,

$$\phi(\theta_f, t) = \int d\Omega(\theta)\tilde{G}(\theta, \theta_f)e^{iS/\hbar}\phi(\theta, 0)\,. \tag{4.14}$$

$d\Omega(\theta) = \sqrt{g(\theta)}d\theta$ is the volume element at θ. Candidates for $\tilde{G}(\theta, \theta_f)$ which are often considered in the literature include the identity operator and $g(\theta)^{-1/4}D^{1/2}g(\theta_f)^{1/4}$, where g is the determinant of the metric on the curved space, and D is the Van-Vleck determinant ($D = \det(-\partial^2 S/\partial\theta\partial\theta_f)$). The different choices give rise to Hamiltonians which differ at order $\hbar^2$ by a certain fraction of $\hbar^2 R$. Ali demonstrates this by choosing locally normal coordinates ξ to evaluate the integrals and considering infinitesimal time so that the exponent and prefactor can be expanded in ξ. The action exponent is then at lowest order (in ξ) quadratic, and the resulting Gaussian integrals are readily performed. Only the even order terms in the expansion of the prefactor about the initial value θ contribute. The $t \to 0$ limit is taken and an effective Hamiltonian can be extracted from the resulting differential equation. The expansion of the potential exponent and the initial wavefunction give the Hamiltonian $-\hbar^2\nabla^2/2m + V$, and it is the quadratic term in the expansion of $\sqrt{g(\xi)}\tilde{G}(\xi)$ that gives rise to the $\hbar^2 R$ discrepancies in the effective Hamiltonian. (Higher order terms give corrections at higher order in $\hbar$.)

The key point is that we may apply the same manipulations to our Eq. 4.12, where $A(\theta(\tau))$ plays the role of the prefactor $\sqrt{g(\theta)}\tilde{G}(\theta)$. Transforming to locally normal coordinates in which there are no linear terms in the action exponent, and expanding $A(\theta(\tau))$ about θ leads to finite $\hbar^2$ corrections in the effective Hamiltonian as in Ali's approach described above. However, it is important to recognize that our corrections emerge from reducing the full, unambiguous coordinate space evolution down to the reduced curved space by taking the constraint limit, whereas Ali's corrections arise from using a modified Feynman kernel for curved space. We observe that our corrections depend not only on the curvature of the space but also on the details of the constraining potential.

Chapter 5

The Whisker Map

In this final chapter we step out of the relative security of integrable systems: we study the quantization and quantum dynamics of a classically chaotic system. the whisker map, or separatrix map.

5.1 Introduction

The separatrix plays a crucial role in determining the behavior of dynamical systems. Indeed, even in fully integrable systems the separatrix trajectory is a very special one, being at the border between qualitatively different motions *e.g.* rotational motion and vibrational motion. It is perhaps not surprising that turning on even the slightest perturbation may cause the motion near the separatrix to go hay-wire, as trajectories are thrown between regions which are very close in phase space yet topologically completely different. Generic systems are not integrable, and can be characterized by a mixed dynamics: stochastic regions of phase space separated by regular stable regions. Typical first-order analyses of such near-integrable systems result in a pendulum Hamiltonian around resonances, and a closer look reveals a stochastic layer around the separatrix. Rather than joining smoothly as in the case of the integrable pendulum, the unstable manifold of the separatrix leaving one hyperbolic fixed point intersects transversely the stable separatrix manifold entering a neighboring hyperbolic point an infinite number of times, oscillating wildly between the intersections: even the smallest perturbation renders the stable and unstable manifolds of the hyperbolic fixed point no longer degenerate. These homo/heteroclinic intersections with their infinitely increasingly tight loops create extraordinarily complicated behavior near the separatrix, yet this happens not in exceptional systems but rather it happens generically. Moreover, near the separatrix of a primary resonance there is an infinite number of secondary resonances, each armed with its own series of elliptic and hyperbolic points, together with the wild motion of the separatrix manifold, which intersect each other as well as the primary resonance. Stochastic motion thus engulfs the original separatrix. The width of the stochastic layer depends on the strength of the perturbation, as we will discuss later in this chapter. As the strength grows, more invariant tori bounding the stochastic layer are destroyed and eventually primary resonances begin to merge, leading to global stochasticity. It is at the separatrix that the seeds of stochasticity are sown.

Arnol'd introduced the terminology of "whisker" for the branches of the separatrix [32] (perhaps in fond (or not so fond) honor of his cat map). There are "departing" and "arriving" whiskers depending on whether the branch approaches the "whiskered torus" (hyperbolic point) as time $t \to -\infty$ or $t \to \infty$. Chirikov was the one who came up with the whisker mapping to describe what happens to these separatrix branches [30]. In generic, near-integrable systems it is clear that the whiskers grow in a far from straight fashion. It is their highly complicated weaving and tangling that the whisker map describes. Stochasticity is born at the separatrix and so the whisker map is instrumental in helping us to understand chaos in generic systems. In section 5.2, we present the classical whisker map and discuss some of its properties.

The quantum mechanics of integrable systems is now on pretty solid ground and its relation to the underlying classical mechanics is also well understood. Semiclassics provides this link: loosely speaking, one may think of the quantum mechanics as composed of classical trajectories put together with phases determined by classical actions and Maslov indices and weighted by classical probability densities. EBK quantized energy states live on the invariant tori of classical phase space. To paint the complete quantum picture and describe classically forbidden processes such as diffraction and tunneling, extension into complex coordinates must be made. Most systems however are not integrable. The quantum mechanics of systems with a chaotic component is not so well understood, although tremendous progress has been made in the last 30 years. Much insight has been gained into the statistical properties (*e.g.* eigenvalue spacing and eigenvector distributions) of the quantum mechanics of fully chaotic systems ([29]). Near-integrable systems, with their mixed phase space, are less understood yet of fundamental importance since typical atomic and molecular systems fall into this class. The fuzzy separatrix is ubiquitous in the phase spaces of generic near-integrable systems. It is clear then that the quantization of the whisker map raises many fascinating questions: what do the quantum states look like and how do their phase space representations compare to dynamics in classical phase space? what does semiclassics say for this system? do states localize? what can we say about the onset of rapid transport between two states in the quantized system as opposed to the classical system? how does the quantum mechanics "smear" over chaos, with the help of a finite Planck's constant? is there tunneling across the stochastic sea, and if so how does it compare with tunneling across resonance zones? We will address only some of the above questions in this chapter (sections 5.3 and 5.4) : the tunneling issue is described only briefly at the end and is left to future work.

From a practical point of view, one can, for example, use the classical whisker map to determine the onset of chaos and hence ionization of orbits near the potential turnover in a hydrogen atom in a microwave field in the presence of a static field [33]. It would be interesting to see what quantum mechanics tells us about this system.

The whiskers of the separatrix play a central role in spawning stochastic motion in classical mechanics: we hope that a quantization of the whisker map will be enlightening for the study of the quantum analogues of such systems.

5.2 The Classical Map

We begin by briefly describing how the whisker map arises in near-integrable systems. Details may be found in [30, 31]. Consider the general perturbed two-dimensional Hamiltonian $H = H_o(\mathbf{J}) + \epsilon H_1(\mathbf{J}, \theta)$. Although a power series expansion may be used in some regular regions to solve for the motion, it fails completely and blows up near a resonance, where the trajectories acquire a modified topology. Techniques of secular perturbation theory have been developed to deal with this difficulty and result in a one-dimensional pendulum Hamiltonian for the modified "slow" action variable p with associated phase ϕ near the resonance $r\omega_1(\mathbf{J}) + s\omega_2(\mathbf{J}) = 0$, with the "fast" modified action I becoming an adiabatic invariant. The process involves averaging over the new angle θ which is much more rapidly varying than ϕ; the latter measures the slow deviation away from resonance. However, to describe the motion near the pendulum separatrix, the averaging is not valid: at the separatrix the local frequency $\omega_1 = \dot{\phi}$ tends to zero, so has an infinite number of secondary resonant interactions with θ. The terms discarded in the averaging spawn a stochastic layer around the separatrix. Reinstating these terms gives, in essence, the Hamiltonian for a driven pendulum [31],

$$H = H_o(I) + \frac{1}{2}Gp^2 - \epsilon F\cos\phi + \epsilon\Lambda\cos(\phi - \theta/r + \chi)$$

The terms in G and F describe the pendulum in the slow variable, and are related to the second p-derivative of the unperturbed Hamiltonian H_o and the $r : -s$ Fourier coefficient in the perturbation H_1 respectively. Only the largest term (Λ) that was neglected in the averaging has been reinstated, since higher Fourier coefficients fall away rapidly [31]. Another simplification, which does not affect the aspects of the behavior much [31], is to consider $\dot{\theta} = \Omega$ as fixed. The whisker map is then the mapping of the action I and the phase θ at the nth crossing of the surface of section at $\phi = \pm\pi$. This is a convenient surface of section in which to study the separatrix layer since the unperturbed ($\Lambda = 0$) motion is simply a straight line; when $\Lambda \neq 0$ a layer of fuzz appears around the line. Also, there is much going on in just one iteration of the mapping: in the infinite time it takes to come back to $\phi = \pm\pi$, θ may undergo many oscillations. One obtains:

$$\begin{aligned} I' &= I - k\sin\theta \\ \theta' &= \theta + \lambda\ln\left|\frac{c}{I' - I_o}\right| \qquad (\mathrm{mod}\, 2\pi) \end{aligned} \tag{5.1}$$

Relating the parameters back to the two-dimensional Hamiltonian problem, $k = 8\pi\Lambda Q_o^2 e^{-\pi Q_o/2}/F$ where the frequency ratio $Q_o = \Omega/r\omega_o$ with $\omega_o = \sqrt{\epsilon FG}$, and $\lambda = Q_o r$. We refer the reader to [31] and [30] for details.

The whisker map is defined on the cylinder. The logarithmic divergence of the angle at the separatrix is familiar from the behavior of the period of a pendulum there. The jump in the action involves an improper integral over all time known as the Melnikov-Arnol'd integral. We refer the reader to the literature [30, 31] for the details and for the identification of the parameters k and λ in terms of the original parameters of the two-dimensional Hamiltonian. There are essentially two independent parameters in the classical whisker map, λ and k, which act in very different ways as will be shortly described. I_o simply translates in action space and c can be absorbed into a scaled action. In our numerical work c is taken to be 1.

We observe that the whisker map is also obtained as the mapping in a $y-p_y$ surface of section of the potential $v(x,y)+\epsilon w(x,y)$, where $v(x,y)$ is of the form $v(x,y)=y^2/2+cos(x)$ and $w(x,y)$ is a perturbation. The mapping is whisker-like near $y_o=\sqrt{2(1-\cos(x_s))}$ where x_s is where the surface of section is erected.

5.2.1 Properties of the classical whisker map: I

Fixed points, their stability, width of stochastic layer The shearing of the angle, wrapped back to the fundamental circle, together with the resulting pseudo-random jumps in the action lead to stochastic motion in a layer around I_o (see figure 5.1 for example). The width of this layer depends on the shearing parameter λ and the jumping parameter k. We can take the two parameters to be as small as we like (but non-zero), yet may still expect instability if we get close enough to I_o due to the blowing up there of the logarithmic shear of the angle. This is of great consequence in non-linear systems: sufficiently close to the separatrix of the pendulum a stochastic layer always exists, however small the perturbation parameter. As the perturbation parameter increases the instability seeded here grows to eventually fill the phase space.

There is an infinite number of fixed points of the whisker map:

$$I_r = I_o \pm ce^{-2\pi r/\lambda},\ \theta_r = 0\,\mathrm{or}\,\pi \tag{5.2}$$

where r is an integer. Their stability is determined by whether the trace of the linearized map at the fixed point M_r has magnitude greater (unstable) or less (stable) than 2:

$$M_r = \begin{pmatrix} \frac{\partial I'}{\partial I} & \frac{\partial I'}{\partial \theta} \\ \frac{\partial \theta'}{\partial I} & \frac{\partial \theta'}{\partial \theta} \end{pmatrix}$$

$$Tr(M_r) = 2 \pm \frac{\lambda k}{|I_r - I_o|}\cos\theta_r \tag{5.3}$$

All fixed points with $|I_r - I_o| < \lambda k/4$ are unstable. The infinite number of unstable fixed points in this action slice converge together exponentially to I_o, their unstable manifolds overlapping. The fixed points $(\theta_r = 0, I_r > I_o+\lambda k/4)$ and $(\theta_r = \pi, I_r < I_o-\lambda k/4)$ are also unstable. Stable elliptic fixed points exist at $(\theta_r = \pi, I_r > I_o + \lambda k/4)$ and $(\theta_r = 0, I_r < I_o - \lambda k/4)$.

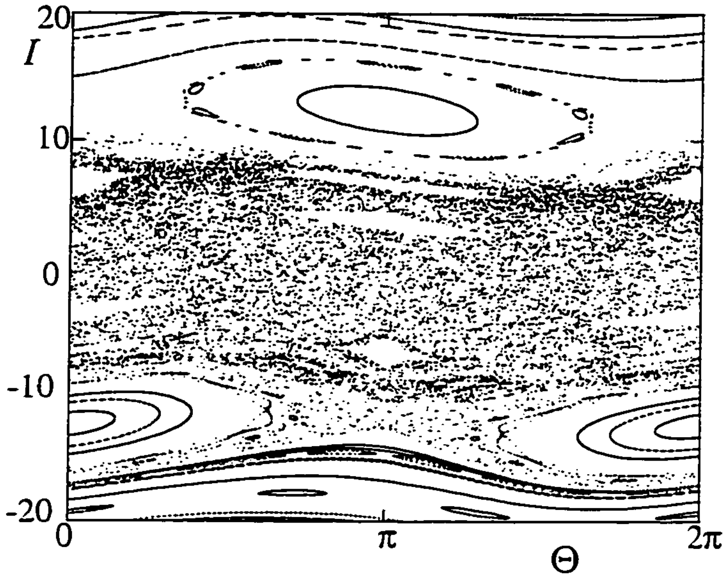

Figure 5.1: Classical whisker phase space: $\lambda = 5, k = 2, I_o = 0$

The islets of stability are clearly seen in the classical phase space in figure 5.1 where we have chosen parameter values $k = 2, \lambda = 5$ and seeded 50 random initial conditions and iterated the map 400 times, plotting the points at each iteration. As we would expect from eqn 5.1, the phase space remains unchanged if we flip the sign of the action-minus-I_o and add π to the angle. Also visible are the stable and unstable manifolds at $|I_r - I_o| > 10$. The motion appears stochastic for roughly $|I_r - I_o| < 10$, except in the islets. To understand this, we improve on the local stability analysis above by transforming the behavior around these first-order resonances to local standard mappings. The effective non-linearity parameter k_{eff} of the local standard map then tells us about the stochasticity in that region. Expanding the logarithmic shearing term around the fixed point action $\ln|I - I_o| \approx \ln|I_r - I_o| + \delta I/(I_r - I_o) + O(\delta I)^2$ where $\delta I = I - I_r$, we find that the whisker map locally looks like

$$\begin{aligned} P' &= P + k_{eff} \sin\theta \\ \theta' &= \theta + P' \end{aligned} \tag{5.4}$$

This represents a standard map in variables

$$\left(P = -\frac{\lambda}{I_r - I_o}(I - I_o), \theta\right) \tag{5.5}$$

with effective nonlinearity parameter

$$k_s = k_{eff} = \frac{\lambda k}{I_r - I_o} \tag{5.6}$$

Work pioneered in [30] and developed by many, in particular by Greene [34], has shown that a standard map with $k_s > k_c$ => 0.9716354... is globally stochastic (see also the next section and appendix): a trajectory started in one area of phase space eventually travels over almost all of it excluding only isolated islets of stability which shrink as k_s grows. This implies that the half-width I_c of the stochastic layer in the whisker map is

$$I_c \approx \lambda k / k_c \tag{5.7}$$

This is supported by the phase space pictures, one example of which is figure 5.1, where the motion appears stochastic for $|I - I_o| < I_c$ and regular for $|I - I_o| > I_c$. Observe that even for the smallest non-zero λ and k there is a thin stochastic layer around the separatrix. This is further emphasized by the following relation between the parameters of the classical map: if we decrease $k \to k \exp(-2\pi/\lambda)$ the map is unchanged provided we scale down $I \to I \exp(-2\pi/\lambda)$. Notice the deformation of the KAM surfaces and periodic orbits: k gives the phase space contours a curvature as a function of the angle, which is evident in the pictures. A perhaps truer border between stochastic and regular motion is something like $I_c + \frac{k}{2}\sin\theta$.

We note that the degree of stochasticity grows as the action moves deeper into the stochastic layer. The parameter k_{eff} increases from critical (k_c) at the layer's border to infinity in the middle at I_o. As a consequence, deep inside the stochastic layer the motion is very random and leads to diffusion in the action (sec. 5.2.2). Further out, the phase space has more structure: in addition to the islets of stability, there are cantori, remnants of KAM invariant tori which slow down the diffusion. There may be several effective cantori within the layer, increasing in their "strength" in inhibiting transport (*i.e.* becoming less broken up) as the border with the regular region is approached. We shall discuss this in more detail next.

5.2.2 Properties of the classical whisker map: II

Dynamics: diffusion and cantori Deep inside the stochastic layer, the effective standard map parameters become very large and approach infinity as $I \to I_o$. This leads to diffusion in the action in the classical whisker map: Given k and λ, for I close enough to I_o, the change in the angle is large enough such that from iteration to iteration after wrapping back to the domain $\theta \in [0, 2\pi)$, there is almost no correlation or memory in the angle. Consequently, it is as if the action is subject to a random force

$$\begin{aligned} \langle I(t)\rangle &= \langle I(0)\rangle \\ \langle I(t)^2\rangle &= \langle I(0)^2\rangle + Dt,\ D = k^2/2 \end{aligned} \tag{5.8}$$

where $\langle\rangle$ represents an ensemble average over many trajectories with initial action $I(0)$. This follows under the assumption of no kick-to-kick correlations. The diffusion out to the regular region is however impeded by barely broken KAM tori ("cantori") further out in the stochastic layer (see figures 5.2 and 5.3). To understand what these structures are and where they lie, and how much they hang up the classical transport, we shall now briefly review some classical theory of non-linear dynamical systems. In the appendix more detail concerning this is provided. The reader is referred to the papers in the references [34, 35, 36, 37, 38, 39, 40, 43].

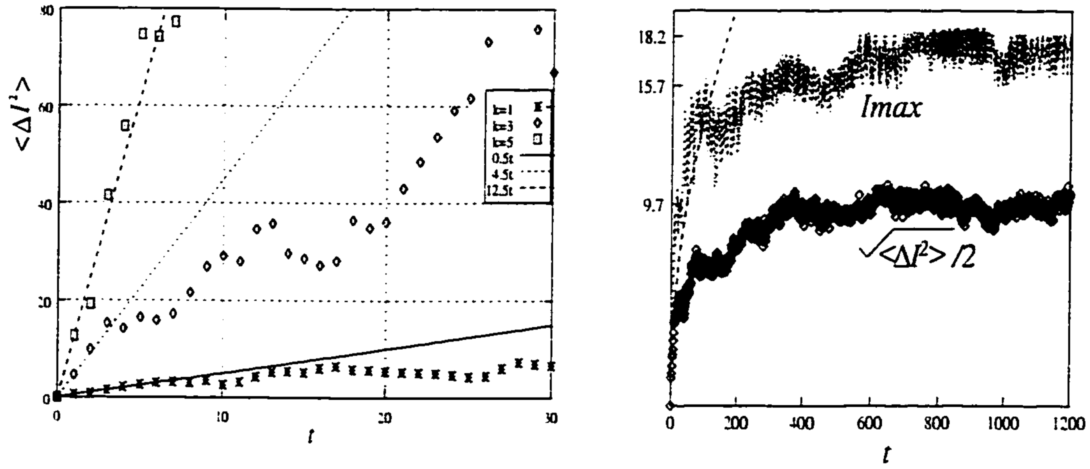

Figure 5.2: (a)Classical diffusion in the whisker map $\lambda = 10$: $\langle \Delta I^2 \rangle$ for a set of initial conditions with 0 action. The initial slopes agree with equation 5.8. (b)Later, diffusion is impeded by cantori. This graph shows the maximum action in the distribution, $\lambda = 10, k = 2$. Also a scaled square root of the dispersion in action is shown. The dashed line corresponds to unimpeded diffusion given by eqn 5.8

In integrable systems all trajectories lie on invariant tori. The winding number

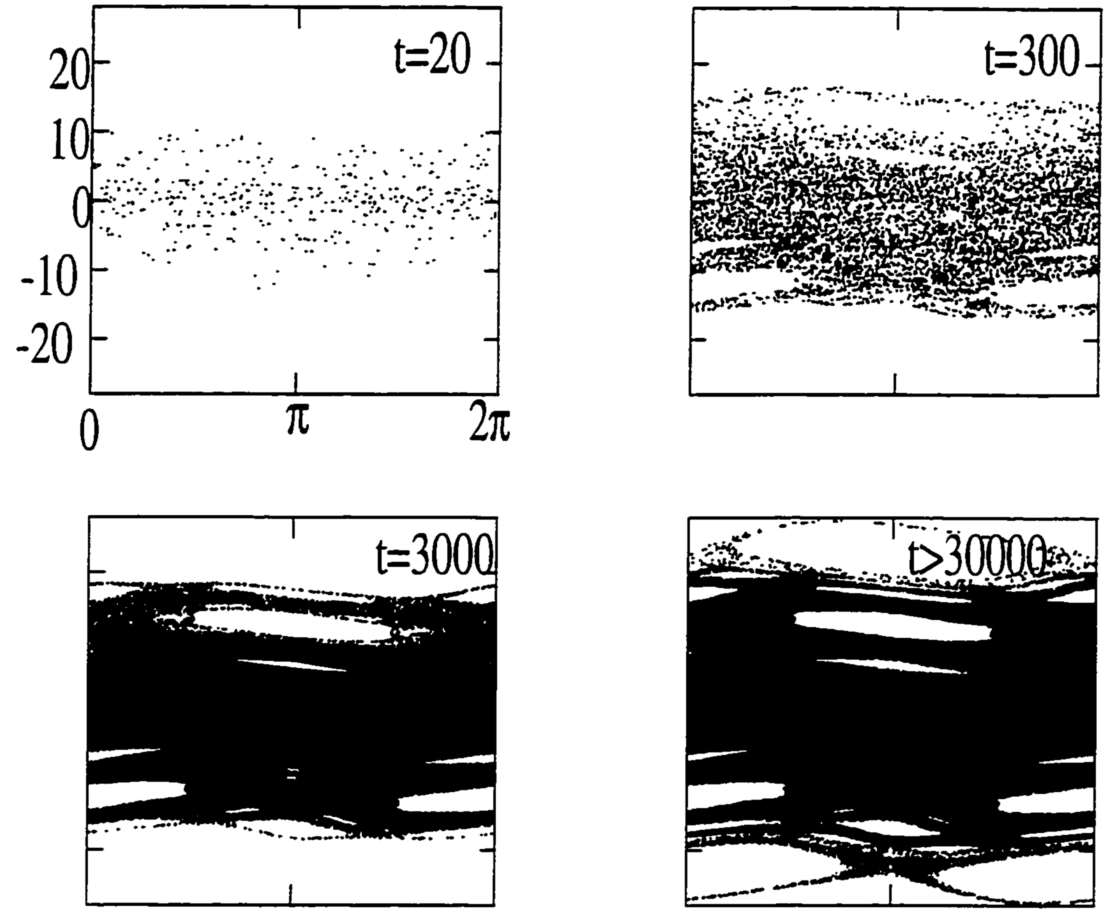

Figure 5.3: Classical evolution of 20 points initially with random θ and $0 < I < 1$. $\lambda = 10, k = 2$. The borders of the distribution at each time shown are at cantori: $t = 20$ shows the cantorus at winding number $4 - \gamma^{-2}$, $t = 300$ shows that at $4 + \gamma^{-2}$; $t = 3000$ shows that at $5 - \gamma^{-2}$ (see text). Finally ($t > 30000$) the outermost cantorus is penetrated and the distribution spreads to the border with the regular region.

$w = 1/r$ characterizes the trajectories: for example in the whisker map, when $k = 0$, if

$$r_o(I) = \frac{1}{w_o} = \frac{\lambda}{2\pi} \ln \left| \frac{c}{I - I_o} \right| \tag{5.9}$$

is a rational number p/q where p and q are relatively prime integers, then the corresponding trajectory is a series of regularly spaced points which repeat after q iterations i.e. a period-q orbit, or q-cycle. If r_o is irrational, the points never repeat, rather they eventually fill the line at I. The rationality or otherwise of unperturbed winding numbers is of great consequence when a perturbation is turned on: Stochastic orbits appear, ones that fill out somewhat randomly an area in phase space (rather than living on a line or a set of points). Some of the periodic q-cycles and orbits of invariant irrational winding numbers are destroyed completely and some persist, albeit deformed. In a perturbation theory approach, one encounters the "small denominator" problem where deformations blow up if the frequencies are commensurate. The KAM theorem [41, 31] states that for small enough but finite perturbation, there are one-dimensional orbits on surfaces that as the perturbation strength goes to zero, go continuously into surfaces with irrational winding number w. w must be irrational enough so that there exists $c > 0$ such that $|w - n/m| > c/m^{2.5}$ for all integers m,n.

Such KAM tori are the last to be destroyed as the perturbation strength increases and they confine other (stochastic) trajectories to lie on one side or the other of the tori. Greene found (see appendix) that the last surviving KAM curve for the standard map (eqn 5.4) has winding number $\pm(\gamma \pm n) = \pm((\sqrt{5}+1)/2 \pm n) \approx \pm(1.618 \pm n)$ where γ is the golden mean and n is an integer.

Note that for the standard map, the winding number is simply $2\pi/I$. This curve remains robust as the standard map parameter k_s increases from 0 to $k_s = k_c = 0.9716354...$ [34], when it breaks up and global stochasticity sets in. The golden mean (and its integer relatives) is, in a sense, the "most irrational" number: the continued fraction representation consists of a series of ones (see appendix). Other irrational winding numbers w correspond to trajectories that lie on an invariant curve under small perturbations but they break up at parameters $k_c^w < k_c$. At the break-up parameter, the KAM curve acquires a scale-invariant fractal structure; this is called a cantorus. A cantorus is an invariant set with an infinite number of infinitesimal gaps ([36, 42]) and present partial barriers to motion across itself for $k_s > k_c^w$ (but not too big), invalidating the diffusion picture. (Of course, for smaller k_s they are complete barriers to transport, and for much larger k_s they totally disintegrate and diffusion may proceed rapidly, as in the stochastic region).

For the whisker map it is not surprising that the strongest restraints on the diffusion in the stochastic layer arise from cantori with winding number $\pm(\gamma \pm m)$, for integer m. The unperturbed winding number w_o is related to the action by equation 5.9. The parameter λ lays down the structures in phase space (islands, cantori); properties such as their size and stochasticity depend on both λ and k. Typically there are several cantori corresponding to winding numbers $w = m \pm \gamma^{-2}$ which are "effective" within the stochastic layer, with varying degrees of "broken-ness". (Note that $\gamma^{-2} = 1 - \gamma^{-1} = 2 - \gamma \approx 0.382$.) Those near the outer border of the stochastic layer are close to critical and present much stronger impediments to diffusion than those further inside the layer; this is as suggested by the local standard map parameter at the cantori (equation 5.6). For example, in figures 5.2 and 5.3, there are three cantori evident, corresponding to winding numbers $4-\gamma^{-2}, 4+\gamma^{-2}$ and $5-\gamma^{-2}$ at $|I - I_o| \approx 9.7, 15.7, 18.2$ respectively. These are of course the values of unperturbed actions: k curves the manifold as is evident in the phase-space pictures. The classical distribution gets hung up at each for some time, which is longer the further out the cantorus is, before escaping further out into the stochastic layer. Of course, ultimately it fills the phase space (except for the islets of stability) up to the regular region (figure 5.3). It is also important to note that each cantorus has a "width" which represents the range in action around the cantorus in which the transport is slowed down due to closely neighboring irrationals (see also appendix and section 5.4.3).

As k increases, the cantori become weaker and the inner ones may disappear (i.e. totally disintegrate) as new ones appear at the growing edge of the stochastic layer. Whether in fact there is an exactly critical cantorus depends on a subtle conspiracy of parameters to produce a golden mean winding number at the border of the stochastic zone: one would need $\lambda k/k_c = \exp(2\pi(m \pm 1/\gamma^2)/\lambda)$. In figure 5.4 we have zoomed in on the border between the stochastic and regular regions in the whisker map with parameters $\lambda = 10, k = 1.77$. There is a critical cantorus at winding number $5-\gamma^{-2}$ at action $I = 18.7$ (the parameter $I_o = 0.5$). Although the cantorus itself is not visible in this picture, which is limited by the number of points iterated, what one can see clearly are the resonance island structures embracing where the cantorus would be. One can make out a period 2, period 3, period 5, period 8 and period 13 chain, alternating between the two sides of the cantorus. Note that this structure is not unique to cantori in the whisker map: the periodic orbit structure occurs around generic cantori. These periodic orbits are called "convergents" to the KAM and they have winding numbers which are successive truncations of the continued fraction representation of the irrational winding number associated with the KAM. For the golden mean, the convergents have period given by the Fibonacci sequence $F_0 = 0, F_1 = 1, F_{i+1} = F_i + F_{i-1}$ with winding numbers F_i/F_{i+1}. As $i \to \infty$ this number approaches γ. Our figure does not have enough points to resolve the structure beyond the 13th level. (Of course for the winding number $n - \gamma^{-2} = n - 2 + \gamma$, $n - 2$ should be added to the winding numbers of the convergents and the KAM above). We refer the reader to the appendix and the literature for more discussion.

The periodic orbit convergents are in a sense responsible for the fractal structure

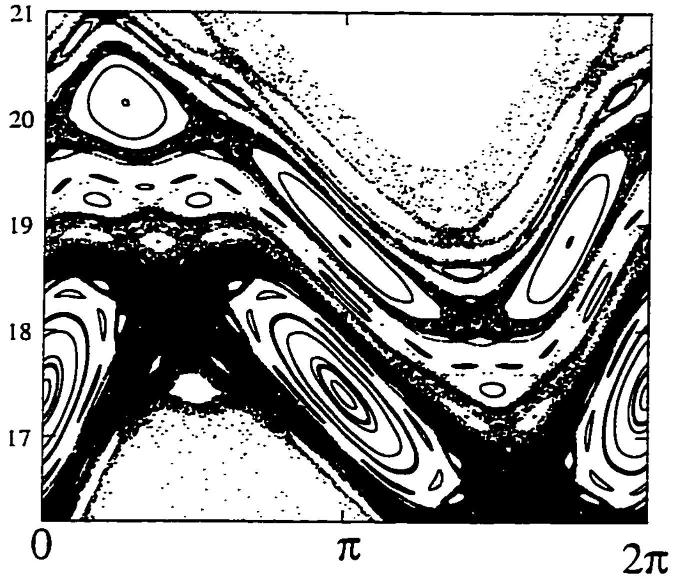

Figure 5.4: Classical phase-space near a near-critical cantorus at the border of the stochastic layer.

at criticality; studying properties of these convergents leads us to scale invariance. Indeed it was a study of their stability as a function of the nonlinearity parameter which led to Greene's result regarding the destruction of the last KAM surface in the standard map [34]. There is an extensive literature on the scaling behavior and renormalization group theories near the cantorus to describe the "structure at all scales". An analytic renormalization approach (see appendix and [39]) can also give predictions for when the KAM torus is destroyed and for the scaling exponents: in [39] a close approximation is found by considering a renormalization procedure between two resonance chains; numerical work in [37] and [35] developed this idea further. The behavior at criticality has universal characteristics: near the critical break-up parameter for other irrational winding numbers and for other maps one finds the same scaling exponents [35] and the same universal map. We expect that the whisker map, being locally a standard map displays many of the same features. Our interest here is in understanding the dynamics near a cantorus: when does a KAM surface break into a fractal set, what is the motion like near the cantorus , "how much" does it inhibit diffusion across it and how all this depends on the parameters. We need to understand this to understand the quantum mechanics of the full system. In the appendix we attempt to briefly discuss these questions, which among others, have been throughly investigated in the literature. One major upshot for us are the scaling relations: asymptotically, the map is invariant under the re-scaling [35, 37, 39]

$$\begin{aligned} \mu &\to \delta\mu \\ \Delta\theta &\to \alpha\Delta\theta \\ \Delta p &\to \beta\Delta p \\ n = F_{r+1} &\to F_r \sim n/w \end{aligned} \tag{5.10}$$

where $\delta \approx 1.628$ is the scaling exponent for the non-linearity parameter μ; $\alpha \approx -1.41(-1.69)$ near $\theta = \pi(0)$ and $\beta \approx -3.07(-2.56)$ near $\theta = \pi(0)$. The non-linearity parameter μ measures the distance away from criticality: for the standard map, $\mu = k_s - k_c$. The last relation expresses time-rescaling, n being the number of iterations of the map, with scaling exponent given by the irrational winding number of the KAM, *e.g.* for the golden mean torus, $w = \gamma \approx 1.618$. It is important to note that the values of α and β correspond to those at the dominant (subdominant) symmetry line (see appendix), which for the standard map of the form in eqn 5.4 with $k_{eff} > 0$ are at $\pi(0)$. This implies that for the whisker map, at $I > I_o$, the relations are as above, but at $I < I_o$ (where k_{eff} is negative), the dominant and subdominant symmetry lines are at $0(\pi)$ respectively and the values of α and β at 0 and π should be switched. As discussed in the appendix, the subdominant symmetry line tends to cross a hyperbolic point of each periodic convergent, whereas the dominant line contains an elliptic point of each periodic convergent. Notice that at both the subdominant and dominant symmetry lines, the product of the phase-space scalings $\alpha\beta \approx 4.34$.

Flux through a cantorus

Perhaps the most important aspect of classical behavior near barely broken tori for our study of the quantized map, is an understanding of "how much" a cantorus slows down transport across itself. In the whisker map there are near-critical cantori near the boundary of the stochastic and regular regions and not so critical cantori deeper in the stochastic layer. A measure of the impedence each provides to transport is given by the flux ΔW swept across the cantoral gaps in one iteration of the map. In the appendix we discuss this in some detail. Essentially, one finds a curve through the cantorus that closes all the gaps and computes the area between this curve and its iteration. The minimum of this over all curves is twice the outward flux through the cantorus (appendix). This construction gives what is often called the "turn-stile". It is somewhat easier however to exploit action principles to compute the flux: as described in the appendix, the flux through a cantorus is given by the action difference between the minimizing orbit (points on the cantorus) and the minimax orbit lying in the middle of the gaps of the cantorus. The former minimizes the action, the latter is a saddle point of the action.

The scaling properties of a near-critical cantorus make the computation of flux at some k_s near k_c easier again for us. The flux follows a scaling relation that is not difficult to guess from eqns 5.10. The flux through periodic orbit convergents ΔW_i and that through the cantorus ΔW_ν scale like

$$\begin{aligned} (\alpha\beta)^i \Delta W_i(k_c + \mu/\delta^i) &\rightarrow \Delta W^*_{cgt}(\mu) \\ (\alpha\beta)^i \Delta W_\nu(k_c + \mu/\delta^i) &\rightarrow \Delta W^*_\nu(\mu) \qquad (5.11) \\ & \qquad (5.12) \end{aligned}$$

The latter implies

$$\Delta W^*_\nu(\mu) \propto \mu^\eta \text{ where } \eta = \frac{\ln \alpha\beta}{\ln \delta} \approx 3.01 \qquad (5.13)$$

That the flux scales as $(\Delta k_s)^3$ holds for a surprisingly wide range of k_s: in [38], the authors show numerically that the diffusion in action goes as $(\Delta k_s)^3$ up to $k_s \sim 2.5$. It is natural to expect that global diffusion in action is limited by the diffusion at cantori and thus is proportional to the cantoral flux, since it is the cantoral regions that provide the most impedance to transport.

From calculations described in ref [36], where ΔW for the golden mean cantorus of the standard map was computed by a study of the convergence of ΔW for the periodic orbit convergents, we deduce the proportionality factor

$$\Delta W^{kr}(k_s) \approx 0.7(\Delta k_s)^3 \qquad (5.14)$$

By universality we expect that the dependence here on the non-linearity parameter (i.e. the scaling exponent η) holds for general one-parameter maps and for irrational winding numbers other than the golden mean, however probably with a different proportionality constant.

Our interest is in the whisker map, and we shall exploit the fact that it is locally a standard map to calculate the cantoral flux (section 5.2.1). We generalize equations 5.5 and 5.6 to the neighborhood of a cantorus, replacing I_r by the action at the cantorus rather than at the fixed point. Note that although we cannot strictly write the whisker map as a local standard map except close to a fixed point there certainly is a sense in which we can associate an effective standard map parameter and corresponding phase-space scalings anywhere inside the stochastic layer.

$$
\begin{aligned}
\Delta W &= \frac{|I_{ct}-I_o|}{\lambda}\Delta W^{kr}\left(\frac{\lambda k}{|I_{ct}-I_o|}\right) \\
&\approx 0.7\frac{|I_{ct}-I_o|}{\lambda}\left(\frac{\lambda k}{|I_{ct}-I_o|}-k_c\right)^{\eta} \qquad (5.15) \\
&\approx \frac{0.7ce^{-2\pi(r\pm\gamma^{-2})/\lambda}}{\lambda}\left(\lambda kce^{2\pi(r\pm\gamma^{-2})/\lambda}-k_c\right)^{\eta} \qquad (5.16)
\end{aligned}
$$

where the last line specializes to the case of a cantorus at winding number $r \pm \gamma^{-2}$.

There is another way to derive the whisker cantoral flux. One can express the dependence of equation 5.13 on the nonlinearity parameter in terms of the residue by making use of the relation A.2. We may write

$$\Delta W_w \approx 0.37\Delta W_{p/q}(R^*)\left(\ln\frac{R_{p/q}}{R^*}\right)^{\eta} \qquad (5.17)$$

which was obtained in reference [43]: the prefactor relates the cantoral flux to the action difference at the critical break-up parameter between the minimizing and minimax orbits of a nearby resonance, with the proportionality factor determined by a numerical study [43]. There, it is also asserted that for a cantorus sandwiched between two periodic orbits of neighboring rationals (*i.e.* $p'q - pq' = \pm 1$) which have residues of significantly different size, one may replace the logarithm in eqn 5.17 with the combination weighted by the inverse "distance" from the resonance to the cantorus. For example, for a cantorus with unperturbed winding number $m + 1/\gamma^2$, $\Delta W_w \approx 0.37\Delta W_m(R^*)\left(\frac{1}{\gamma}\ln\frac{R_m}{R^*} + \frac{1}{\gamma^2}\ln\frac{R_{m+1}}{R^*}\right)^{\eta}$. (Note that $1/\gamma + 1/\gamma^2 = 1$). It is straightforward to calculate the components of this expression for cantori in the whisker map using the fixed points for the periodic orbit pivots on the right-hand side. Their residues may be found by the frequency Ω of small oscillations around around the orbit: for elliptic orbits, R may be written as $\sin^2(\Omega T/2)$, T being the period of the orbit (see eqn A.1). So we compute $\ddot{\theta} = d(\lambda \ln|c/(I-I_o)|)/dt = \lambda k \sin\theta/(I-I_o) = k_{eff}\sin\theta$ near a fixed point. Linearizing gives $R = \Omega^2/4 = k_{eff}/4$. The action difference between the minimizing fixed point (hyperbolic point) and the minimax (elliptic point) is $2k$ (*e.g.* consider the F_1 generating function discussed in section 5.3.2). At the critical break-up parameter, when $R = R^*$, $k_{eff} = \lambda k/|I_r - I_o| = k_c$ and so the action difference at R^* is $2k_c|I_r - I_o|/\lambda = 2k_c c\exp(-2\pi r/\lambda)/\lambda$. Putting this all together, we get for a cantorus at winding number $m \pm 1/\gamma^2$

$$\Delta W \approx \frac{0.7ce^{-2\pi r/\lambda}}{\lambda}\left(\frac{1}{\gamma}\ln\left(\frac{\lambda kce^{2\pi r/\lambda}}{k_c}\right)+\frac{1}{\gamma^2}\ln\left(\frac{\lambda kce^{2\pi(r\pm 1)/\lambda}}{k_c}\right)\right)^{\eta} \tag{5.18}$$

This was also obtained in reference [53].

We notice this is *almost* exactly the same as our earlier formula 5.16: the terms in the large parentheses may be combined as

$$\ln\left(\frac{\lambda kce^{2\pi(r\pm\gamma^{-2})/\lambda}}{k_c}\right)$$

which gives the same term as that taken to power η as in eqn 5.16 once the argument of the logarithm is expanded around 1. The only difference with equation 5.16, is then an overall factor of $e^{\pm 2\pi/(\lambda\gamma^2)}$. The difference, we think, comes about because in the formula 5.18 only the closest resonance is accounted for in the prefactor, but in our formula 5.16, an effective weighted combination from both resonances occurs from the local standard correspondence.

Because of this we are inclined to trust 5.16 more when calculating the flux. In section 5.4.3 we shall provide numerical evidence supporting our approximation.

5.3 Quantization

We are not the first to give a quantization of the whisker map: in [53] the quantization in action representation is given. It is however the angle representation which is of greatest interest from the semiclassical point of view (and this has not been studied). We address the semiclassical issues in section 5.3.2, but first discuss the full quantization in angle representation and in action representation.

It is not a priori obvious what a quantization of a classical map means given that the concept of a conserved energy does not exist in the conventional sense. We may however write down a Hamiltonian which gives rise to the mapping: for the whisker map

$$H = \lambda(I - I_o)\left(\ln\left|\frac{c}{I - I_o}\right| + 1\right) - k\cos\theta\sum_n \delta(t - nT). \tag{5.19}$$

Integrating the equations of motion $\dot{\theta} = \partial H/\partial I, \dot{I} = -\partial H/\partial\theta$ over a period T yields the whisker map (eqn 5.1). We note this is not a unique choice for a Hamiltonian: the following function, with the "potential" term acting first and then the "kinetic" term,

$$H \;=\; -\frac{1}{z}k\cos\theta,\ 0 < t < zT$$

$$= \frac{\lambda(I - I_o)}{1 - z}\left(\ln\left|\frac{c}{I - I_o}\right| + 1\right), \; zT < t < T.$$

where $0 < z < 1$, also effects the whisker map equations. The non-uniqueness is not surprising considering that the map only "sees" the system at discrete times, every period, and not in between. The quantum evolution operator over one period (Floquet operator), $U = \left[\exp(-i \int_0^T H dt/\hbar)\right]_{+}$ (with $[]_+$ denoting positive time-ordering) *is* unique as we would expect: all choices of H give the operator

$$U = e^{-i\lambda(I-I_o)\left(\ln\left|\frac{c}{I-I_o}\right|+1\right)/\hbar} e^{ik\cos\theta/\hbar} \tag{5.20}$$

θ and I are now of course quantum operators. The unitary operator U may be thought of as defining the quantum map. The phases ν of its eigenvalues $e^{-i\nu}$ are called quasi-energies and are defined mod 2π. The corresponding quasi-energy eigenstates are also called Floquet states.

We note one ambiguity in the quantization arises from the non-commutativity of the I and θ operators: different orderings of the exponentials give different quantizations. Our choice of ordering follows that dictated by our choice in the classical map 5.1: the equation mapping the angle depends on the mapped action (I' rather than I). (This is done to ensure area preservation, see *e.g.* [54]; another choice would be to have instead the equation mapping the action depend on the mapped angle with the equation mapping the angle depending on the unmapped action).

One can study the quantized system via U in a number of different ways. We shall begin by computing its matrix elements in the angle and action bases *i.e* by examining the one-step propagator. A semiclassical calculation surprises us by being a remarkably good approximation to the full quantum mechanics which at first glance we may not expect. The quantum one-step dynamics gives by iteration the quantum long-time dynamics and this is what we shall study in 5.4. The main feature we shall discuss there is the nature of localization in the stochastic layer.

5.3.1 The one-step propagator

The quantum probability amplitude for being at θ_f after one iteration of the whisker map having started at θ_i is given by the propagator:

$$\begin{aligned} K(\theta_i,\theta_f) &= \sum_n \langle\theta_f + 2\pi n|U|\theta_i\rangle \\ &= \sum_n \int dI \frac{1}{2\pi i\hbar} e^{iI(\theta_f-\theta_i+2\pi n)/\hbar} e^{-i\lambda(I-I_o)\left(\ln\left|\frac{c}{I-I_o}\right|+1\right)/\hbar+ik\cos\theta_i/\hbar} \end{aligned} \qquad (5.21)$$

where the sum over n is a sum over domains in angle representing the action of taking mod 2π in the map. In the second step we have inserted the identity in the form of the closure relation $\int dI|I\rangle\langle I| = 1$. We also note $\langle I|\theta\rangle = \exp(iI\theta/\hbar)/\sqrt{2\pi i\hbar}$ which follows from action and angle being canonically conjugate variables with commutator $[\theta, I] = i\hbar$.

The sum over domains may be transformed into a sum in action space (Poisson's Summation Formula):

$$\sum_n e^{iI2\pi n/\hbar} = \sum_j \hbar\delta(I - j\hbar)$$

yielding the quantum quantization rule for allowed actions. This ensures periodic boundary conditions in angle. Inserting this into 5.21 would give an infinite sum over I-matrix elements of oscillating exponentials. To avoid this divergence, we truncate the phase space to a finite (rather than infinite) cylinder symmetric about I_o:

$$\theta \in [0, 2\pi),\ I \in [-I_c + I_o, I_c + I_o)$$

The number of quantum states is $N = 2I_c/\hbar$ which allows each state an area of Planck's constant h in phase space. The closure relation in action becomes $1 = \sum_{j=-N/2}^{N/2-1} |I_j\rangle\langle I_j|$ where $I_j = j\hbar$ for example (or $j\hbar +$ integer$\hbar$). Finally, we replace $\sqrt{1/(2\pi i\hbar)}$ with $\sqrt{\hbar/(2I_c)}$ as the normalization factor and $\int dI$ with $\hbar\sum_j$, to obtain

$$K(\theta_i, \theta_f) = \left(\frac{\hbar}{2I_c}\right) e^{ikcos\theta_i/\hbar} \sum_{j=\left[\frac{-I_c+I_o}{\hbar}\right]_+}^{\left[\frac{I_c+I_o}{\hbar}\right]_-} e^{ij(\theta_f-\theta_i)-i\lambda(j-I_o/\hbar)\left(\ln\left|\frac{c}{j\hbar-I_o}\right|+1\right)/\hbar+ik\cos\theta_i/\hbar} \qquad (5.22)$$

θ_f and θ_i can also only take on quantized values: only N angle states may fit into 2π, so each allowed state has support integer$\times\pi\hbar/I_c$. Choosing states θ_p to be centered at $p\pi\hbar/I_c$ gives periodic boundary conditions in action.

Let us comment on the role of I_o. We observed in the classical map that I_o acts only as a translation in action, shifting the entire phase space by a constant. Indeed, I_o

plays the same role here: if we rotate our basis to $|\tilde{\theta}\rangle = e^{-iI_o\theta/\hbar}|\theta\rangle$, then the propagator $K(\tilde{\theta}_i, \tilde{\theta}_f)$ has no I_o-dependence. The quantization changes as the delta function becomes $\delta(I - I_o - j\hbar)$. I_o is much like a gauge variable: any choice of I_o leads to the same quantum mechanics *provided* the basis is rotated.

The propagator in action may be obtained from a double Fourier transform of $K(\theta_f, \theta_i)$, or directly:

$$\begin{aligned} K(I_f, I_i) &= \langle I_f | e^{-i\lambda(I-I_o)\left(\ln\left|\frac{c}{I-I_o}\right|+1\right)/\hbar} e^{ik\cos\theta/\hbar} | I_i \rangle \\ &= \frac{\hbar}{2I_c} e^{-i\lambda(I_f-I_o)\left(\ln\left|\frac{c}{I_f-I_o}\right|+1\right)} \sum_{p=0}^{2I_c-1} e^{-i\pi(I_f-I_i)p/I_c+ik\cos\left(\frac{p\pi\hbar}{I_c}\right)/\hbar} \end{aligned} \tag{5.23}$$

where we inserted the identity in the form of a complete set of angles in the middle of the factorized propagator. This result was also obtained in [53]. Again, we see the gauge nature of I_o: if we define $|\bar{I}\rangle = |I - I_o\rangle$, then I_o drops out of $K(\bar{I}_f, \bar{I}_i)$ *i.e.* the propagator is the same for all gauge choices provided we translate the basis (*c.f.* the classical mechanics case, sec 5.2).

In section 5.4 we shall study the long-time properties of the quantized whisker map by iterating the propagator for long times and also by looking at its eigenstates. Before doing so, we consider what a semiclassical quantization gives for the whisker map.

5.3.2 Semiclassics

Semiclassical quantization of maps proceeds much like that of continuous time systems: amplitudes are expressed as the square root of a classical probability times an exponential whose phase is the appropriate classical action. If more than one classical path links the two endpoints in question, then a sum of such terms, one for each classical path, is needed. Pictorially, the one-step semiclassical propagator from an initial state $|i\rangle$ to a final state $|f\rangle$ may be represented as summing with appropriate complex weights, the intersections of two manifolds in classical phase space: one, the distribution corresponding to $|f\rangle$, the other the distribution obtained by evolving the bunch of points corresponding to $|i\rangle$ for one iteration. This yields a very interesting picture for the whisker propagator in angle-representation, Fig. 5.5a: there are an infinite number of intersections converging towards I_o with any final angle state (a vertical line). This raises an interesting question for semiclassics: the quantization of action in the full quantum mechanics (sec 5.3.1) smears over structure in phase space below the level of $\hbar$, yet within an $\hbar$-slice of I_o there are an

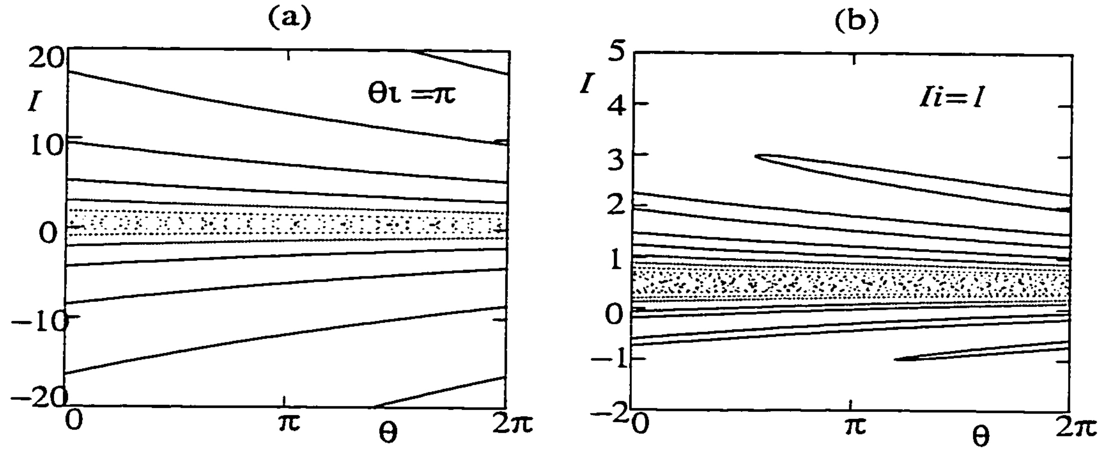

Figure 5.5: Classical one-time step evolution on whisker map $\lambda = 10, k = 2, I_o = 0.5$ (a)Initial distribution at $\theta = \pi$(b)Initial distribution at $I = 1$.

infinite number of semiclassical contributions to be summed. Does the quantum mechanics "see" them all? In fact, as we shall see shortly, it does.

One may compute the semiclassical angle propagator from the type 1 classical generating function F_1:

$$K^{sc}(\theta_i, \theta_f) = \sum \sqrt{-\frac{i}{2\pi\hbar}\frac{\partial^2 F_1}{\partial\theta_i \partial\theta_f}} e^{-iF_1(\theta_i,\theta_f)/\hbar} \tag{5.24}$$

where $I_i = \partial F_1(\theta_i, \theta_f)/\partial\theta_i$ and $I_f = -\partial F_1(\theta_i, \theta_f)/\partial\theta_f$ and the sum is over different branches of the action function, (i.e. different classical paths). For the whisker map. $F_1(\theta_i, \theta_f) = -I_o(\theta_f - \theta_i) \pm c\lambda \exp(-(\theta_f - \theta_i)/\lambda) - k\cos\theta_i$, where the two signs represent the classical paths above and below I_o respectively. This gives for the whisker map:

$$\begin{aligned} K^{sc}(\theta_i, \theta_f) &= \frac{1}{I_c}\sqrt{\frac{i\pi c\hbar}{2\lambda}} \sum_{n=n_c}^{\infty} e^{-(\theta_f-\theta_i+2\pi n)/2\lambda} e^{iI_o(\theta_f-\theta_i+2\pi n)/\hbar} e^{ik\cos\theta_i/\hbar} \\ &\times \left(e^{-ic\lambda e^{-(\theta_f-\theta_i+2\pi n)/\lambda}/\hbar} - ie^{ic\lambda e^{-(\theta_f-\theta_i+2\pi n)/\lambda}/\hbar} \right) \end{aligned} \tag{5.25}$$

where the sum is over different domains in angle, arising from taking mod 2π after the shearing. We note again the gauge role of I_o is manifest: using the rotated basis as described in sec 5.3.1 the I_o-dependence in the propagator drops out. The sum has a lower limit at

$$n_c = \left[\frac{1}{2\pi}\left(\lambda \ln\left|\frac{c}{I_c}\right| - (\theta_f - \theta_i)\right)\right]_+ \tag{5.26}$$

where $[]_+$ rounds up to the closest integer, to correspond to the truncation of the cylinder in the action coordinate. The two terms for each n represent the two classical paths that

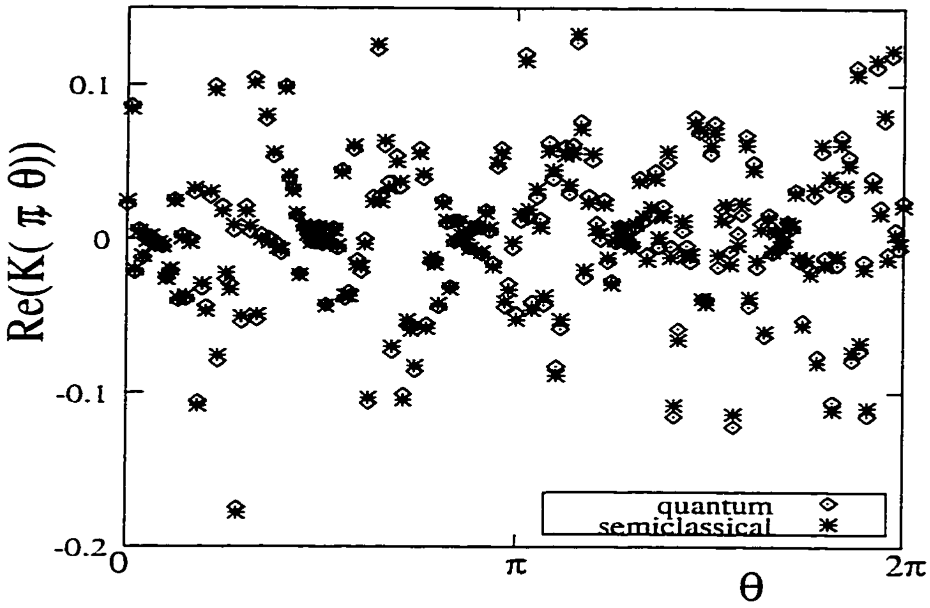

Figure 5.6: Quantum and semiclassical one-step propagators for the whisker map $\lambda = 10, k = 2, I_o = 0.5, \hbar = 0.2, \theta_i = \pi$.

has been sheared over to angle $\theta_f + 2\pi n$ before taking mod 2π; one with actions staying above and one below I_o respectively. The upper limit of the sum extends to infinity with the differences between the terms becoming exponentially small as the classical paths they represent shear farther and farther. At the same time this part of the manifold is becoming thinner and thinner as it stretches out, which is reflected in the exponential decay of the Van-Vleck prefactor in eqn 5.25. Each term represents a topologically distinct classical path, having traversed 2π in angle a different number of times, and is an independent and exponentially decreasing contribution to the semiclassical amplitude. This is why the semiclassical sum works so well despite the hairy phase-space close to I_o. Moreover, there are no caustics in the angle-representation; the manifold in figure 5.5b never is tangent to an angle-state. The semiclassical approximation is very good as seen in figure 5.6 where the quantum and semiclassical one-step propagators are plotted. One mild warning to the reader: diffraction at the cut-off introduced at large actions affects the quantum sum over action matrix elements and the semiclassical sum over angle domains in different ways. The consequence is that they differ more in certain ranges of final angle than in others.

We can also get eqn 5.25 from a stationary phase Fourier transform of the action integral in eqn 5.21, each stationary phase point being the classical action at a given intersection. In fact not only can we get the semiclassical expression starting from the quantum one, but we can retrieve a fully quantum propagator starting from semiclassics, if we write the map as an involution of two (non-commuting) maps: $T = T_2 \circ T_1$ where

$$\begin{aligned} T_1 &: \theta' = \theta,\ I' = I - k\sin\theta \\ T_2 &: \theta' = \theta + \lambda \ln|c/(I - I_o)|,\ I' = I \end{aligned} \tag{5.27}$$

The semiclassical propagator for each map is exact, since each map only changes either action or angle, not both. To construct the angle propagator for T we compose the θ to I propagator for T_1 with the I to θ propagator for T_2:

$$K(\theta_i, \theta_f) = \sum_n \int dI \frac{i}{2\pi\hbar} e^{iF_3^{(T_1)}(I,\theta_i)/\hbar} e^{iF_2^{(T_2)}(\theta_f + 2\pi n, I)/\hbar} \tag{5.28}$$

The generating functions F_3 and F_2 above are each bilinear in the mixed term and the Van-Vleck prefactor for each is just 1; this tells us again that the semiclassical expression is exact. It is not difficult to calculate these and one finds exactly formula 5.21 which was derived purely quantum mechanically. Performing the sum over domains exactly as described there gives the quantum propagator eqn 5.22 and performing the I-integral by stationary phase gives the semiclassical eqn 5.25.

One may also calculate the semiclassical action propagator. Graphically, this is represented by the intersection of a horizontal I-state with the manifold in figure 5.5b. The phase-space representation of this is not as interesting as in the angle case however there are some points we would like to make. There are two ordinary caustics in this representation due to the curving created by k, and we would expect the semiclassics to fail here. However one may at first be more concerned about what happens when both I_i and I_f are taken close to I_o where the manifold stretches out with very little curvature in action and may seem to resemble the supercaustic of chapter 2. In fact this poses no problem for the semiclassics: the naive picture is of course deceiving unless we consider the thickness of the manifold in this region. The manifold is exponentially thin, which cancels out any tangency effect. In other words, one can perform a transformation on the phase-space that squeezes in θ and stretches out in I; in this scaled phase-space it is clear there is no problem with the semiclassics. Another way to illustrate this last point is to consider the θ to I propagator, represented semiclassically by the intersection of a horizontal I-state with the manifold in fig 5.5a; the same issues discussed above arise at an action near I_o. Consider for simplicity $k = 0$, this doesn't affect the essentials of the hairiness near I_o.

That the semiclassics behaves (and is indeed exact at $k = 0$) for this propagator is clearly demonstrated by considering what the picture would be for the I to θ propagator which is remarkably simple: the intersection of a horizontal I-state with a vertical θ-state, just as in free particle propagation but with a phase!

For completeness, we give the semiclassical action propagator:

$$\begin{aligned} K^{sc}(I_i, I_f) &= \sqrt{\frac{1}{2\pi i\hbar k}}\left(\frac{1}{1-\left(\frac{I_f-I_i}{k}\right)^2}\right)^{\frac{1}{4}} \\ &\times\ e^{\frac{i}{\hbar}\left(k\sqrt{1-\left(\frac{I_f-I_i}{k}\right)^2}+(I_f-I_i)\sin^{-1}\left(\frac{I_f-I_i}{k}\right)-\lambda(I_f-I_o)\left(\ln\left|\frac{c}{I_f-I_o}\right|+1\right)\right)} \end{aligned}$$

We conclude this section by considering a quantity independent of representation which shows the difference between the semiclassical and quantum propagators.

$$\chi \equiv \frac{1}{N} Tr(U^{qm} - U^{sc})^{\dagger}(U^{qm} - U^{sc}) = \frac{1}{N}\sum_i \sum_j |K^{qm}(\theta_i, \theta_j) - K^{sc}(\theta_i, \theta_j)|^2 \qquad (5.29)$$

where U^{qm} is the quantum evolution operator and U^{sc} would be the evolution operator that gives the semiclassical propagator. In figure 5.7 we plot this as a function of I_o and notice that the difference is very small. We also plot the difference between the quantum and the semiclassical sum cut off within $\hbar$ of I_o and find a bigger difference - the contributions within $\hbar$ of I_o are indeed important. Notice also the $\hbar$- periodicity with I_o as expected from its role as a gauge parameter: it is clear from the amount of rotation or shift needed to yield the same quantum mechanics for different I_o's (section 5.3.1) that I_o's differing by $\hbar\times$integer are equivalent.

5.4 Localization in the Stochastic Layer

In this section we find that the long-time properties of the quantized whisker map are very different from those of the classical map. In particular, the eigenstates are exponentially localized in action and consequently transport across the layer is much impeded. This is in contrast to the classical diffusion in action: diffusion is fast deep in the stochastic layer and although it is slowed down near cantori, at long times trajectories roam all over phase-space. A trajectory started deep in the stochastic layer eventually gets out to the

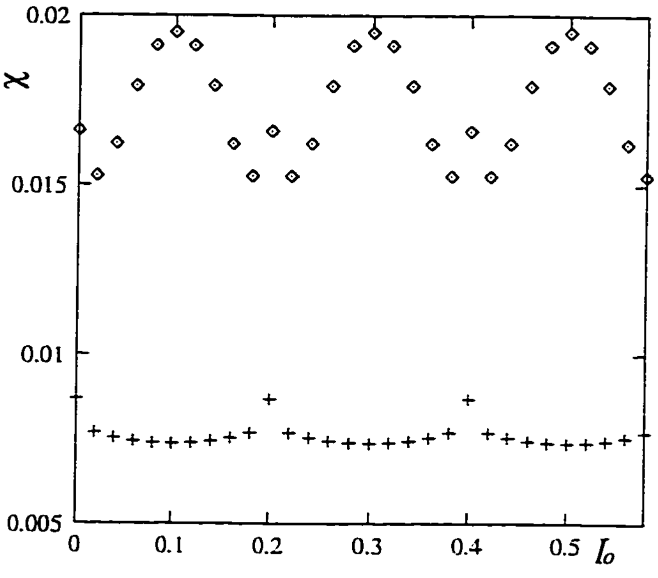

Figure 5.7: Difference between quantum and semiclassical propagators, equation 5.29 as a function of $I_o(+)$. Also plotted is the difference between the quantum and the semiclassical sum cut off within $\hbar$ of $I_o(\diamond)$. Parameters are $\lambda = 10, k = 2, \hbar = 0.2$. The cut-off in action is 20.

border of the regular region whereas in the quantum case the probability is exponentially suppressed. (In fact, the probability to go even three-quarters of the way out may be down by several orders of magnitude, whereas the classical system easily gets there in finite time. Eigenstates centered anywhere within the stochastic layer are localized, although the localization length is not the same everywhere, nor is the localization mechanism. There is an earlier study of localization in the whisker map in [53] which raises some of the issues we discuss here. Our study is an independent one in many ways as will be discussed in the summary 5.4.4. Also, we draw conclusions which are true for quantum transport through generic near-critical cantori.

5.4.1 Time-averaged probability and husimi plots

We may study the long-time properties of a quantized map either by studying its eigenstates, or a closely related property, the time-averaged probability of being at final state $|f\rangle$ having started at initial state $|i\rangle$:

$$P(f,i) = \lim_{T\to\infty} \frac{1}{T} \sum_{t=0}^{T} |\langle f|U^t|i\rangle|^2$$

$$= \sum_n |\langle f|n\rangle|^2 |\langle i|n\rangle|^2 \tag{5.30}$$

where in the last line the sum goes over the quasi-energy eigenstates.

For our purposes there are two particularly useful representations in which to study this object: one is a phase-space representation (a husimi plot), the other is action space. The phase-space representation helps us to understand qualitative aspects of the localization and it also indicates that our quantization is a correct one. We take circular coherent states $\alpha(\theta) = \exp\left(-(\theta - \theta_\alpha)^2/2\hbar + iI_\alpha\theta/\hbar\right)/(\pi\hbar)^{1/4}$ as final and initial states in eqn 5.30. θ_α and I_α denote the center coordinates of the coherent state. Figure 5.8 is a contour plot of the logarithm of the time averaged density in a whisker map of $\lambda = 10, k = 2, \hbar = 0.2$ where the initial coherent state is centered at $\theta = \pi, I = 0$. (I_o is 0.1). The shading reflects the magnitude, with light being high and dark low, however it is important not to be misled by regions of dense contours which make the region look dark when it is not. Such regions indicate a rapid exponential change in the magnitude of the probability. We see structures which we recognize from the corresponding classical phase space: islets of stability centered at $|I - I_o| = (12.3, 6.6)$ and $\theta = \pi(0)$ at $|I - I_o| > 0(< 0)$ respectively. The stochastic layer covers almost all of the shown phase space for these parameters. The shading out from the initial state indicates an exponential decay in the deep stochastic layer. This then meets a series of lines, one set at $|I - I_o| \sim 10$, another set at $|I - I_o| \sim 16$, and yet another at $|I - I_o| \sim 18$. These are at the cantori in the stochastic layer and indeed their shape in the husimi plot resembles their shapes in the classical phase space, figure 5.3. In a time averaged classical phase space they would not be visible, as classical trajectories eventually penetrate them, yet we see that in the quantum mechanical case they act as much stronger barriers. One advantage of the phase-space plot over a plot in action representation, figure 5.9, is that we can clearly see the cantoral curves in phase space. The exponential decay in the deep stochastic layer and at the cantori is clearly seen in the action plot: it is these exponential slopes that will tell us more about the mechanisms for localization across the layer. We shall be studying the slopes in some detail for a whisker map with $\lambda = 5, k = 1.5$. A husimi plot of this for $\hbar = 0.2$ is given in figure 5.10. We notice cantori at winding numbers $1 + \gamma^{-2}$ and $2 - \gamma^{-2}$ (actions $|I - I_o| \approx 5.7$ and 7.64 respectively) We shall come back to this plot shortly.

There is a more efficient way than the expansion in eigenstates of eqn 5.30 to

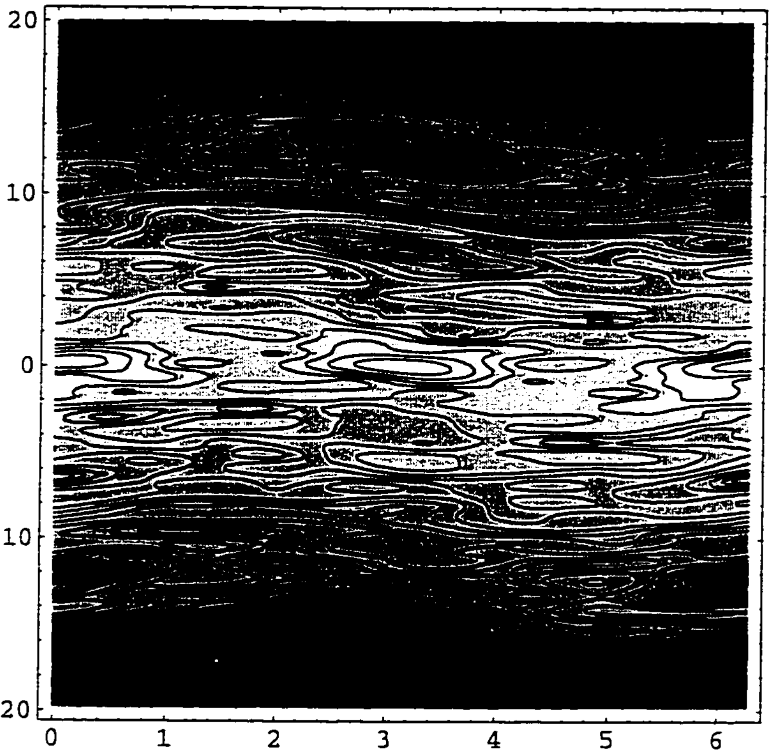

Figure 5.8: Husimi plot with logarithmic contours for the time-averaged probability in the whisker map with $\lambda = 10, k = 2\hbar = 0.2, I_o = 0.1$. Initial state is a coherent state centered at $\theta = \pi, I = 0$.

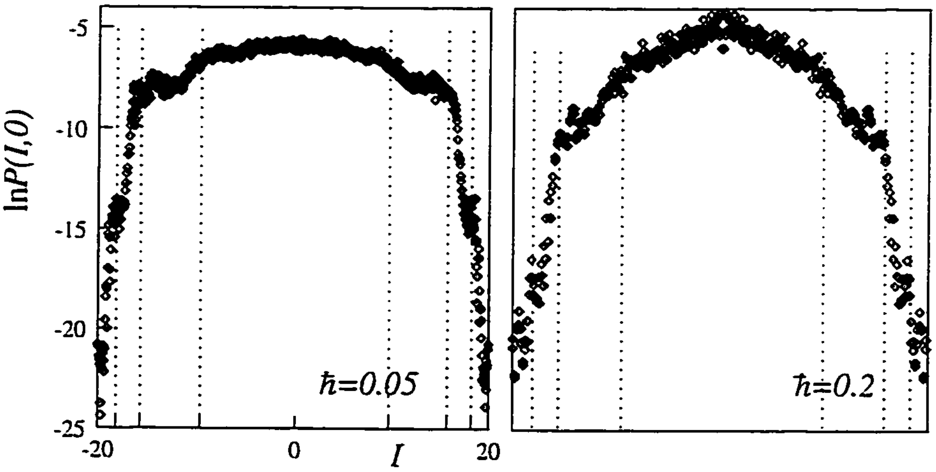

Figure 5.9: $\lambda = 10, k = 2, \hbar = 0.2, I_o = 0.1$, logarithm of the time-averaged probability in action $I = 0$. The dashed lines indicate the cantori (see text).

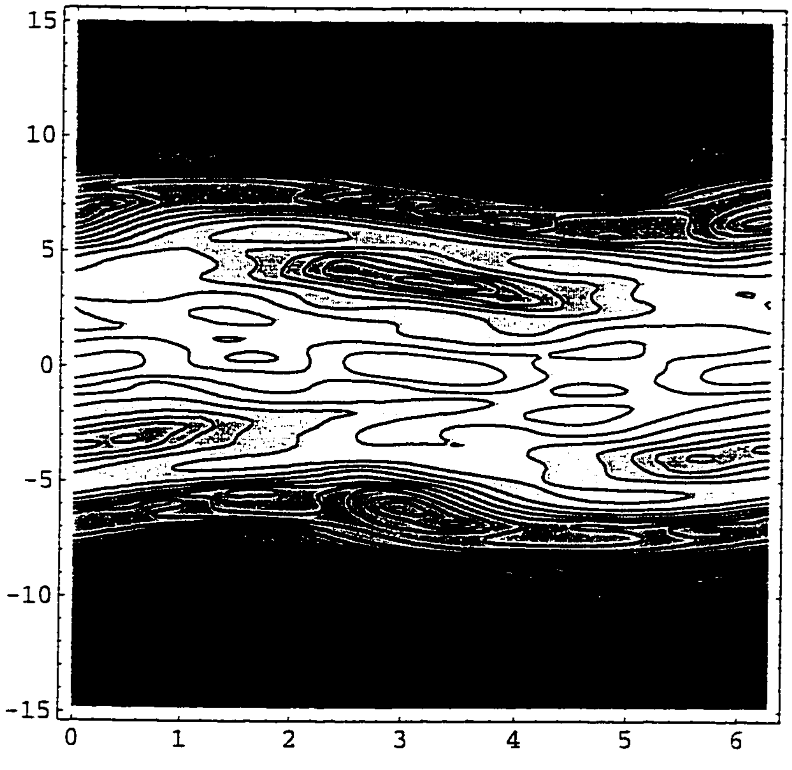

Figure 5.10: $\lambda = 5, k = 1.5$, initial coherent state centered at $\theta = \pi, I = 0$

calculate the time-averaged probability in action. This involves performing a forward and backward fast-fourier transform at each time-step:

$$\begin{aligned}
\langle I_f|U^t|\psi_i\rangle &= \sum_j \langle I_f|U|I_j\rangle\langle I_j|U^{t-1}|I_i\rangle \\
&= \frac{\hbar}{2Ic} e^{-i\lambda(I_f-I_o)\left(\ln\left|\frac{c}{I_f-I_o}\right|+1\right)} \sum_{p=0}^{2I_c/\hbar-1} e^{-i\theta_p I_f/\hbar} e^{ik\cos\theta_p/\hbar} \sum_{j=-I_c}^{I_c} e^{-i\theta_p I_j/\hbar}\langle I_j|\psi_i(t-1)\rangle
\end{aligned} \tag{5.31}$$

where $\theta_p = p\pi\hbar/I_c$. The squared norm of this is then summed over all times. For the computations we used the program "fftw" [57], which held true to its full name ("fastest Fourier transform in the West").

5.4.2 The Deep Stochastic Layer

Let us first discuss the localization deep inside the stochastic layer. It is now pretty well established that for systems which are classically chaotic, the quantized system displays dynamical localization. That is, destructive interference develops in the quantum dynamics which leads to exponentially localized states, putting an end to classical diffusion. Early papers on this are [44, 45, 46] where the standard map at large kicking strength was studied and, in contrast to the classical behavior, the energy was found to be bounded at long times. The energy and momentum become quasiperiodic in time. Crucial for this kind of quantum localization is the existence of two time scales in the classical system [47]: the fast quasi-random jumps in the angle (due to taking mod 2π) and the slower diffusion in action (sec 5.2.2). In some sense this time scale separation can be interpreted as giving rise to a slow almost conserved action variable, and hence localization in this variable [47]. In the classical kicked rotor system $\langle\Delta I^2(t)\rangle = Dt$ grows without bound and for k_s large enough that the angle jumps may be considered independent and random, the diffusion constant is $D = k_s^2/2$. In the classical whisker map if we start in the deep stochastic layer a similar behavior occurs $D = k^2/2$, as described earlier (5.8), until a cantorus is reached and diffusion is slowed down. At short times the quantum system follows classical diffusive behavior. But before $\langle\Delta I^2\rangle$ gets "too big" (which will be quantified shortly) quantum interference between classical paths becomes important and the system begins to localize. $\langle\Delta I^2\rangle$ stops growing and undergoes quasiperiodic behavior in time. In some sense the quantum mechanics is over at what is called the "break time": the system has resolved the finite spectrum and already explored all of its eigenstates. When the classical diffusion is linear in time, as it is for sufficiently chaotic classical systems, as in the deep stochastic layer, the localization length in action may be calculated by the following simple argument ([45]): The quantum system diffuses until the "break time" t_b, and the action explored until this time defines a localization length $\bar{l}$:

$$\langle \Delta I^2(t_b) \rangle = (\bar{l}\hbar)^2 = Dt_b$$

$\bar{l}$ is also the number of eigenstates spanned by the wavepacket from the break time onwards [30]:this, with Heisenberg's uncertainty relation gives a relation between $\bar{l}$ and t_b: if ΔE is the total range of accessed quasienergies and δE the average energy spacing,

$$\bar{l} = \Delta E/\delta E = 2\pi\hbar/\delta E \propto t_b$$

We then arrive at the localization length in action

$$\bar{l}\hbar \propto \frac{D}{\hbar} = \frac{k^2}{2\hbar} \tag{5.32}$$

$\bar{l}$ gives the exponential decay factor for the eigenstates (and time averaged probability) up to a factor: if we assume states to have the form $\psi \sim e^{-\Delta I/l\hbar}$, then the expectation value of the dispersion $\langle \Delta I^2 \rangle$ in this state would be $(l\hbar)^2/2$. Thus the localization length in the time domain $\bar{l}$ is related to the exponential decay localization length in the time-averaged domain l by $\bar{l} = l/\sqrt{2}$. For the kicked rotor, it has been numerically verified in the literature that states are localized with

$$l\hbar = \frac{k_s^2}{2\hbar} \tag{5.33}$$

for large enough k_s. Before we verify numerically that the same relation holds for the whisker map, we note another approach which proves that dynamical localization occurs in kicked-rotor-like and also whisker-like maps. There is a mapping of the standard map on to the problem of a quantum particle in a one-dimensional lattice with random impurities [48]. Such a mapping also exists for the whisker map. In the lattice problem, if the site energies are randomly chosen from some fixed distribution then it can be proven ([49]) that all electron eigenstates are exponentially localized around a lattice site (Anderson localization). The quantum transport vanishes and the quantum particle undergoes quasiperiodic motion. In the quantum kicked rotor or the whisker map there is no randomness in the

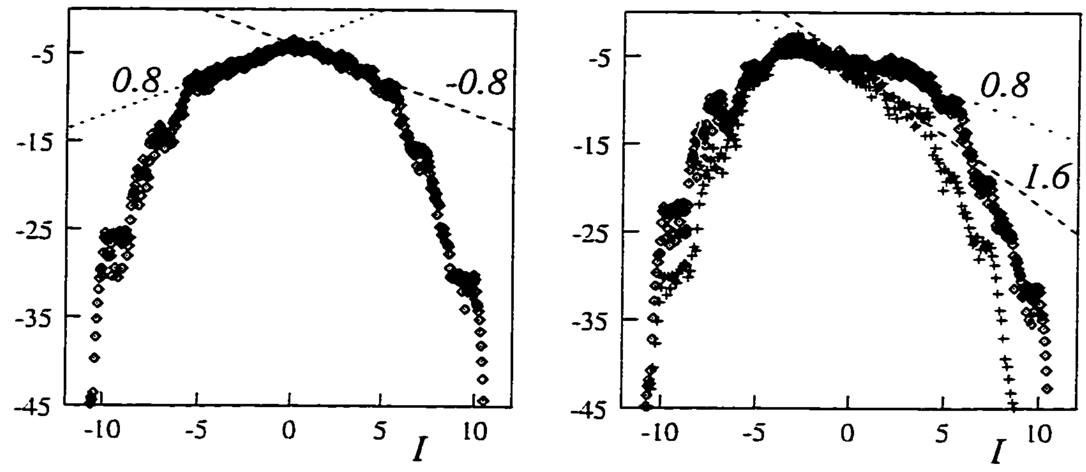

Figure 5.11: Localization slopes in the deep stochastic layer. $\lambda = 20, k = 0.5$. On the left, the initial state is at $I = 0$ and $\hbar = 0.05$; on the right, the initial state is at -3 with $\hbar = 0.05(\diamond)$ and $\hbar = 0.1(+)$. The slopes are as predicted by equation 5.33: slope $= 4\hbar/k^2 = 2/l\hbar$ since $P \sim \exp(-2\Delta I/l\hbar)$.

Hamiltonian, rather the randomness emerges out of the dynamics; hence the term "dynamical localization". In the mapping of the whisker (or the kicked rotor) to the lattice problem it is essentially the kinetic term $K = \lambda(I - I_o)(\ln|c/(I - I_o)| + 1)$, mod 2π, with $I = \hbar \times$integer which plays the role of the site energies. Although this sequence is uniformly distributed in 0 to 2π, there are correlations ($\langle K_m K_{m+r}\rangle \neq 0$) which lead to a pseudorandom rather than random distribution, similar to the case of the kicked rotor [48]. Although no rigorous theorems exist for the pseudorandom case we do expect states are localized: weak correlations do not alter the physics in this case too much.

In figure 5.11 we have plotted the logarithm of the time-averaged probability in the whisker map when $\lambda = 20, k = 0.5$. The slopes in the deep stochastic layer are as predicted by equation 5.33. The much sharper exponential decays further out are due to cantori (see section 5.4.3).

Notice a difference with the kicked rotor: for the kicked rotor k must be large enough in order for the stochasticity to be strong enough to cause destructive interference effects which localize the quantum mechanics. In contrast, for the whisker map, there is in principle no limit on how small k can be in the whisker map: even for a very skinny stochastic layer, provided $\hbar$ is small enough to resolve it and also is smaller than k, we would expect dynamical localization to hold in the middle of the layer. (Recall that the effective local standard map parameter eqn 5.6 goes to infinity here).

There is another important difference with the kicked rotor case: whatever the width of the stochastic layer, the localization length in equation 5.33 may not be realized due to cantori in the stochastic layer. If the quantum distribution reaches a cantorus before it diffuses out to the localization length $\bar{l}\hbar$, there is not enough time for the coherence effects responsible for the Anderson localization length to develop. In figure 5.12 we have plotted the logarithm of the time-averaged probability for $\lambda = 5, k = 1.5$. (We have separated the distributions by displacing them down in action to get a clear picture. Only the slopes matter for current purposes). At $\hbar = 0.2$, the Anderson length breaks down because the cantorus at winding number $1 + \gamma^{-2}$ is reached before the localization length is achieved. The resulting exponential decay is sharper; the localization length is shorter due to the interference of the cantorus. A time domain picture, figure 5.13, elucidates this. The quantum distribution at $\hbar = 0.4$ (top graph) localizes in the deep stochastic layer before the cantorus can have effect, however the quantum distribution at $\hbar = 0.2$ bumps into the cantorus too early. This can be seen by considering the maximum of a distribution of points along $I = 0$ evolved classically. We shall come back to what happens at the cantorus in the next section.

5.4.3 Localization at Cantori

The dynamical localization in the deep stochastic layer does not survive through to the regular region: we notice much sharper exponential decays further out in the stochastic layer, at cantori, the remnants of broken KAM surfaces. (In fact a cantorus may be reached before the deep stochastic localization length $l\hbar = k^2/2\hbar$ can be resolved as we discussed in the previous subsection). Classically we observed that (non-critical) cantori reign in the fast diffusion deeper in the layer, trajectories take many iterations to get out; in the quantum case the transport is much more severely impeded, the probability of penetration being exponentially suppressed. Typically, the further out in the stochastic layer the cantorus is, the steeper is the "cliff" in the logarithm of the time-averaged probability (see for example, figure 5.9).

There are two quite different mechanisms responsible for the exponential decay at cantori: one is dynamical localization, similar physics to that in the deep stochastic layer, but with somewhat different characteristics, the other is a "re-tunneling" where the size of $\hbar$ is such that the quantum mechanics sees a closed surface rather than a broken cantorus

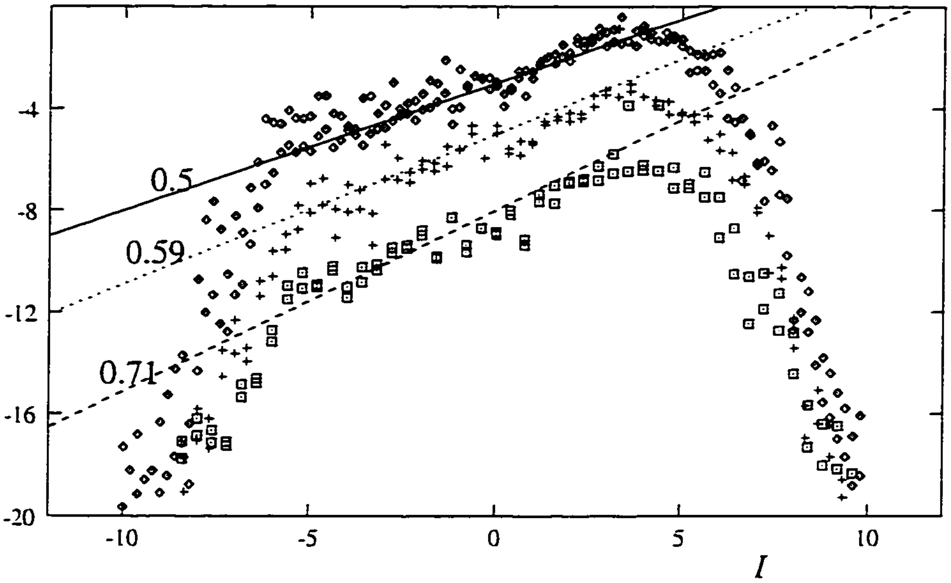

Figure 5.12: Localization slopes in the deep stochastic layer, $\lambda = 5, k = 1.5$. The graphs with $\diamond, +$ and $\Box$ correspond to $\hbar = 0.2, 0.3\dot{3}$,and 0.4 respectively. The slopes for $\hbar = 0.3\dot{3}$ and 0.4 are as predicted by equation 5.33, however the slope for $\hbar = 0.2$ is larger than predicted (smaller localization length); this is due to bumping into the cantorus at winding number $1 + \gamma^{-2}$ before being able to attain the Anderson localization length. See text and figure 5.13.

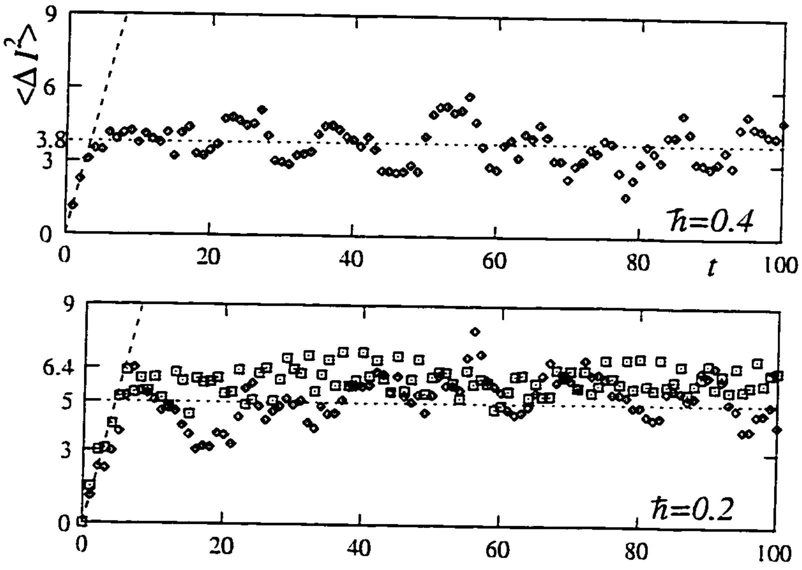

Figure 5.13: Suppression of diffusion in the deep stochastic layer in the quantized map, $\lambda = 5, k = 1.5$. The initial state is an action state at $I = 0$. The top graph shows initial diffusion following classical behavior (dashed line), then localization as predicted by 5.33. In the bottom graph, the cantorus at winding number $1+\gamma^{-2}$ (which has extremal action 6.4) is reached before the Anderson length can be realized. The ◇ is the quantum $< \Delta I^2 >$: the □ is the value of the maximum classical action reached at time t from an initial distribution at 0. The dashed has slope $1.125 = k^2/2$, as the quantum initially follows the classical diffusion. See text and also section 5.4.3.

($\hbar$ is bigger than the gaps in the cantorus). We shall discuss these two effects in some detail: we shall see that the classical scaling properties near a cantorus play an important role in determining the quantitative properties of the localization. Before turning to this we make some observations which will help us understand what is going on.

Preliminary Observations

A phase-space representation helps us to understand some preliminary aspects of localization near a cantorus. First, observe that the contours near a cantorus trace out curves which follow the shape of the cantorus. This is consistent with the observation in [38] of the motion near a cantorus in the *classical* kicked rotor: they found that classical trajectories in a strip around the cantorus tend to follow curves parallel to the cantorus, with a much slower diffusion in a direction normal to the cantorus. Our husimi plots suggest that the quantized system has a related property: the localization mechanism (be it dynamical or re-tunneling) respects this. We expect that the exponential decay occurs not just right at the golden mean cantorus, rather, in a strip around it; again, either from dynamical localization due to slow classical diffusion or from re-tunneling through other cantori in the strip whose gaps are smaller than $\hbar$. This is clear both in the husimi plots and in the action plots. We shall come back to this point soon. Second, when looking at the time-averaged probability in action, it is important to bear in mind the curvature of the phase space caused by k which is evident in the phase-space pictures. Consider figure 5.14 where we focus on the logarithm of the time-averaged probability near the cantorus at winding number $4+\gamma^{-2}$ in the whisker map with $\lambda = 10, k = 2$. The plot where the initial state is deep in the stochastic layer at 0 begins a sharp exponential decay at -16 whereas the onset of sharp decay for starting at -15 is at -17. This is explained by two points: that the cantorus is curved and spans a range of horizontal action states and that there is a "width" associated with each cantorus in which high-order periodic convergents and cantori associated with other very irrational winding numbers lie. A more natural quantum basis associated with a cantorus would be to curve the action state to fit the curvature laid out by the cantorus. From the graph in figure 5.14where we start in the deep stochastic layer, it appears that the cantoral region starts at -16, but in fact that is the value of the extremal action of the inner end of the cantoral strip (not the extremal edge of the actual cantorus but rather, of the cantoral width). The time-averaged probability in action space essentially

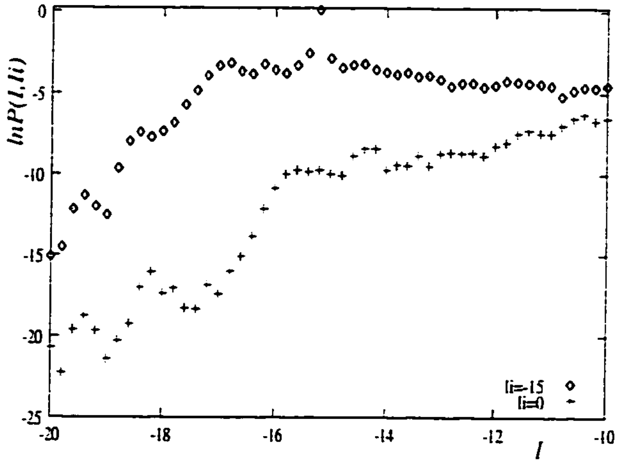

Figure 5.14: $\lambda = 10. k = 2$ and $\hbar = 0.2$, time-averaged probability in action space, where the initial action is $I = -15(\diamond)$ and $I = 0(+)$

projects the husimi plots onto action: the apparent onset of decay in the action plot is at an action which is the extremal action of the inner end of the cantoral strip. The husimi plot of figure 5.8 supports this. Starting at -15 cuts across a range of the "natural" curved states and there is no resistance to being carried across to action -17 by such a curve. This is further elucidated by the husimi plot of the time-averaged propagator having started in the action state -15, as shown in figure 5.15.

Now we have an understanding of where exponential decay near a cantorus starts in phase-space representation and in action representation.

Quantitative Aspects; Dynamical Localization versus Re-tunneling

The quantitative aspects of the time-averaged transport are a consequence of what the classical scaling properties imply for the quantized system. The effect of scaling on quantum mechanics has been discussed to a certain extent in the literature [50, 55]; in the appendix A.3 we provide an outline of the issues and results pertinent to us. To first-order, the scaling properties carry over to the quantized motion near a cantorus, provided Planck's constant is also scaled: the relation [50, 55]

$$\hbar \to |\alpha\beta|\hbar \tag{5.34}$$

joins equations 5.10. However, as time evolves, $\hbar$ gets scaled to larger and larger values and there comes a time when $\hbar$ gets larger than the scaling region ([50] and see A.3). At this

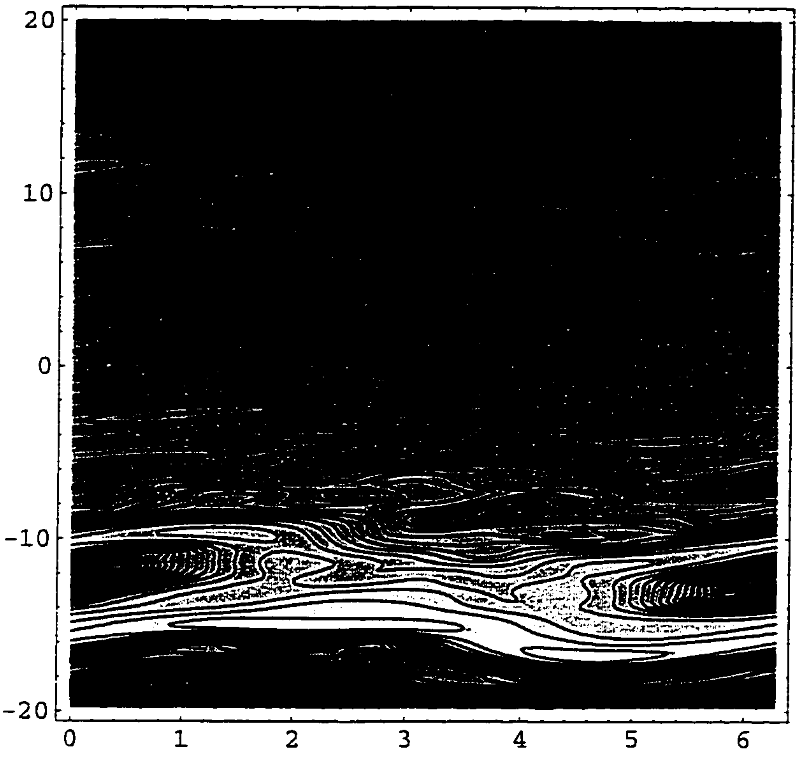

Figure 5.15: $\lambda = 10, k = 2, \hbar = 0.2$, initial action state $I = -15$

time, scaling breaks down as $\hbar$ is too big to resolve the structures which give rise to scaling. The breakdown happens at the time t^* which scales as $t^* \sim \hbar^{-1/\gamma}$, $\gamma = \ln|\alpha\beta| / \ln\omega \approx 3.05$. It is on the same time scale that quantum effects such as interference begin to become important. A consequence of the scaling breakdown for quantum diffusion in the kicked rotor at $k > k_c$ is the onset of localization. Quantum dynamics follows the classical diffusion, scaling with k as does the flux ($\sim (\Delta k)^3$), but begins to keel over at a time that scales with $\hbar$ as $t^* \sim \hbar^{-1/\gamma}$. We refer the reader to [50] for graphs of this behavior. There is some diffusion in action after t^*, albeit slower; the system does not completely localize in the sense of $\langle \Delta p^2 \rangle$ not reaching a steady state until much after. The approach to complete localization is not a simple one.

Armed with this understanding, we now return to the more quantitative aspects of localization at cantori.

Dynamical Localization at Cantori

Classical motion in the scaling region near an open cantorus (*i.e* non-critical) is a slow diffusion in action, the diffusion constant being proportional to the flux transported across the cantorus, ΔW (equation 5.16). We may then expect that the quantum counterpart displays dynamical localization, similar in principle to that in the deep stochastic layer. However the details are quite different: not only is the localization length much longer, since the classical diffusion is slower, but the onset of localization happens at a time scaling like $\hbar^{-1/\gamma}$ (rather than $\hbar^{-2}$) and the subsequent approach to complete localization shows a more complicated dependence on time than in the strong chaotic case (section 5.4.2). The simple argument given there for the localization length in the strong chaotic case no longer holds and we shall see that as a consequence the $\hbar$- and ΔW-dependence of the localization length are more complicated. The slope of the logarithm of the time-averaged propagator gives the exponential decay factor and is inversely related to the localization length. (For ψ of the form $\exp(-2\Delta I/L)$, the decay length L is twice the inverse slope). In figure 5.16 we have plotted the logarithm of this slope at the inner cantorus of the whisker map with $\lambda = 5$ and $k = 1.5$ (see also figure 5.10). This cantorus is at winding number $1 + \gamma^{-2}$ and corresponds to the unperturbed action ~ 5.68. The extremal value of the cantorus is at ~ 6.4.

A typical graph of the time-averaged probability near this is shown in the top graph of figure 5.17. In this figure the initial state is at 4; however most initial conditions decay with about the same slope at the cantori and the error-bars in figure 5.16 account

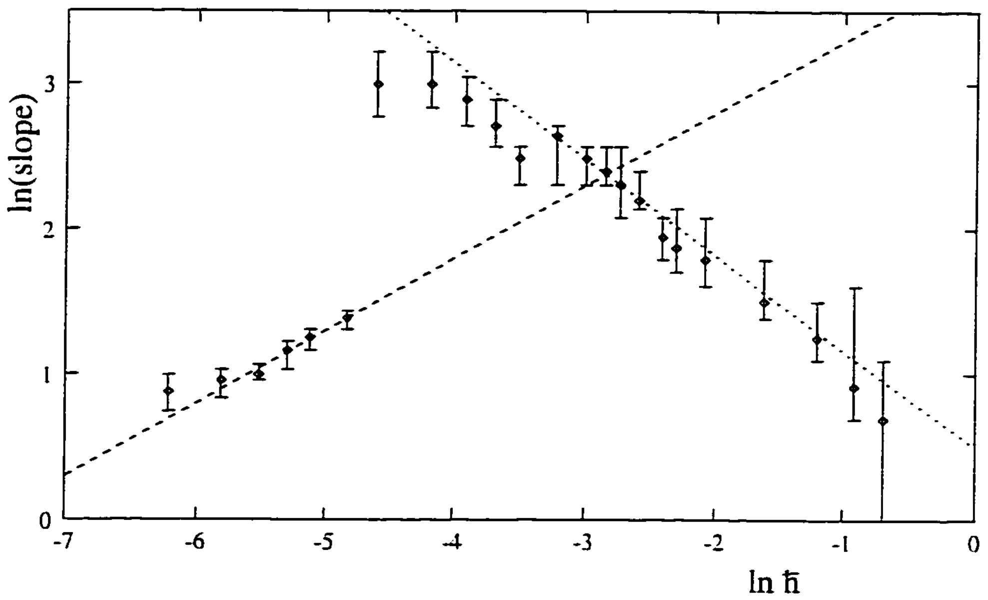

Figure 5.16: Slopes at the inner cantorus (winding number $1+\gamma^{-2}$) as a function of $\hbar$. The classical parameters are $\lambda = 5, k = 1.5$. The dashed lines have slopes 0.5 and -0.66 (see text).

for the variation. Exceptions are when the initial state lies well in the cantoral strip (see section 5.4.3) or when tunneling interactions into resonances around the cantorus enhance the probability of being found there. Classical diffusion in the strip is limited by the flux across the golden mean cantorus (eqn. 5.16) and we expect this to determine the slope in the quantum probability. Near the golden mean cantorus are other cantori with fluxes very close to that of the golden mean cantorus, by continuity. As we move away from the cantorus, because of the resonance structure and the slightly larger fluxes across other broken-up irrational surfaces in the strip, we are not surprised to find that the slope is not uniform as we move out to the borders of the strip. The slope recorded in fig 5.16 is that *at* (the outer edge of) the cantorus. (This is independent of the initial action as said before).

The range in $\hbar$ currently under discussion is the low-$\hbar$ end of the graph ($\ln \hbar < -4$). Notice the slopes increase slower than they would in the strong chaotic case (the slope goes as $\hbar^{\rho}$ where ρ goes something like 0.5 rather than as $\hbar$ as in the deep stochastic layer). One can show that having a slower than linear approach to complete localization in the time domain in an argument along the lines of [45] (see 5.4.2) would lead to an $\hbar$-dependence of the localization length $l\hbar$ weaker than in the linear case ($1/\hbar$). For $\hbar$ too small the localization length would be too large to be resolved within the cantoral width.

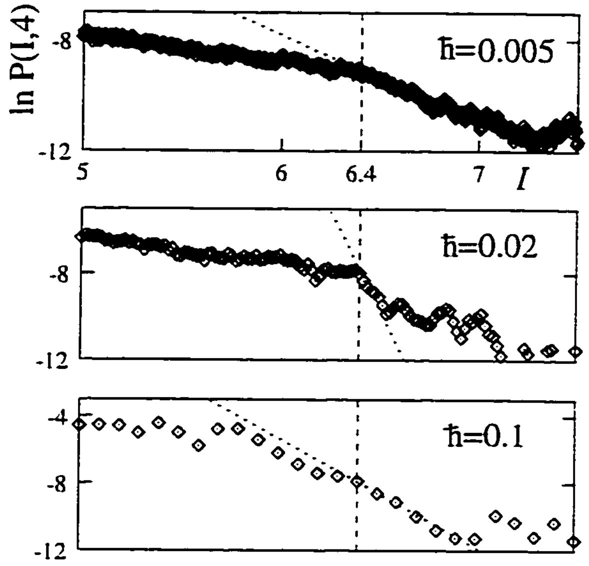

Figure 5.17: Logarithm of the time-averaged probability near the cantorus at winding number $1+\gamma^{-2}$, whose outer edge is at I=6.4. The slopes are 3.2,18 and 6.5 respectively. Note the scale differences on the vertical axis.

We can look at this in the time domain too. as shown in figure 5.18 and the $\hbar = 0.001, 0.008$ traces in figure 5.20. The initial state is at $I = 0$ and all the quantum curves as well as the classical initially diffuse out at the classical rate $k^2/2$ (see figure 5.20). We notice that for small enough values of $\hbar$ the quantum dynamics follows the classical into the cantoral region. This is the $\hbar$ regime we are currently discussing. The quantum states then localize, falling away from the classical distribution at various times after that. We shall come back to these plots shortly.

As the approach to localization is not a simple one we cannot predict the ΔW-dependence of the localization length other than to expect that it goes as some positive fractional power of the flux. We have checked that this is true. Recall that locally the whisker map is a kicked rotor (eqn 5.4). In figure 5.19 we have plotted the slopes of the logarithm of time-averaged probability for the kicked rotor at non-linearity parameter $k_{eff} = \lambda k/|I_{ct} - I_o| = 1.32$ corresponding to the whisker parameters $\lambda = 5, k = 1.5$ at the cantorus at $1 + \gamma^{-2}$. We notice that the quantum kicked rotor slopes are roughly a factor of 1.3 higher than those in the whisker (in the dynamical localization regime). What we can draw from this is that the flux for the whisker is larger than that for the corresponding kicked rotor since we expect that the localization is stronger for a smaller flux. This supports

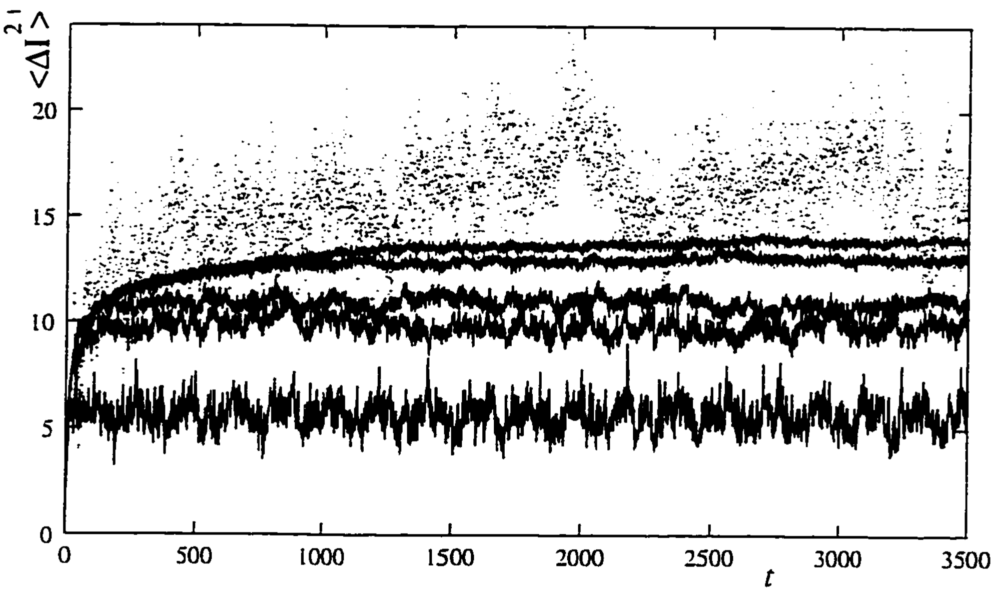

Figure 5.18: $< \Delta I^2 >$ for the whisker map, $\lambda = 5, k = 1.5$. The dots represent a classical average, the curves from the top down are at $\hbar = 0.001, 0.002, 0.008, 0.02, 0.1$ respectively. The dashed line shows the initial classical and quantum diffusion with diffusion constant $1.125 = k^2/2$.

our formula 5.16 over that in [53], 5.18: our formula says that the flux through the whisker cantorus is that through the corresponding kicked rotor times $|I_{ct} - I_o|/\lambda = 1.14$ whereas that of eqn 5.18 says that the factor relating the two is $|I_r - I_o|/\lambda = 0.7$.

Re-tunneling

At a larger value of $\hbar$, the time-averaged probability graph develops a sharp kink at the cantorus (lower two pictures of figure 5.17). This signifies the beginning of a different type of localization mechanism at the cantorus. Quantum diffusion cannot happen for any length of time when $\hbar$ is larger than ΔW, the flux across a cantorus: the quantum mechanics can no longer resolve the gaps (turn-stiles) in the cantorus when $\hbar > \Delta W/\pi$. In fact we first see a kink when $\hbar \approx 0.01$ and indeed $\Delta W/\pi = 0.01$ using our formula 5.16. The barrier to transport caused by the finite $\hbar$ characterizing quantum mechanics is however overcome by a behavior which is also a characteristic of quantum mechanics: tunneling. We shall call this "re-tunneling" to distinguish it from tunneling that generally refers to quantum transport which is classically forbidden. In our case, there is no problem with classical transport across the cantorus, but there is an obstruction to (even short-time) classical-type transport in the quantum mechanics. The slopes plotted in the figures are the

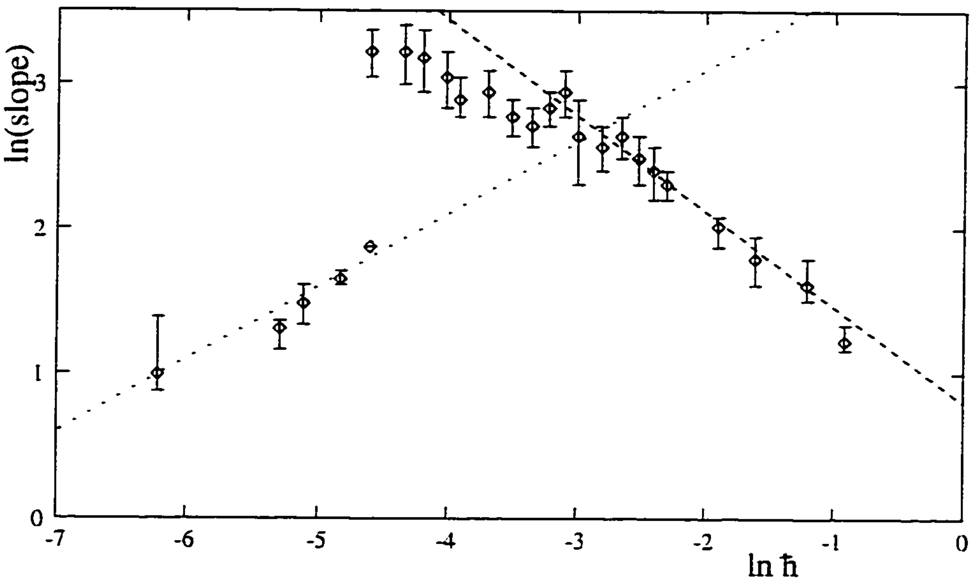

Figure 5.19: Slopes of the quantum kicked rotor, $k_s = 1.32$. The dashed lines have slope 0.5 and -0.66.

local slopes at the cantorus: of course immediately around the cantorus there are typically other cantori with $\hbar > \Delta W$, but also resonance chains. This affects the "overall slope" or overall transport property in the region. However in this figure we concern ourselves only with the local slope at the cantorus. We can see the distinction between exponential decay due to dynamical localization and tunneling in the time domain also. First consider again figure 5.18. It is clear that quantum mechanics at $\hbar = 0.1$ does not manage to diffuse into the inner cantoral region, as it collapses at $\langle \Delta I^2 \rangle \approx 5.7$ just as the corresponding classical distribution has reached the cantoral region (see also fig 5.13 which was for $\hbar = 0.2$). To see whether the higher $\hbar$'s manage to penetrate the cantorus (without having to resort to tunneling over long times), we focus in on shorter times in figures 5.20 and 5.21. Here we have also plotted the maximum of a classical distribution of points with initial $I = 0$ and evenly spaced in angle. The dashed line at 6.4 is the outer edge of the cantorus at $1 + \gamma^{-2}$: the classical distribution gets hung up by this cantorus between about $t = 40$ and $t = 200$. In the range of time plotted in these two figures, the quantum spread at $\hbar = 0.001$ follows the classical average: in this time regime we can think of this curve as representing the classical average. (It in fact penetrates this cantorus and then localizes). The quantum spread at $\hbar = 0.008$ appears to follow the classical into the cantoral region and then fall away and localize shortly before around $t = 200$. It localizes within the cantoral strip (with the

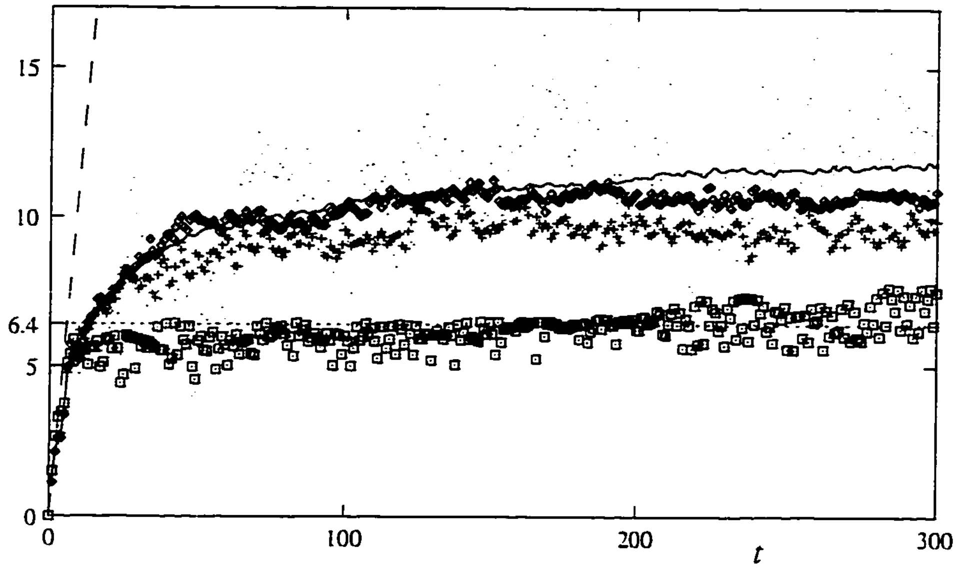

Figure 5.20: $< \Delta I^2 >$ for the whisker map, $\lambda = 5, k = 1.5$. The dots represent a classical average. The curves from top down are at $\hbar = 0.001$ (line), $0.008(\diamond), 0.02(+)$. The $\square$ represents the maximum action of the classical distribution. The dashed line indicates the initial diffusion of all quantum and classical curves, with diffusion constant 1.125.

corresponding localization length in the time-averaged picture as plotted in 5.16). However the graph at $\hbar = 0.02$ never makes it in there: if we look closely, the graph falls away from the classical average (and the smaller $\hbar$ quantum plots) when the classical maximum reaches the edge of the cantorus. $\langle \Delta I^2 \rangle$ can still grow somewhat after that time; that time is when the highest actions in the evolved distribution reach the cantorus, subsequently more of the distribution can diffuse out there and so the expectation value $\langle \Delta I^2 \rangle$ grows. Figure 5.21 shows a similar plot for different $\hbar$'s. The $\hbar = 0.01, 0.02, 0.05$ curves fall away from the $\hbar = 0.001$ (and the classical) when the classical maximum strikes the outer edge of the cantorus. That they all fall away at the same time is another indication that the cantorus presents an un-diffusible barrier to them through which they can only tunnel. (If it was a dynamical localization effect that we were seeing, different $\hbar$'s would fall away at different times.)

From figures 5.16 and 5.19 we observe that the $\hbar$-dependence of the re-tunneling does not go as $e^{-a\Delta I/\hbar}$ as in ordinary tunneling across a KAM torus or a potential barrier. Rather, when $\hbar$ is somewhat bigger than ΔW it fits a dependence more like $e^{-a\Delta I/\hbar^\sigma}$ where σ is a fraction like 0.66. When $\hbar \simeq \Delta W$ or a bit larger, the dependence is weaker. We shall

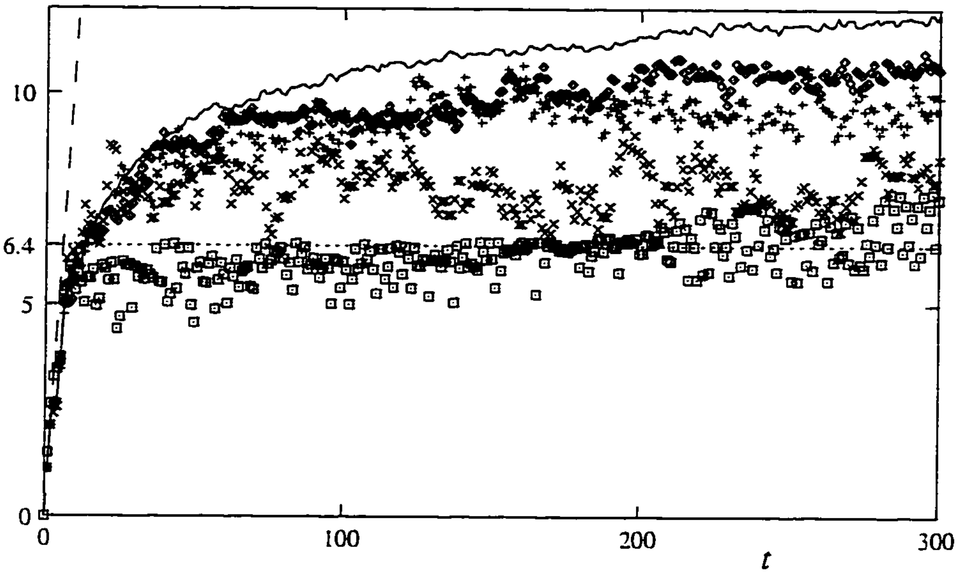

Figure 5.21: As in figure 5.20 but with the quantum data being at $\hbar = 0.001, 0.01, 0.02, 0.05$ respectively.

come back to this shortly.

First we note that there is another effective cantorus in this whisker map, one at winding number $2 - \gamma^{-2}$, with unperturbed action 7.64. This cantorus is very close to criticality, with $k_{eff} \approx 0.98$. Figure 5.22 shows a logarithmic plot of the slope of the logarithm of the time averaged probability at this outer cantorus. Again, the $\hbar$-dependence of the re-tunneling in this near-critital cantorus is close to $e^{-a\Delta I/\hbar^{0.66}}$. In the *critical* case, this exponent has been previously discovered in the quantum kicked rotor. We now turn to a discussion of this.

For a *critical* cantorus ($\Delta W = 0$) of the kicked rotor it has been found numerically that the tunneling probability goes as $\hbar^{-\sigma}$ where $\sigma \approx 0.66$ [52]. In [50], this exponent is shown to be related to scaling exponents in this region. We give a different (but related) argument to that in [50]: one based on perturbation theory. Consider the basis of deformed action states, which have curvature in phase space following the curvature of the nearby cantorus. Let us label these states by their extremal value of action $|I_m^{ex}\rangle$. Then , in the neighborhood of a near-critical cantorus, a transition between two such curved states $|I_m^{ex}\rangle$ and $|I_n^{ex}\rangle$ is very weak; as we have seen in the husimi plots, the transition is exponentially small, and in the classical picture, trajectories follow along the curve but transport between different curves is very slow. In such a case, we might expect a perturbation matrix element

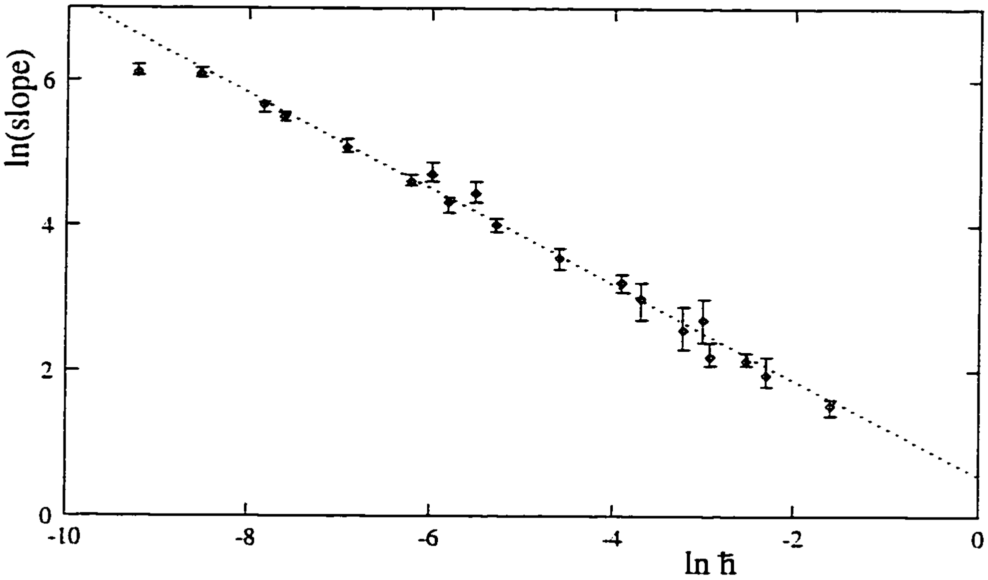

Figure 5.22: Slopes at the outer cantorus (winding number $2-\gamma^{-2}$). The slope of the dashed line is -0.66.

could well give the transition probability amplitude and hence the tunneling rate across the cantorus. If v is the appropriate perturbation potential for this, then

$$\begin{aligned} \langle I_m^{ex}|v|I_n^{ex}\rangle &= v(\Delta I,\hbar,\Delta k) \\ &= \beta^{-r} v(\beta^r \Delta I, |\alpha\beta|^r \hbar, \delta^r \Delta k) \end{aligned} \tag{5.35}$$

where in the first step we have expressed the amplitude in terms of all the parameters it could depend on and in the second step we have used scaling properties (see A.6). We use the shorthand ΔI for $I_m^{ex} - I_n^{ex}$. Let us first consider a critical cantorus where $\Delta k = 0$. r is arbitrary and at criticality we can choose it such that all the $\hbar$-dependence appears in a factor in front on ΔI: letting $r = -\ln\hbar/\ln|\alpha\beta|$, then

$$v(\Delta I,\hbar,0)|_{criticality} = \hbar^{\sigma} v(\hbar^{-\sigma}\Delta I, 1, 0) \tag{5.36}$$

where

$$\sigma = \left(1 + \frac{\ln|\alpha|}{\ln|\beta|}\right)^{-1}$$

This implies that, in the critical case, whatever the transition matrix element may be, $\hbar$ and action appear together as $\Delta I/\hbar^{\sigma}$. This then gives the tunneling dependence. Now near the subdominant symmetry line, $\sigma \approx 0.65$ whereas near the dominant symmetry line

$\sigma \approx 0.76$: the numerically measured value 0.66 is very close to that near the subdominant symmetry line. Before we discuss this, we note that this result was also obtained in [50] where scaling was invoked similarly but inside a time-integral whose upper limit extended to infinity. Scaling does not hold for most of the times in the integral. Their result turns out to be valid since numerical evidence shows that the exponential dependence of the integral is almost independent of time. But why this is so, is still an open question.

We suggest that the subdominant symmetry line provides the pertinent scaling exponents for tunneling by the following argument: in the cantoral region the motion follows curves parallel to the cantorus, moving through all angles. The overall quantum tunneling across the curves will then be dominated by the scaling exponents giving the smallest σ and this is at the subdominant symmetry line. We do not think that this has anything to do with the extremal action at the cantorus being near the subdominant line as is suggested in [50, 52]: first, as is supported by our husimi plots, this region does not distinguish itself from the other angles: we re-iterate that the contours near the cantorus evenly follow curves parallel to the cantorus and the classical motion does this also. We tried to test their hypothesis in a numerical study: we compared the slopes for entering the cantoral region from one side to that for entering from the other side. The relevant extremal actions are clearly at different angles: for example for a whisker cantorus at $I > I_o$, the extremal action from entering at actions below the cantorus is around $0 - 1$ but for entering from actions above the cantorus the extremal action is around $4 - 5$. Yet, there was no discernible difference in the slopes. (In [50, 52] only one direction of approach was considered). We do recognize that the difference between a dependence like $\hbar^{0.65}$ and $\hbar^{0.76}$ would be a small one, however there was no such difference that we could detect.

We comment now on the non-critical case. For "classically open but quantum-mechanically closed" cantori (*i.e.* non-critical but with $\hbar > \Delta W$) it is not so simple to come up with a form for v that bundles all the $\hbar$- and ΔI-dependence together. If we use the same r as above, $\delta^r \Delta k \to \hbar^{-\ln\delta/\ln\alpha\beta}\delta k$. Evaluating the exponent and writing in terms of the flux, we get

$$\langle I_m^{ex}|v|I_n^{ex}\rangle| = \hbar^{\sigma} v(\hbar^{-\sigma}\Delta I, 1, (\Delta W/\hbar)^{1/3}) \tag{5.37}$$

Although we cannot conclude a general dependence from here, we can say that when $\hbar \gg \Delta W$, we expect the dependence to tend towards that of the critical case, $\hbar^{-\sigma}\Delta I$. Our numerical results support this (figures 5.22, 5.19 and 5.16). This is what we might expect:

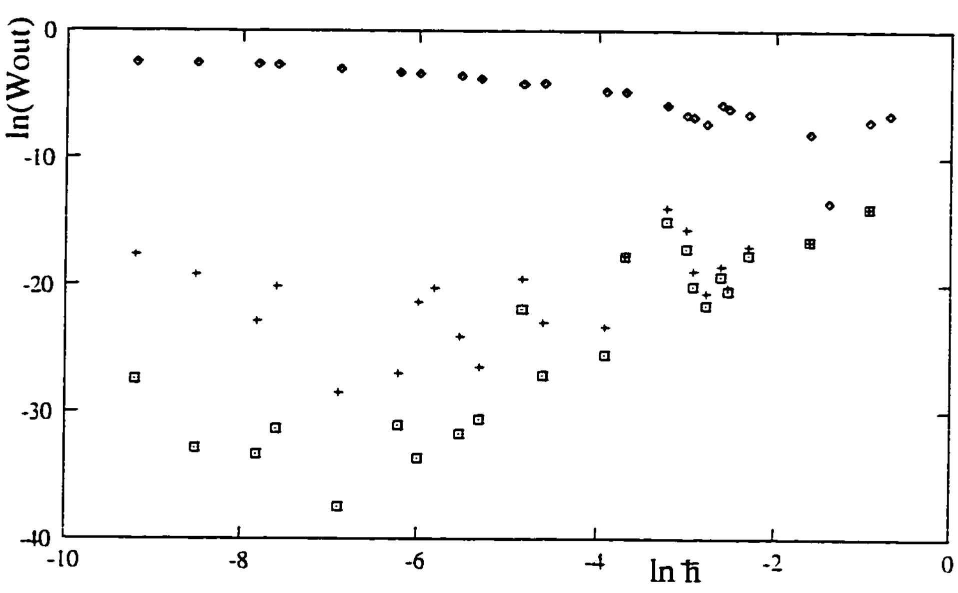

Figure 5.23: Probability of being found outside the inner cantorus (◇), outer cantorus (+) and inside the regular region (□)

if $\hbar \gg \Delta W$, to the quantum mechanics, the cantorus and its immediate neighborhood does not look that different from criticality.

Finally, as an indication of the overall transport properties through a stochastic layer, we plot in figure 5.23 the probability of being found anywhere outside the outer bend of the inner cantorus, the outer cantorus and anywhere in the regular region having started in the deep stochastic layer at 0:

$$W_{out} = \sum_{I > I_{lim}} P(I, 0) \tag{5.38}$$

where I_{lim} is outermost bend of the respective cantorus (or torus, in the case of the regular region). Because this is an indication of "overall" slopes in regions of the layer, we do not expect the behavior to have a simple dependence on $\hbar$.

Quantum Kicked Rotor at criticality.

We now wish to clarify a point made in the literature which is perhaps misleading. The kicked rotor *at* criticality is numerically studied in [52] where a major result is that the probability distribution decays exponentially at the extremal value (*i.e* the outermost bend) of a critical cantorus as $e^{-a|p-p_c^+|/\hbar^\sigma}$, $\sigma = 0.66$. Yet it is evident from the close-up pictures around the peak of the distribution figure 5.24 that the onset of exponential decay depends on where we start: if we begin at 3, the exponential decay near the golden mean cantorus of winding number $\gamma - 1 = 1 - \gamma^{-2}$ starts close to 4, whereas for values of the initial action displaced from 3, the decay begins at actions displaced by roughly the same amount. The extremal value of the golden mean torus is 4.269. There are two observations which we have raised in previous sections, regarding the classical phase space which explain this. They are closely related to the issues discussed in section 5.4.3. First, just as we discussed there, a natural basis for the phase space would be states that followed the curvature of the phase space near the golden mean. Classical trajectories near the cantorus tend to follow such curves: the periodic orbit chains approximating the cantorus have this curvature. Any I-state cuts across several of these natural curves, so an initial I can be easily carried across to any other I-value that cuts across these curves. So the quantum time-averaged probability shows almost no decay until a limiting action, the extremal action that can be reached by any of the natural curves that the initial action state lies on. As the initial action state changes, the limiting value of the action changes correspondingly. The onset of the exponential decay is where this limiting action is, *not* at the extremal I of the cantorus as suggested in the literature. The decay then occurs over a range of actions, because close to the critical cantorus the transport from one extremal action to another is very slow classically, which leads to either a short localization length in the quantum mechanics or re-tunneling. This is as described in the above chapters.

5.4.4 Summary

We have presented a study of the classical and quantum dynamics of the whisker map. This problem is of considerable interest from the point of view of quantum mechanics, semiclassics and classical mechanics for a number of reasons. It is a study of quantum behavior in a stochastic layer near a typical separatrix.

Its quantization in angle-representation may at first seem hopeless, because of the infinite number of infinitesimally close intersections within $\hbar$ of each other in phase space that must be summed. Yet these pose no problem, each representing a different, topologically independent classical contribution.

The classical whisker map has very interesting dynamics and dynamical structures, the quantization of which tells us much about quantum behavior in classically stochastic regions in general systems and in the much less stochastic regions near critical structures

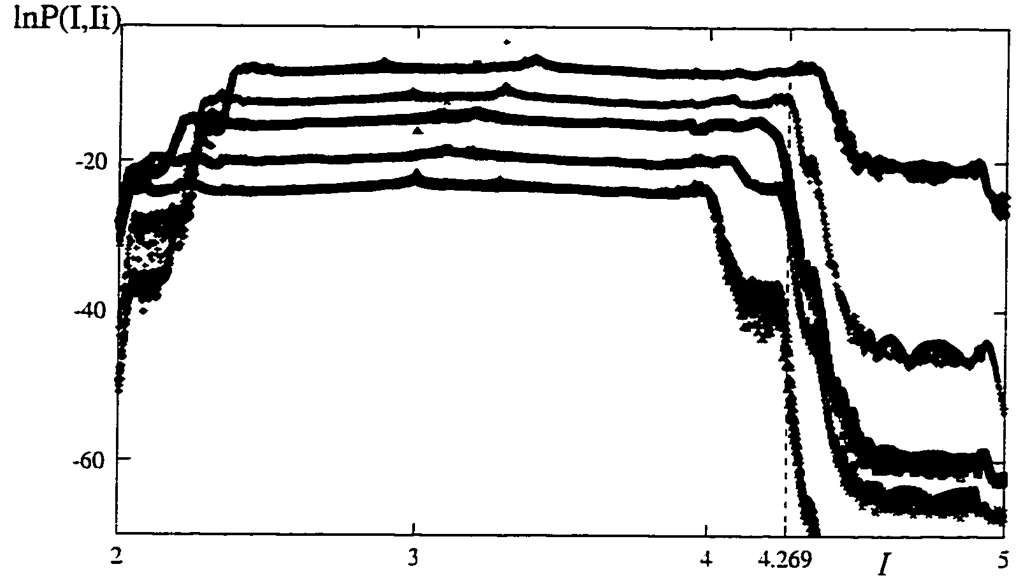

Figure 5.24: Quantum kicked rotor at criticality, $\hbar = 0.001$. Initial actions are, from top to bottom, 3.4, 3, 3, 3.2, 3.1, 3.

in general systems. We show how a local effective standard map parameter can tell us much about the degree of stochasticity in the layer in the classical map and also about the flux through cantori. Deep in the stochastic layer, where the classical dynamics is one of diffusion at a rate determined by the action-jump parameter, the quantum states, in contrast, are exponentially localized. This phenomenon, dynamical localization, or Anderson localization, is well-established, being first discovered in the kicked rotor at large kicking parameter. We find the same behavior in the whisker map, however the cantori further out in the stochastic layer may prevent the Anderson length from being realized.

There may be several effective cantori in the layer, increasing in their effectiveness to slow down transport the further out in the layer they are. This brings us to a major part of the study: localization mechanisms and $\hbar$-dependences of transport properties at cantori. We point out that our new results concerning this hold not just for cantori in the whisker map, but rather for any non-critical cantori in generic maps due to the universality of behavior near cantori. We found there were two mechanisms resulting in quantum exponential decay at cantori: one, when $\hbar < \Delta W$, is a dynamical localization similar to that in the deep stochastic layer, the other, at $\hbar > \Delta W$ is a re-tunneling when quantum mechanics sees a closed cantorus, due to the finite $\hbar$ being too big to resolve the gaps. Both mechanisms have different characteristics and $\hbar$-dependences than the usual dynamical localization and ordinary tunneling as described in the text. This is due to the intricate structure of the phase space there and the resulting scaling properties. Which mechanism is at work can be deduced either by looking in the time domain or at a time-averaged probability. That cantori act as stronger barriers in the quantum case than in the classical has been discussed before in the literature ([52, 50]); it is however specifically the re-tunneling phenomenon that is discussed for $\hbar > \Delta W$ and only at criticality is the $\hbar$-dependence discussed. We point out here that cantori can be strong (exponential) barriers also when $\hbar < \Delta W$, as we have seen above. We also show that there are good indications that the exponential $\hbar$-dependence which is discussed at the critical kicked rotor cantorus in the literature, holds for an almost critical cantorus in the whisker map and also holds for non-critical cantori provided $\hbar$ is somewhat bigger than ΔW. Numerical evidence as well as an argument based on scaling and perturbation theory imply this. We stress again that these properties should hold for generic cantori.

We present a phase-space representation of the quantum mechanics which shows the cantoral regions in the quantum mechanics more clearly than in an action representation. This picture is also useful to bear in mind when considering behavior near cantori and the onset of exponential decay.

Localization in the quantized whisker map was observed in the study of [53], which was largely qualitative. They discuss Anderson localization deep in the stochastic layer, however they state a condition that implies this cannot coexist with localization at cantori. They demonstrate that cantori act as exponential barriers in the case when $\hbar > \Delta W$; we expand on this in several ways as described above. We provide a calculation of the (classical) flux through a whisker cantorus based on considering a local standard map there, which our numerical results show is a better approximation to the flux than the formula used in [53].

We have discussed cases where the classical parameters of the map are bigger then $\hbar$. We have not discussed for example when $k << \hbar$, where the jump in action is too small to transport across even one state in action. This kind of effect was first studied by Shuryak [56] and was also discussed in [53]: the quantum behavior is close to unperturbed behavior. Another example not studied is when the stochastic layer has width smaller than $\hbar$. The quantum mechanics smears over the layer, and appears not much different than in the regular case.

Because the whisker map describes motion near a separatrix in a generic near-integrable system we also believe that the results of our study may help understand aspects of behavior in generic mixed systems, like transport properties across separatrices.

Tunneling Across a Stochastic Layer.

The whisker map has the discrete phase space symmetry

$$T : \theta \to \theta + \pi \,(\mathrm{mod} 2\pi), \quad I - I_o \to -(I - I_o)$$

However, under T, the whisker Hamiltonian, equation 5.19, changes sign. This discourages tunneling across the stochastic layer, because the quasi-energies of corresponding states (*e.g.* period 1 islands) which are related by T are almost equal but opposite each other.

In order to look at tunneling across a stochastic layer, we can however modify the whisker map to obtain a symmetric kinetic term: consider the map

$$\begin{aligned} I &= I + k\sin\theta \\ \theta' &= \theta + \lambda \mathrm{sgn}(I' - I_o) \ln\left|\frac{c}{I' - I_o}\right| \end{aligned} \tag{5.39}$$

where sgn represents the signum function, $\mathrm{sgn}(I' - I_o) = 1(-1)$ if $(I' - I_o) > 0(< 0)$. The Hamiltonian becomes

$$\tilde{H} = \lambda|I - I_o| \left(\ln|c/((I - I_o)| + 1\right) - k\cos(\theta) \sum_n \delta(t - n).$$

Under the symmetry

$$\tilde{T} : \theta \to -\theta \,(\mathrm{mod} 2\pi), \quad I - I_o \to -(I - I_o)$$

not only is the map invariant, but so is the Hamiltonian. The quasi-energies of related states across the stochastic layer are now near-degenerate. The quasi-energy eigenstates appear now as doublets across the layer. We can use this modified map to study the nature of the tunneling across a stochastic layer. This raises many interesting questions. It has been found that tunneling across a few isolated resonance zones is controlled by the particular resonance in the zone corresponding to the quantum number difference between the two tunneling states [58]. (Also see for example [59] for a review of approaches to tunneling in mixed phase-space systems). We may think of the stochastic sea as a convergence of resonance zones: then does the tunneling matrix element between two states across the sea simply pick out the resonance chain with the appropriate quantum number ratio? Another question relates to the role that chaos may play in the tunneling process: it has been found that chaos can enhance the tunneling probability in some studies [60], for example, by picking up an exponentially small tail of a state on a torus and carrying it to the other side. How the localization of states in the stochastic layer affects this is another question we leave to further study.

Bibliography

[1] N.T. Maitra and E.J. Heller, *Phys. Rev. A* **54**(6), 4763 (1996).

[2] L.D. Landau and E.M. Lifshitz, *Quantum Mechanics (Non-relativistic Theory)*, Pergamon Press, New York, (1977).

[3] R. Feynman and A. Hibbs, *Quantum Mechanics and Path Integrals*, McGraw-Hill, New York (1965).

[4] B.R. Holstein and A.R. Swift, *Am.J.Phys.* **50**(9), 829 (1982).

[5] M.V. Berry and K.E. Mount, *Rep.Prog.Phys.* **35**, 315 (1972).

[6] L.S. Schulman, *Techniques and Applications of Path Integration*, Wiley, New York, (1981).

[7] M.C. Gutzwiller, *J.Math. Phys.* **8**(10), 1979 (1967).

[8] N.T. Maitra and E.J. Heller, *Phys. Rev Lett.* **78** (16), 3035 (1997).

[9] N.T. Maitra and E.J. Heller, *Classical, Semiclassical and Quantum Dynamics in Atoms*, Springer Lecture Notes in Physics, Eds. H. Friedrich and B. Eckhardt, Berlin (1997).

[10] M.J. Davis and E.J. Heller, *J. Chem. Phys.* **75**, 246-54 (1981).

[11] E. J. Heller. *J. Phys. Chem.* **99**, 2625 (1995).

[12] A. M. Ozorio de Almeida, *J. Phys. Chem.* **88**, 6139 (1984).

[13] F.L. Roberts and C. Jaffé, *J. Chem. Phys.* **99**, 2495 (1993).

[14] T. Uzer and R. A. Marcus, *J. Chem. Phys.* **81**, 5013 (1984).

[15] T. Uzer, D.W. Noid and R.A. Marcus, *J. Chem. Phys.* **79**, 4412 (1983).

[16] M. Carioli, E.J. Heller and K. Möller, *J. Chem. Phys.* **106**(20), 8564 (1997).

[17] Lebedev N.N., *Special Functions and Their Applications*, Dover Publications Inc., New York (1972).

[18] Rajaraman R. *Phys. Rep.* **21c**, 227 (1975).

[19] Keshavamurthy S. and Miller W.H. *Chem. Phys. Lett.* **218**, 189 (1994).

[20] Grossman F. and Heller E.J. *Chem. Phys. Lett.* **241**, 45 (1995).

[21] C. Grosche and F. Steiner, *J. Math. Phys.* **36**, 2354 (1995).

[22] H. Kleinert and I. Mustapic, *J. Math. Phys.* **33**, (2) 643 (1992).

[23] W. H. Miller *Adv. Chem. Phys.* **XXV**, 69, (1974).

[24] N. L. Balazs and A. Voros (1989) *Annals of Physics* **199**, 123 (1989).

[25] L. Kaplan, N. T. Maitra and E. J. Heller, *Phys. Rev. A* **56** (4), 2592 (1997).

[26] For example, P. A. M. Dirac, *Lectures on Quantum Mechanics*, Academic Press, New York (1967); M. C. Gutzwiller, *Chaos in Classical and Quantum Mechanics*, Springer-Verlag, New York (1990); K.S. Cheng, J. Math. Phys, **13**, 1723 (1972); B.S. Dewitt, Phys. Rev **85**, 653 (1952); see reference [25] for more references.

[27] M. K. Ali, *Can. J. Phys.* **74**, 255 (1996).

[28] V. I. Arnol'd, *Mathematical Methods of Classical Mechanics*, Springer-Verlag, New York (1978); C. Lanczos, *The Variational Principles of Mechanics*, Dover (1986).

[29] G.M. Zaslavski and N.N. Filonenko *Sov. Phys. JETP* **38**, 317 (1974); M.V. Berry and M. Tabor *Proc. R. Soc. Lond* **A349**, 101 (1976); M.V. Berry in *Les Houches Session XXXVI 1981, Chaotic Behavior of Deterministic Systems* eds. G. Iooss, R. H. Helleman, R. Stora, North-Holland, Amsterdam (1983).M. L. Mehta *Random Matrices and the Statistical Theory of Energy Levels*, Academic, New York (1965); C. E. Porter (ed.) *Statistical Theory of Spectra*, Academic, New York (1965).

[30] B.V. Chirikov *Phys. Rep.* **52**, 263 (1979).

[31] A.J. Lichtenberg and M.A. Lieberman, *Regular and Chaotic Dynamics*, Springer-Verlag, New York (2nd ed) (1992).

[32] V.I. Arnold, *Dokl. Akad. Nauk. SSSR* **156**, 9 (1964).

[33] S. Cocke and L.E. Reichl, *Phys. Rev. A* **41**(7), 3733 (1990).

[34] J.M. Greene, *J.Math. Phys*, **20**, 1183 (1979).

[35] S.J. Shenker and L.P. Kadanoff J. Stat. Phys. **27**, 631 (1982).

[36] R.S. MacKay, J.D. Meiss and I.C. Percival *Physica* **13 D**, 55 (1984).

[37] R.S. Mackay *Physica* **7D**, 283; in *Nonlinear dynamics of particle accelerators*, Ed.s J.M. Jowett, M. Month, S. Turner, Springer Lecture Notes in Physics 247, 390 (1986).

[38] I. Dana and S. Fishman *Physica* **17D**, 63 (1985).

[39] D.F. Escande and F. Doveil *J. Stat. Phys.* **26**, 257 (1982)

[40] D. Bensimon and L.P. Kadanoff *Physica* **13 D**, 82 (1984).

[41] A.N. Kolmogorov, *Dokl. Akad. Nauk. SSSR* **98** 527 (1954); V.I. Arnold, *Soviet Math. Dokl.* **2** 501 (1961); J. Moser *Nachr. Akad. Wiss. Göttingen, Math. Phys.* Kl. 1.

[42] I. Percival, *Nonlinear Dynamics and the Beam-Beam Interaction*, Ed.s M. Month ad J.C. Herrera, Am Inst. of Physics Conf Proc No 57, 302 (1979); S. Aubry in *Solitons and Condensed Matter Physics*, Ed.s A.R. Bishop and T. Schneider, Springer, Berlin, 264 (1978); J.N. Mather *Topology* **21**, 457 (1982).

[43] R.S. MacKay and J.D. Meiss, *Phys. Rev A* **37**, 4702 (1988).

[44] G. Casati, B.V. Chirikov, F.M. Izrailev and J. Ford in *Stochatsic Behavior in Classical and Quantum Hamiltonian Systems* **93** of Lecture Notes in Physics, Eds. G. Casati and J. Ford, Springer, Berlin (1979)

[45] B.V. Chirikov, F.M. Izrailev and D.L. Shepelyansky *Sov. Sci Rev. Sec. C***2**, 209 (1981).

[46] Hogg and B.A. Huberman, *Phys. Rev. Lett.* **48**, 711 (1982).

[47] F. Haake *Quantum Signatures of Chaos*, Springer-Verlag, Berlin Heidelberg (1991).

[48] D.R. Grempel, R.E. Prange and S. Fishman *Phys. Rev. A* **29** (4), 1639 (1984).

[49] P.W. Anderson *Phys. Rev. Lett.* **109**, 1492 (1958); P.W. Anderson *Rev. Mod. Phys.* **50**, 191 (1978);

[50] S. Fishman, D.R. Grempel and R.E. Prange *Phys. Rev. A* **36** (1), 289 (1987).

[51] J.H. Jensen and Q. Niu *Phys. Rev. A* **42**, 2513 (1990).

[52] G.Radons, T.Geisel and J.Rubner, *Adv. Chem. Phys.* **73**, 891 (1989); T.Geisel, G.Radons and J.Rubner, *Phys. Rev. Lett.* **57**, 2883 (1986).

[53] N. Bubner and R. Graham, *Phys, Rev. A* **43** (4), 1783 (1991).

[54] M. Tabor, *Chaos and Integrability in Nonlinear Dynamics*, John Wiley & Sons Inc., New York (1989).

[55] G. Györgi, R. Graham, R.E. Prange *J. Stat. Phys.* **68** (1/2), 175 (1992).

[56] E.V. Shuryak, *Sov. Phys. JETP* **44** 1070 (1976).

[57] M. Frigo and S.G. Johnson (MIT) http://theory.lcs.mit.edu/ fftw

[58] E.J. Heller *J. Phys. Chem.* **99**, 2625 (1995).

[59] S. Creagh in *Tunneling in Complex Systems*, Ed. S. Tomosovic, World-Scientific, Singapore (1998).

[60] S. Tomsovic and D. Ullmo *Phys. Rev. E* **50**(1), 145 (1994); O. Bohigas, D. Boosé, R. Egydio de Carvalho and V. Marvulle, *Nucl. Phys.* **A560**, 197 (1993).

Appendix A

Appendix

A.1 KAM convergents and scaling relations

We refer the reader to the literature, for example,[31, 34, 35, 36, 37, 39] and more references therein for detail of what we are about to review.

A big clue to understanding the scale-invariance and hence the dynamics, comes from a study of periodic orbits near the KAM whose winding numbers are successive approximants to the irrational of the KAM [34]. A winding number w may be expressed in a continued fraction expansion:

$$w = a_o + \cfrac{1}{a_1 + \frac{1}{a_2 + \frac{1}{a_3 + \dots}}} \equiv [a_o, a_1 ....]$$

where the partial quotients a_i are positive integers. Rational numbers have a finite expansion, whereas irrationals have an infinite number of partial quotients. The larger a_N is the closer $[a_o, a_1 .... a_N]$ is to $[a_o, a_1 .... a_{N-1}]$. It is perhaps not surprising then that the number that is "farthest from the rationals", the golden mean, has continued fraction representation

$$\gamma = \frac{\sqrt{5}+1}{2} = [1, 1, 1....].$$

Truncating the continued fraction expansion after n partial quotients gives an approximation to the irrational, called the nth convergent. For example, convergents to γ are F_{i+2}/F_{i+1} and convergents to $1/\gamma$ are $W_i = F_i/F_{i+1}$ where F_i are the Fibonacci numbers, defined by $F_o = 0, F_{i+1} = F_i + F_{i-1}$. The first few are $0, 1, 1, 2, 3, 5, 8, 13....$ The cycles converge to the KAM at a rate $\delta = \lim_{i \to \infty}(W_{i+1} - W_i)/(W_i - W_{i-1}) = -(1/\gamma)^2$.

The nth convergent corresponds to the periodic orbit, which out of all the periodic orbits of length n or shorter, approaches most closely the most irrational torus. The scaling theory and the existence or otherwise of a KAM torus rests on the properties of these convergents, perhaps the most crucial of which is their stability.

The stability of a periodic orbit is determined by its residue:

$$R = \frac{1}{4}(2 - TrM) = \frac{1}{4}(2 - \nu - 1/\nu) \tag{A.1}$$

where M is the tangent map of the periodic orbit (i.e. the linearised mapping over q iterations) and ν and $1/\nu$ are its eigenvalues.

$0 < R < 1$ corresponds to complex eigenvalues of modulus 1; tangent space orbits are stable and lie on ellipses about the origin. When $R < 0$ or $R > 1$ eigenvalues are real and positive or real and negative; tangent space orbits lie on hyperbolae and almost all initially small deviations are exponentially unstable (the exceptions lying on the eigenvector of M corresponding to the eigenvalue of magnitude < 1). In the integrable case, $R = 0(\lambda = 1)$: all periodic orbits lie on surfaces composed of periodic orbits, so there must be a line of periodic orbits in the tangent space too. For non-zero perturbation parameter k there is an even number of periodic orbits of winding number p/q, half with $R > 0$ and half with $R < 0$; in fact for the standard map, there is one orbit of each type ([34]). As k increases $|R|$ does and the positive residue orbit goes from being stable to unstable: the change in stability of the convergents tells us whether the KAM surface exists or is a broken cantorus. For the standard map, $|R| \propto k^q$, q being the length of the orbit. A crucial result of Greene's regards the existence of KAM torus: that there is an infinite discontinuity in the residue at the critical k. This provides a precise way to find the critical parameter for when a particular KAM torus breaks into a cantorus. At $k < k_c^w$ the residues of the $R > 0(R < 0)$ periodic orbits associated with the convergents $w_i = p_i/q_i$ approach 0 from above (below) as $q_i \to \infty$. At $k > k_c^w$, they approach $\infty(-\infty)$. At $k = k_c^w$, they approach a finite constant. For example for the golden mean, $R^+_{i\to\infty} \to 0.2500888, R^-_{i\to\infty} \to -0.255426$ and $k_c = k_c^\gamma = 0.9716354....$ Greene also asserts and numerically shows that if the torus of winding number w exists then so does that of the golden mean, where w is any other irrational number. It then follows that the standard map is globally stochastic for any $k > k_c$.

The convergents thus provide a very powerful way to study the KAM curve. It would be perhaps impossible to track down a surface of irrational winding number otherwise.

One can numerically construct the KAM curve by taking high-order convergents to it. To find a q-cycle one may exploit a reversibility property of the map ([35]): T may be written as the product of two involutions each of whose fixed points forms two lines in the phase plane. There is a point belonging to one of the two q-period orbits on each line ([34]); this clearly eases the task of finding the orbit in phase space. One of the lines is called the "dominant symmetry line" and the elliptic cycle (R^+) always has a point on this line. For the standard map 5.4 with positive nonlinearity parameter k this is at $\theta = \pi$. Another line, the "subdominant symmetry line" is at $\theta = 0$ (see also text).

We refer the reader to the literature (in particular, [35]) where the fine scale structure of the KAM at criticality is beautifully shown. Both a phase-space representation and a Fourier transform which shows similar structure repeated between the primary peaks of the spectrum demonstrate this clearly. A numerical analysis of this structure-at-all-scales provides scaling exponents and scaling functions for characteristics of the behavior. The residues of the elliptic and hyperbolic periodic orbits converge to their critical values as:

$$R_i^{\pm} \sim R_{\infty}^{\pm}(\gamma^*)^{2.3\mu q_i},$$

where $\mu = k - k_c$. In particular, observe that

$$\ln(R_i^{\pm}/R_{\infty}^{\pm}) \sim \mu \tag{A.2}$$

Positions of neighboring minimax points near the dominant symmetry line $\theta = \pi$ converge together as

$$\Delta\theta_{i+1} = \alpha_{\pi}^{-1}\Delta\theta_i$$

where the scaling exponent $\alpha_{\pi} \approx -1.41$. The positions of the minimax points on the line converge together as

$$\Delta I_{i+1} = \beta_{\pi}^{-1}\Delta I_i$$

with the scaling exponent $\beta_{\pi} \approx -3.07$.

The scaling near the subdominant line $\theta = 0$ goes similarly, but with $\alpha_0 \approx -1.69$ and $\beta_0 \approx -2.56$. Notice that both at $\theta = \pi$ and at $\theta = 0$, the product of the phase-space scaling exponents $\alpha\beta \approx 4.34$.

Fixing a value for the residue R_o, where $0 < R_o < \infty$ is arbitrary but the same for each periodic orbit corresponding to the convergents, one finds that the corresponding values of the non-linearity parameter k converge to k_c^w as

$$\Delta k_{i+1}(R_o) = k_{i+1}(R_o) - k_c^w = \delta^{-1}\Delta k_i(R_o)$$

where $\delta \approx 1.628$. Note that although typically the convergence goes as δ, if we pick the special value $R_o = R^*$ the convergence is faster, as $\delta' \approx 0.6108$.

These scaling results are universal: for one-parameter maps other than the standard map, and irrational winding numbers other than the golden mean and its relatives, the same exponents are observed to dictate the behavior. They imply that asymptotically, the map is invariant under the re-scaling [37, 35, 39]

$$\begin{aligned} \mu &\rightarrow \delta^{-1}\mu \\ \Delta\theta &\rightarrow \alpha^{-1}\Delta\theta \\ \Delta p &\rightarrow \beta^{-1}\Delta p \\ n = F_r &\rightarrow F_{r+1} \sim wn \end{aligned} \tag{A.3}$$

where the last relation expresses time-rescaling, n being the number of iterations of the map, with scaling exponent given by the irrational winding number of the KAM, *e.g.*for the golden mean torus, $w = \gamma \approx 1.618$.

Phrased in language closer to that of renormalization-group theory, there exist coordinate and parameter changes $B_n(x, y, \mu)$ such that

$$\begin{aligned} B_n...B_oT^{q_n}R^{p_n}B_o^{-1}...B_n^{-1}(x, y, \mu) &\rightarrow T^*(x, y, \mu) \\ B_n(x, y, \mu) \rightarrow B^*(x, y, \mu) &= (\alpha x, \beta y, \delta\mu) \end{aligned} \tag{A.4}$$

where $R(x, y) = (x - 2\pi, y)$ expresses the periodic property of the map.

The limit map T^* is universal: it is the same for all typical one-parameter maps (up to rescaling).

The above behavior has been well couched in renormalization-group theory, [39, 37, 35]. One searches for a fixed point in the space of maps of the following renormalization procedure: start with some map, zoom in on a region, iterate the map there, then rescale. The scale factors that work to eventually give the fixed point of the renormalization, give the scaling exponents. If we start in the stable manifold of the renomalization operator $\mathcal{R}$, then this procedure takes us to the fixed point of $\mathcal{R}$. In the case of one-parameter maps, such as the kicked rotor, the renormalization procedure can tell us the critical value of k: $k \neq k_c$ lies on the unstable manifold of $\mathcal{R}$ and if we start with a map here, k grows under iteration of the renormalization procedure. k is a "relevant" variable, lying, in a sense, orthogonal to the stable manifold. In [39], an explicit renormalization method is presented for KAM tori between two resonance chains. They describe higher and higher resonances in between by successive renormalizations of the Hamiltonian. They are able to determine the existence or otherwise of a KAM torus from their scheme.

A.2 Cantoral Flux

A measure of how much a cantorus slows down transport is given by the flux δW swept across the cantoral gaps in one iteration of the map.

The flux across a *closed* curve C is defined as the phase space area occupied by the points mapped from the interior R of C to the exterior in one iteration. If C' is the image of C and R' the image of R under the mapping, then the outward flux across C is the area in C' which is not inside C. For area-preserving maps, the inward flux is equal to the outward flux. Consider a curve going through the cantorus closing all of its gaps. Then the flux through the cantorus is defined as the outward flux through the curve that minimizes the flux over all such curves [36, 40]. One way to obtain this curve is the following [36]: we choose a gap in the cantorus and iterate the endpoints of the gap backward in time for n steps, bringing us to another gap in the cantorus. We close that gap with a straight line (between the back-iterated endpoints) and then iterate the line forward n steps. This gives a curve $W^u(G)$ that closes all the gaps that are backward images of the original gap. We repeat the process, starting from the original gap, but doing the forward-time iteration of the endpoints first, and then the backward-time iterates of the line. This gives a curve $W^s(G)$. Now $W^u + W^s$ gives a curve closing all the gaps uniquely except for the original gap in which there are 2 curves, which intersect once in the middle of the gap, to choose from. The rest of the curve is invariant by construction, *i.e.* a barrier to transport. The "turnstile" in the original gap represents the total flux across the cantorus, and it is a minimum flux: if we choose W^u to close the gap then in one iteration, the curve is mapped to W^s. Then the upward flux through the cantorus is the area of the left-hand side of the turnstile: points in the left-hand area get mapped from below the original curve to above it. For area-preserving maps this is the same as the right-hand area, which represents the downward flux through the cantorus. We note two details: (i) if there is more than one turnstile in the gap, which would happen if W^u and W^s intersect more than once, we take a sum over the left-hand or right-hand areas (ii) sometimes, but not often, more than one original gap may be needed to fill all the cantoral gaps through the iteration process described above.

In practice, fortunately, one may exploit action principles to calculate ΔW rather than performing the above procedure. We recall that for each winding number, there are two periodic orbits for the standard map, with residues of opposite sign. The p/q-orbit with $R < 0$ minimizes the action sum $W = \sum_{t=0}^{q} F(x_t, x_{t+1})$ over arbitrary variations of the intermediate x_t, with $x_q = x_o + p$ fixed [42, 36]. $F(x, x')$ is the generating function for one iteration of the map. This can be generalized to irrational winding numbers,[42, 36]: a minimising orbit of winding number w is either a closed circle (KAM surface) or a cantorus, with a dense set of gaps.

The minimising cantorus is the limit set of minimising periodic orbits corresponding to the convergents to the KAM. The orbit with $R > 0$ is a minimax orbit, that is, a saddle of the action. The saddles lie in between the points of the minimizing orbits: a minimizing orbit started at some point is equivalent to the orbit started at that point shifted by one iteration, so has the same minimum action. By continuity then, there must be a saddle of the action in between the two points, which is also a periodic orbit of the same winding number. For irrational winding numbers, one may generalize the argument above to show there is a minimax orbit in the gaps of the cantorus, since each of the endpoints of a gap belong to a minimizing orbit in the cantorus. The minimax orbit is homoclinic to the cantorus, since it lives in the gap and gap widths go to zero as $t \to \pm\infty$. In fact, the limit set of the minimax periodic orbits is the cantorus plus all homoclinic points in the gap.

The flux through the cantorus is given by the action difference between the minimizing and minimax orbits. The curve created by the construction described to minimize the flux resulted in a turnstile in the original gap, whose pivot is at the minimax orbit, since it approaches the cantorus in both backward and forward time. The area in the left-hand turnstile is, by Stokes Theorem, given by $\int_{l_o}^{c_o}(p^-(x_o) - p^+(x_o))dx_o$ where $p^{\pm}(x)$ are the two upper/lower branches of the turnstile, l_o and c_o being the minimizing orbit on the cantorus at the left and the minimax orbit in the gap respectively. The momenta can be expressed in terms of the action function for the area-preserving map: $p^-(x_o) = \partial F(x_{-1}, x_o)/\partial x_o$ and $p^+(x_o) = -\partial F(x_o, x_1)/\partial x_o$, where $x\mp$ are the x-coordinates at the previous/next iteration. This makes the area

$$\Delta W = F(c_{-1}, c_o) + F(c_o, c_1) - F(l_{-1}, l_o) - F(l_o, l_1) = \sum_{t=-\infty}^{\infty} (F(c_t, c_{t+1}) - F(l_t, l_{t+1}))$$

where the last step follows from stationarity of the action (the intermediate terms add to

0)

So the flux across a cantorus may be calculated by taking the difference in action between the orbit of an endpoint of a gap on the cantorus and the centerpoint of the turnstile in the gap. We note that if the orbit corresponding to the irrational winding number is actually a circle (not broken), there is no minimax orbit and $\Delta W = 0$ as it must be.

Near the broken-up KAM in question are other irrationals, and by continuity, their ΔW's are approximately the same. The transport in the region is limited by the smallest one.

A similar quantity $\Delta W_{p/q}$ may be defined for periodic orbits as the difference in action between the minimizing periodic orbits and the minimax orbit. To compute the flux acorss a cantorus it is easiest to find the orbits for the periodic convergents (see A.1) and their actions $\Delta W_{p/q}$ and take the limit as $p/q \to w$. We refer the reader to the tables and trees in references [36, 37] to see this process in action. As the order of the convergent increases, $\Delta W_{p/q}$ decreases and approaches a limit [42]. It is interesting to note that the minimum of ΔW_w in any interval between neighboring rationals p/q and p'/q', where $pq' - p'q = \pm 1$ is at the winding number $(p + \gamma p')/(q + \gamma q')$. Numbers of this form are called "noble" numbers and are in a sense the most irrational numbers in the interval $[\frac{p}{q}, \frac{p'}{q'}]$. Indeed, their continued fraction expansion has $a_n = 1$ for all $n \geq N$ where N is the smallest it can be while still being in $[\frac{p}{q}, \frac{p'}{q'}]$.

A.3 Scaling in Quantum Mechanics

What are the consequences for quantum mechanics of the intricate structure of the classical phase space near a cantorus and the resulting scaling properties (section 5.2.2)? In fact, in a first approximation, scaling carries over to the quantized motion near a cantorus, provided Planck's constant is also scaled (in renormalization-group-speak, $\hbar$ is a "relevant" variable): one must add [50, 55]

$$\hbar \to |\alpha\beta|\hbar \tag{A.5}$$

to equations 5.10. On the one hand it may be surprising that the quantum scaling exponent is given by classical exponents and indeed that $\hbar$ even obeys a universal scaling relation considering that quantum mechanics can give very different physics than classical. We shall come back to this point shortly. $\hbar$ represents a quantum uncertainty or "noise", yet it scales so simply unlike classical noise. On the other hand, from the perspective that

$\hbar$ is an area in phase-space, it may be expected to scale as the classical phase-space area does 5.13. That this is the correct scaling to leading order has been shown in reference [50]. A renormalization-group theory approach to quantum mechanics, generalizing the RNG theory method for classical systems supports the scaling factor for $\hbar$ for lowest-order fluctuations: $|\alpha\beta|$ emerges as an eigenvlaue of the linearized renormalization transformation [55]. A numerical study based on the Wigner function [51] has shown consistency up to $\hbar^4$.

In reference [50] the Wigner function corresponding to a quantum wavefunction is used to demonstrate the scaling to lowest order. The Wigner function has the useful property that the expectation value of any Weyl-ordered quantum operator (*i.e.* symmetric ordering of x and p) is equal to the corresponding classical quantity: the phase-space integral of the classical function corresponding to the operator weighted by the Wigner function of the quantum state. This enables the comparison of a quantum object with a classical one for which scaling properties are known, and leads to the result A.5 above to lowest order in $\hbar$. For example, the expectation value G_ψ of a Weyl-ordered operator $G(x,p)$ at the nth iteration of the map in an initially coherent state ψ with width σ in x, scales like

$$G_\psi(x,p,\sigma,\hbar,\Delta k,t) = \Lambda^{-r} G_\psi(\alpha^r x, \beta^r p, \alpha^r \sigma, |\alpha\beta|^r \hbar, \delta^r \Delta k, t/\omega^r) \tag{A.6}$$

where Λ depends on the nature of the operator, $\Lambda = \alpha$ for example if $G = x$. We may think of time $n \sim t \sim \omega^r$, so that this equation relates quantities at time t to quantities at one iteration of the map. We now arrive at at crucial observation: as we go to larger times (n), Planck's constant $\hbar$ is taken to larger values under the scaling back to the time 1. Yet if the scaled $\hbar$ gets bigger than the scaling region itself, which is $O(1)$ in our units, the quantum mechanics cannot detect the structures giving rise to the scaling behavior [50]. There thus comes a critical time t^* when $\hbar$ becomes of order one when scaling breaks down in the quantum mechanics and quantum behavior begins to deviate from classical. The breakdown happens at a time t^* which scales as $t^* \sim \hbar^{-1/\gamma}$, $\gamma = \ln|\alpha\beta|/\ln\omega \approx 3.05$. This is simply obtained from the scaling exponents for time and for $\hbar$.

We have so far discussed the scaling only to lowest order in the quantum mechanics: we need to consider higher-order corrections to Weyl-ordering. We may expand an arbitrary operator in a series of Weyl-ordered terms with each term being of order $\hbar$ up from the previous:

$$G =: G : +i\hbar : G_1 : -\hbar^2 : G_2 : +...$$

where the :: denotes Weyl-ordering. The terms odd in $\hbar$ are actually zero if G is a Hermitian operator. At short times, for small enough $\hbar$, the zeroth order Weyl term dictates the behavior and so quantum mechanics follows the classical mechanics. But deviations from classical behavior and scaling emerge when the higher order terms in this expansion get large. In fact it has been shown numerically that quantum effects from the higher order terms kick in appreciably at the same time scale as when the scaling breaks down due to the scaled $\hbar$ being too big in the initial wavepacket [50, 51]. In fact, in [51] it is shown that the leading corrections scale in the same way. So quantum expectation values follow the corresponding classical averages with the extra scaling relation A.5 until the critical time $t^* \sim \hbar^{-1/\gamma}$. Subsequently, scaling breaks down and quantum effects such as interference become important.

PHYSICAL REVIEW A VOLUME 56, NUMBER 4 OCTOBER 1997

Quantizing constrained systems

L. Kaplan
Harvard Society of Fellows and Department of Physics, Harvard University, Cambridge, Massachusetts 02138

N. T. Maitra and E. J. Heller
Department of Physics and Harvard-Smithsonian Center for Astrophysics, Harvard University, Cambridge, Massachusetts 02138

(Received 27 May 1997)

We consider quantum mechanics on constrained surfaces which have non-Euclidean metrics and variable Gaussian curvature. The old controversy about the ambiguities involving terms in the Hamiltonian of order $\hbar^2$ multiplying the Gaussian curvature is addressed. We set out to clarify the matter by considering constraints to be the limits of large restoring forces as the constraint coordinates deviate from their constrained values. We find additional ambiguous terms of order $\hbar^2$ involving freedom in the constraining potentials, demonstrating that the classical constrained Hamiltonian or Lagrangian cannot uniquely specify the quantization: the ambiguity of directly quantizing a constrained system is inherently unresolvable. However, there is never any problem with a physical quantum system, which cannot have infinite constraint forces and always fluctuates around the mean constraint values. The issue is addressed from the perspectives of adiabatic approximations in quantum mechanics and Feynman path integrals, and semiclassically in terms of adiabatic actions. [S1050-2947(97)08910-5]

PACS number(s): 03.65.Sq, 02.40.Ky

I. INTRODUCTION

The controversy over the proper way to quantize a constrained dynamical system has had a long and interesting history in 20th century physics. One treatment of the subject opens by saying that "if you like excitement, conflict, and controversy, especially when nothing very serious is at stake, then you will love the history of quantization on curved spaces" [1]. The possibility of resolving the ambiguities experimentally for rigid body systems was the subject of a conference discussion in 1957 among DeWitt, Wheeler, and Feynman [1]. The problem was also treated in Dirac's famous text of 1967 [2]. Yet many years later we still seem far from attaining a consensus regarding quantization on curved spaces. The "quasipermanent discussion among the specialists" [3] has by no means come to an end. In fact, a recent paper [4] laments that "in spite of all the successes of quantum mechanics and after years of efforts on quantization, we are still not absolutely sure about the correct quantization of as simple a system as the double pendulum." The subject also received early attention in the works of Cheng [5] and DeWitt [6]. In this paper we do not attempt to review the extensive research on the subject of constrained quantization, and refer the interested reader to the literature [7]. Our approach to this problem is quite independent of all previous methods.

The canonical quantization prescription has served us well in defining a straightforward and unambiguous way of quantizing a classical system in flat space. However, it immediately runs into problems where constrained dynamics is involved. It is easy enough to restrict the potential term to the constraint surface — the difficulty arises in treating the operator ordering ambiguities in quantizing the kinetic term $K=-(\hbar^2/2m)(1/\sqrt{g})(\partial/\partial q^i)[g^{ij}\sqrt{g}(\partial/\partial q^j)]$. These ambiguities, at order $\hbar^2$, are proportional to the local Gaussian curvature of the constraint surface, which is the only available coordinate-invariant quantity. Thus for constrained systems with flat constraints (e.g., the simple pendulum or a particle confined to a one-dimensional curve), the ambiguity does not arise, whereas for systems with constant curvature (e.g., motion on a sphere) it leads only to a physically unobservable shift in the zero-point energy. In the latter case, the semiclassical Van Vleck approximation can be used to fix the "correct" energy offset [3]. In three dimensions this requires adding an R term to the Laplacian (R being the scalar curvature). For a two-dimensional surface of constant negative curvature, the semiclassical approximation becomes exact (though only at distances large compared to the curvature radius) if the quantity added to the Laplacian is $R/4$. Even if one (somewhat arbitrarily?) requires that the Van Vleck approximation should be as close as possible to being exact for the constant curvature case, it is by no means clear that this prescription is valid in the generic case of varying curvature, where the ambiguities are most physically relevant.

One might think that Feynman's path-integral approach [8] would help to resolve these uncertainties. However, as remarked by Schulman in this context, "there is no free lunch." In the path-integral method, the ambiguity arises in choosing how to incorporate the metric into the kernel and in deciding at what point in the infinitesimal time interval to evaluate functions of the metric [1,4]. Two commonly used kernels give answers that differ by an effective $R/6$ contribution to the Laplacian (and naturally enough both differ from the canonical quantization result). These issues are discussed at some length in Ali's recent paper [4], and here we will not go into the details.

Given this history, we have decided to attack this old problem using a somewhat different, and in our view, more physically motivated approach. The principle governing our view is that arriving at a unique quantization is essential only in real systems. That is, quantization should be *physically* unambiguous. For example, quantization of the usual rigidly constrained classical double pendulum is not a physical problem, because the requirement that the pendulum lengths remain exactly constant is not realizable. To make the problem as close as possible to physical, the constraints should be imposed through a limiting procedure, fluctuations remaining physically allowable along the way. We call this the "limit quantization," as opposed to direct quantizations which do not pass through a limiting procedure. This procedure is carried out in Sec. II using a Hamiltonian formalism, and later in Sec. III from a path-integral point of view. The limit quantization embodies the idea of classical constraints arising as the limit of ever larger restoring forces normal to the constraint surface, an idea discussed in Arnol'd, for example [9] (see also Lanczos [10]). In this way the constraint coordinates appear as part of the full dynamical system in the usual Euclidean metric. As the constraint forces are increased, the constrained degrees of freedom acquire a very high frequency, and their actions remain adiabatically constant as the slow variables move. This, however, does not imply that the fast variables (which we here call the r variables) are *energetically* decoupled from the slow ($\theta-$) variables. We discuss the classical and semiclassical issues of constrained dynamics further in Sec. IV, where from still another perspective we will see that the direct quantization is intrinsically ambiguous at order $\hbar^2$: different limiting constraint potentials give the *same* classical constrained motion but *different* quantum dynamics at order $\hbar^2$.

The uncertainty principle requires that in any real physical system there will be quantum fluctuations around the surface of constraint. By examining the effects of these fluctuations in the limit of ever tighter constraints, we find unavoidable ambiguities in the quantum dynamics along the surface of constraint. Our claim is that these ambiguities are an inherent part of any reasonable quantization procedure, and need not be more bothersome in principle than the Aharonov-Bohm effect, which shares the property of identical classical dynamics giving rise to different quantum dynamics. As the Aharonov-Bohm effect illustrates, there is no good reason why a quantum system should be uniquely determined by its classical (or even semiclassical) limit, and the richness of the new phenomena that can occur in physical quantum systems can well be viewed as a positive aspect of the quantum theory rather than as a shortcoming.

In any case, we hope our contribution to the literature will be a valuable one, in spite of this concluding warning by Schulman: "Additional papers on curved space path integration are legion, and we do not attempt to list them all. Some are correct; some are less correct. Some have original features; some are less rich in this praiseworthy property" [1].

II. QUANTUM MECHANICS OF CONSTRAINED SYSTEMS

A physically natural way of defining a constrained dynamical system in classical mechanics is through a limiting procedure where a strong attractive potential forces the system at any fixed energy to live closer and closer to the constraint surface [9]. The effective classical dynamics obtained in this limit turns out to depend only on the intrinsic properties of the constraint surface (e.g., the curvature) and not on the details of the constraining potential chosen on the embedding space. We will use an analogous procedure in quantum mechanics, and consider the quantization of a constrained classical system as the limit of quantizations of classical systems with large potentials away from the surface of constraint. This approach is in accord with our intuition about physical constraints. It is also appealing because once a specific squeezing potential is chosen, the resulting quantum mechanics is entirely unambiguous, and can be obtained equivalently via a canonical or path-integral method. Ambiguities will nonetheless arise in this approach, but are due to the freedom in selecting a constraining potential. The effective quantum dynamics in the squeezing limit will have corrections at order $\hbar^2$ which depend on the details of the way in which this limit is taken. These ambiguities are analogous to operator-ordering effects in canonical quantization approaches, and to ambiguities which arise in the choice of kernel (particularly in the choice of evaluation points for functions of the metric) in path-integral methods. However, the physical ambiguities we find are considerably more general in that they need not be functions only of the intrinsic properties of the constraint space. Even for a flat constraint space a large set of possible quantizations are available, each having its own physical realization in an embedding space, but all having the same classical and semiclassical limits. The existence of such quantum ambiguities in constrained systems all leading to the same classical physics in our view overshadows any attempt to resolve the operator ordering questions and terms involving the curvature.

We begin with a Lagrangian

$$L=\tfrac{1}{2}g_{ij}\dot{q}^i\dot{q}^j-V(q)-\bar{V}_\lambda(q) \qquad (1)$$

on the full coordinate space, with flat metric g_{ij} and potential V (we take the mass to be unity throughout). The additional potential $\bar{V}_\lambda$ enforces the constraint in the limit $\lambda\to\infty$. Classically we require $\bar{V}_\lambda$ to have the same value everywhere on the constraint surface S, for each λ. We now transform to the Hamiltonian

$$H=\tfrac{1}{2}g^{ij}p_ip_j+V(q)+\bar{V}_\lambda(q), \qquad (2)$$

where $p_i=\partial L/\partial\dot{q}^i=g_{ij}\dot{q}^j$ is the momentum coordinate and g^{ij} is the inverse of g_{ij}. Canonical quantization now requires that we replace $g^{ij}p_ip_j=\vec{p}\cdot\vec{p}$ with the operator $-\hbar^2\nabla^2$, which in coordinate system q has the form

$$-\hbar^2\nabla^2=-\hbar^2\frac{1}{\sqrt{g}}\frac{\partial}{\partial q^i}g^{ij}\sqrt{g}\frac{\partial}{\partial q^j}, \qquad (3)$$

where g is the determinant of the metric (i.e., the square of the volume element). Notice that there is no operator ordering ambiguity here because the full metric g_{ij} is flat.

Now locally, near some region of the constraint surface S we may separate the coordinates q into "slow coordinates" θ parametrizing S and "fast coordinates" r orthogonal to the surface (see Fig. 1). We will be looking for an effective theory of the coordinates θ when the constraining potential $\bar{V}_\lambda(r)$ allows only small fluctuations in r (small compared to the length scale associated with the physical potential V, the curvature scale of the constraint surface S, and the scale on

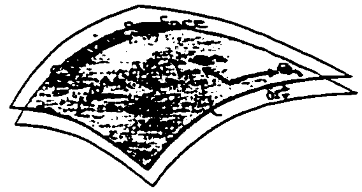

FIG. 1. Schematic showing the fast motion along r and slow motion along θ_1,θ_2 coordinates for finite confining forces (finite λ).

which $\bar{V}_C^{\theta}$ varies as a function of θ). The quantum wave function on the full space can be written as

$$\Psi(q)=\Psi(\theta,r)=\phi_0(\theta)\Psi_{\rm GR}^{(\theta)}(r)+\phi_1(\theta)\Psi_1^{(\theta)}(r)+\cdots, \tag{4}$$

where $\phi_0,\phi_1,\ldots$ are arbitrary functions of the slow variables. $\Psi_{\rm GR}^{(\theta)}(r)$ is the ground state of the fast variables r, treating θ as a fixed parameter. $\Psi_1^{(\theta)}(r)$ is the first excited state, and so on. More precisely, $\Psi_{\rm GR}$, Ψ_1, etc. are the eigenstates of the fast Hamiltonian,

$$H_r=-\frac{\hbar^2}{2}\frac{1}{\sqrt{g}}\frac{\partial}{\partial r^i}g^{ij}\sqrt{g}\frac{\partial}{\partial r^j}+\bar{V}_C^{\theta}(r), \tag{5}$$

where i and j are summed over the fast variables only, and the metric is evaluated at a fixed value of θ. Note that g here is the determinant of the full metric on the (r,θ) space.

Now we want to consider the effective Hamiltonian $H_{\rm eff}$ acting on the slow wave function $\phi_0(\theta)$ which multiplies the ground state of the r variables. We will argue toward the end of this analysis that this effective theory is in fact unitary in the limit $\lambda\to\infty$, as the transition probabilities connecting the ground states to the excited states of the fast variables disappear in the constraint limit (due to adiabaticity).

We have mentioned previously that in order to obtain the correct classical motion in the constraint limit, we must make $\bar{V}_C^{\theta}(r=0)$ be independent of θ and have the potential increase away from $r=0$. In order for the quantum mechanics to have a sensible semiclassical limit, we must further enforce that the energy of the ground state $E_{\rm GR}^{(\theta)}$, defined by

$$H_r\Psi_{\rm GR}^{(\theta)}=E_{\rm GR}^{(\theta)}\Psi_{\rm GR}^{(\theta)}, \tag{6}$$

must be θ independent, for any λ, and the energy of the first excited state must be well separated from it, with the separation growing with λ. This can be implemented in a number of ways, but two particularly simple scenarios present themselves. In the first we take $\bar{V}_C(q)=\lambda v(q)$, where v is a smooth function vanishing on the constraint surface and having its minimum there (but with a nonsingular second derivative matrix with respect to the fast variables). Near the constraint surface, the constraining potential will have the harmonic-oscillator form

$$\bar{V}_C^{\theta}(r)=rA^{(\theta)}r+O(r^3), \tag{7}$$

where the matrix function $A^{(\theta)}$ is smooth. The ground states $\Psi_{\rm GR}^{(\theta)}$ will to first approximation be harmonic oscillator ground states with spatial extent of order $\hbar^{1/2}/\lambda^{1/4}$ and energy $E_{\rm GR}$ of order $\hbar\lambda^{1/2}$. As discussed above, the coefficient of this energy must be θ independent, to prevent infinite effective forces in θ from arising in the $\lambda\to\infty$ limit. The matrices $A^{(\theta)}$ can easily be adjusted to satisfy this condition. In the case of more than one constraint variable, this still allows for much freedom in the function $A^{(\theta)}$ and the resulting eigenstates $\Psi_{\rm GR}^{(\theta)}$ (energy can flow from one fast degree of freedom to another as a function of θ, as long as the total energy remains constant). One may choose to adjust (some of) the anharmonic parts of the potential as well, but this is not really necessary or natural. The quartic term will lead to order $\hbar^2$ (λ independent) corrections to the ground-state energy and thus (if these anharmonic corrections vary with θ, which in general they will) to the effective potential in θ.[1] We will later see that this effect is of the same order as other terms that are encountered in the effective potential. We might also mention at this point that if in finding the ground state of r at a given θ we used normal coordinates centered at $(\theta,r=0)$, $g_{ij}=\delta_{ij}+O(r^2)$ for fixed θ, and neglected the $O(r^2)$ curvature correction, we would also make an error of order $\hbar^2$ in the ground-state energies and therefore in the effective potential for θ.

A second scenario involves a hard-wall potential with the cross section of the allowed region shrinking toward S as $\lambda\to\infty$. Thus we may instead take

$$\bar{V}_C^{\theta}(r)=0,\quad a^{(\theta)}(\lambda r)<1 \tag{8}$$

$$=\infty,\quad a^{(\theta)}(\lambda r)>1, \tag{9}$$

where the function $a^{(\theta)}$ defines a θ-dependent region shrinking as $1/\lambda$ in which the fast eigenstates live. The energy of the ground state is of order $\hbar^2\lambda^2$, and can again be adjusted to be θ independent while allowing for substantial freedom in the shapes of the ground states. In the following we will focus on the original (smooth potential) scenario, but this one could be used to obtain similar results.

We now see what happens when we compute the effective Hamiltonian for the slow variables $H_{\rm eff}(\theta,\partial/\partial\theta)$, defined by

$$\langle\phi_0|H_{\rm eff}|\phi_0\rangle=\langle\Psi|H|\Psi\rangle, \tag{10}$$

with

$$\Psi(\theta,r)=\phi_0(\theta)\Psi_{\rm GR}^{(\theta)}(r). \tag{11}$$

The potential $V(q)$ clearly induces an effective potential $V(\theta,r=0)$, up to corrections which disappear in the constraint limit, since $V(\theta,r)$ varies slowly in r over the extent of $\Psi_{\rm GR}^{(\theta)}(r)$. The constraint potential $\bar{V}_C$, combined with the

---

[1] For the purpose of dimension counting, every power of r in an expression contributes a factor of $\hbar^{1/2}/\lambda^{1/4}$ to the expectation value whereas $\partial/\partial r$ acting on $\Psi_{\rm GR}$ (but not the metric) contributes $\lambda^{1/4}/\hbar^{1/2}$. Derivatives acting on the "slow" wave function $\phi_0(\theta)$ and the metric g, as well as $\partial/\partial\theta$ acting on $\Psi_{\rm GR}$ all produce factors of order unity.

fast part of the kinetic term, gives, by assumption, a θ-independent effective potential which we can therefore drop. We are left with the slow (θ) part of the full q-space Laplacian, as well as mixed terms involving one derivative each with respect to the slow and fast variables.

In the Born-Oppenheimer spirit, consider first the action of the "slow" part of the Laplacian on the full wave function. We are interested in matrix elements of the form

$$\left\langle \phi_0'\Psi_{\rm GR}\left| -\frac{\hbar^2}{2}\frac{1}{\sqrt{g}}\frac{\partial}{\partial\theta^i}\left(g^{ij}\sqrt{g}\frac{\partial}{\partial\theta^j}\right)\right|\phi_0\Psi_{\rm GR}\right\rangle . \quad (12)$$

The two derivatives can act on the slow wave function ϕ_0, or in the ground state $\Psi_{\rm GR}$, or on the metric and its determinant. Consider terms where both derivatives act on the ground state or the metric. After integrating over the fast variables, this leads to $\langle \phi_0'| -\hbar^2 f(\theta)|\phi_0\rangle$, an effective potential scaling as $\hbar^2$.[2] (Note that both the metric and the ground state are changing over typical scales of order unity in θ.) Furthermore, this effective potential is λ independent for large λ, since $\Psi_{\rm GR}$ maintains its functional form (that of a Gaussian plus higher-order corrections) and simply shrinks toward $r=0$ as $\lambda\to\infty$.

Now suppose one of the derivatives acts on the metric or on $\Psi_{\rm GR}$, while the other acts on the slow wave function. We then obtain

$$\left\langle \phi_0'\left| -\hbar^2 h^i(\theta)\frac{\partial}{\partial\theta^i} + {\rm H.c.}\right|\phi_0\right\rangle , \quad (13)$$

where h^i are real functions of θ (because the ground state $\Psi_{\rm GR}$ can be chosen to be real, and the metric is real as well). Taking the Hermitian part we again obtain an effective potential of order $\hbar^2$. Finally, if both derivatives act on the slow wave function ϕ_0, we obtain the usual kinetic term for the slow variables, *including* order $\hbar^2$ terms proportional to the curvature of the constraining surface, as discussed in Sec. I. This concludes the discussion of the pure θ-derivative part of the kinetic energy, and we move on to the mixed terms next.

If the $\partial/\partial r$ derivative acts on the metric, we obtain a contribution of order $\hbar^2$ to the effective potential as before (all derivatives are of order unity). If $\partial/\partial r$ acts on $\Psi_{\rm GR}$ while $\partial/\partial\theta$ acts on g or the wave function ϕ_0, we obtain

$$\hbar^2\left\langle \Psi_{\rm GR}\left| b^i(\theta,r)\frac{\partial}{\partial r} + {\rm H.c.}\right|\Psi_{\rm GR}\right\rangle , \quad (14)$$

where b is a slowly varying real function. So to this order in $\hbar$ only the commutator of b with $\partial/\partial r$ survives, and once again the resulting contribution to the effective potential is of order $\hbar^2$. The remaining term is the one where both derivatives act on the ground state; it has the form

$$\hbar^2\left\langle \Psi_{\rm GR}\left| c(\theta,r)\frac{\partial}{\partial\theta}\frac{\partial}{\partial r}\right|\Psi_{\rm GR}\right\rangle . \quad (15)$$

Since $\Psi_{\rm GR}(r)$ is even in r, the slowly varying function $c(\theta,r)$ must be expanded to first order in r to obtain a nonvanishing contribution. We then obtain yet another contribution to the effective potential of order $\hbar^2$ [since $r(\partial/\partial r)$ acting on $\Psi_{\rm GR}(r)$ is of order unity].

Finally, we argue by adiabaticity that there is no mixing between $\phi_0(\theta)$ and the excited wave functions $\phi_1(\theta)$, etc. This follows because the splitting between $\Psi_{\rm GR}^{(\theta)}$ and the excited states of r scales as $\hbar\sqrt{\lambda}$ in the constraint limit (or as $\hbar^2\lambda^2$ in the case of a hard-wall potential), whereas the matrix elements do not grow with λ. So assuming a finite amount of energy in the initial $\phi_0(\theta)$ wave function, transition probabilities vanish in the $\lambda\to\infty$ limit, and we obtain a probability-conserving effective quantum mechanics. The effective Hamiltonian is

$$H_{\rm eff} = -\frac{\hbar^2}{2}\frac{1}{\sqrt{g}}\frac{\partial}{\partial\theta^i}\left(g^{ij}\sqrt{g}\frac{\partial}{\partial\theta^j}\right) + V(\theta) + \hbar^2 V_{\rm eff}(\theta). \quad (16)$$

This is the key result of this paper. $V_{\rm eff}$ is essentially an arbitrary smooth function, depending in a complicated way on both the curvature properties of S and on the constraining potential around S (together these determine the ground-state wave functions). $\sqrt{g}$ can be taken to be the square root of the determinant of either the full metric or of the metric restricted to the constraint surface. Any difference between these expressions can be absorbed into $V_{\rm eff}$.

III. LAGRANGIAN FORMALISM

A path-integral analysis also shows that quantization on the constrained surface is ambiguous at order $\hbar^2$. We begin with the propagator on the full coordinate space. Because the space is flat, this is given by the usual Feynman prescription $\int \mathcal{D}(q(\tau))\exp(iS(q(\tau))/\hbar)$ where $S(q(\tau)) = \int L(q(\tau),\dot q(\tau),\tau)\,d\tau$. The Lagrangian L on the full space is given by Eq. (1) in Sec. II; we follow the notation introduced there. We extract the effective dynamics for the "slow" variables θ by performing a trace over the "fast" variables r in the adiabatic limit. Specifically, we calculate $\langle\theta_f|\rho(t)|\theta_i\rangle$, where $\rho(t)={\rm Tr}_r(W(t))$ is the trace over the fast variables of the density operator on the full space. The time t is taken to be small on the time scales of θ motion, but r may undergo many oscillations during this time. Noting that the evolution of the full density operator is given by $W(t)=e^{-iHt/\hbar}W(0)e^{iHt/\hbar}$, and inserting identities in the form of complete sets of states, we have

$$\langle\theta_f|\rho(t)|\theta_i\rangle = \int dR\,dr'\,dr''\,d\theta'\,d\theta''\langle\theta_f R|e^{-iHt/\hbar}|\theta' r'\rangle \times\langle\theta' r'|W(0)|\theta'' r''\rangle\langle\theta'' r''|e^{iHt/\hbar}|\theta_i R\rangle . \quad (17)$$

We take the initial density operator to be the "product" state $|\Psi_{\rm GR}^{(\theta)}\rangle\otimes|\phi\rangle$, where the initial state of the fast variables is the

---

[2] The derivatives acting on the metric only will give the usual curvature-dependent corrections to the effective potential. Terms coming from derivatives acting on the ground state are of the same order and will give rise to additional corrections.

(purely real) ground state $\Psi_{GR}^{(\theta)}(r)$, with θ regarded as a fixed parameter (see Sec. II). $\phi(\theta)$ is an arbitrary initial wave function of the slow variables θ. Replacing the two propagators by path integrals, we then have

$$\langle\theta_f|\rho(t)|\theta_i\rangle = \int d\theta'\,d\theta''\int_{\theta(0)=\theta'}^{\theta(t)=\theta_f}\mathcal{D}\theta(\tau)\times\int_{\bar\theta(0)=\theta''}^{\bar\theta(t)=\theta_i}\mathcal{D}\bar\theta(\tau)\,\phi(\theta')\,\phi^*(\theta'')\times\mathcal{F}(\theta(\tau),\bar\theta(\tau)), \qquad (18)$$

where

$$\mathcal{F}(\theta(\tau),\bar\theta(\tau)) = \int dR\,dr'\,dr''\int_{r(0)=r'}^{r(t)=R}\mathcal{D}r(\tau)\times\int_{\bar r(0)=r''}^{\bar r(t)=R}\mathcal{D}\bar r(\tau)\,e^{iS^{(1)}/\hbar-iS^{(2)}/\hbar}\times\Psi_{GR}^{(\theta'')}(r'')\,\Psi_{GR}^{(\theta')}(r'). \qquad (19)$$

$S^{(1)}=S(r(\tau);\theta(\tau))$ and $S^{(2)}=S(\bar r(\tau);\bar\theta(\tau))$ are the actions along the respective paths. In performing the path integrals over the fast variables, $\theta(\tau)$ $(\bar\theta(\tau))$ is to be treated as an external forcing function with the property $\theta(0)=\theta'$, $\theta(t)=\theta_f$ [respectively, $\bar\theta(0)=\theta''$, $\bar\theta(t)=\theta_i$].

We evaluate $\mathcal{F}$ using the stationary phase approximation with respect to $\hbar$ on the path integrals, the trace, and the integrals over the intermediate fast variables. In fact the stationary phase approximation becomes exact in the adiabatic limit: we shall now show that the errors due to stationary phase evaluation are of order $\hbar^{1/2}/\lambda^{1/4}$, so they vanish as $\lambda\to\infty$. Recall that

$$\int g(x)\,e^{if(x)/\hbar}dx = \sum_n\left(\frac{2\pi i\hbar}{f''(x_n)}\right)^{1/2}g(x_n)\,e^{if(x_n)/\hbar}\times\left[1+O\left(\hbar^{1/2}\frac{f'''(x_n)}{f''(x_n)^{3/2}}\right)\right], \qquad (20)$$

where the sum is over stationary phase points x_n satisfying $f'(x_n)=0$. Stationary phase evaluation of path integrals, although different in the details, scales in the same way. $f(x)$ corresponds to the action S. The stationary paths are the classical paths and we now argue that $S\sim O(\lambda^{1/2})$ to leading order in λ. The leading behavior of the action in the fast variables arises from the kinetic term in r and the constraint potential: $L_r\sim g_{ij}\dot r^i\dot r^j/2-V''_\lambda(r)$, where the sum is over fast variables only. This Lagrangian corresponds to the fast Hamiltonian of Eq. (2) discussed in Sec. II, which gives harmonic motion for r at least throughout the range of the fast variable ground state. Because the initial fast state is this ground state, the leading behavior of $e^{iS/\hbar}$ gives

$$\int dr'\int\mathcal{D}r(\tau)\,e^{iS^{(1)}/\hbar}\,\Psi_{GR}^{(\theta')}(r')\sim e^{-iE_{GR}t/\hbar}\,\Psi_{GR}^{(\theta)}(r), \qquad (21)$$

where we note that $E_{GR}\sim O(\hbar\sqrt{\lambda})$ is required to be θ independent to avoid infinite torques acting on the slow variables (Sec. II). This shows the leading behavior of the action on the ground state is simply to multiply it by an evolving phase. The fast variable $r(t)$ does not stray from the domain of faithful harmonic approximation to the constraint potential. Subleading terms are a factor of $1/\sqrt{\lambda}$ smaller. Thus the dominant behavior of the action and its derivatives is simply that of a harmonic potential of frequency $O(\sqrt{\lambda})$. The errors in the stationary phase evaluation of the path integrals are of order $\hbar^{1/2}/\lambda^{1/4}$, vanishing in the adiabatic limit [see Eq. (20)]. The errors in using stationary phase to compute the trace and integrals over the intermediate variables r' and r'' scale in the same way. In the harmonic approximation to the action and the ground state it is readily seen that the stationary phase points are $R=r'=r''=0$, the constrained value of the fast variable. Corrections to this approximation due to subleading terms vanish in the adiabatic limit, $\lambda\to\infty$.

We then have,

$$\mathcal{F}(\theta(\tau),\bar\theta(\tau)) = \left(\frac{\partial^2\ln\Psi_{GR}^{(\theta')}}{\partial r'^2}\right)^{-1/2}\left(\frac{\partial^2\ln\Psi_{GR}^{(\theta'')}}{\partial r''^2}\right)^{-1/2}\times\left(\frac{\partial^2 S_{cl}^{(1)}}{\partial R\,\partial r'}\right)^{1/2}\left(\frac{\partial^2 S_{cl}^{(2)}}{\partial R\,\partial r''}\right)^{1/2}e^{iS_{cl}^{(1)}/\hbar-iS_{cl}^{(2)}/\hbar}, \qquad (22)$$

where the derivatives are evaluated at $R=r'=r''=0$. $S_{cl}^{(1)}$ (respectively, $S_{cl}^{(2)}$) is the action along the classical path starting and ending at the constraint value $r=0$ subject to the Lagrangian of Eq. (1) with $\theta(\tau)$ [respectively, $\bar\theta(\tau)$] treated as an undetermined forcing function. In the adiabatic limit, we shall now show that the action exponent is just the action for the reduced slow variable system on the constraint surface, i.e., the action we would have written down had we begun in the reduced space. The kinetic term in r together with the constraint potential give a θ-independent term in the exponent as discussed above. This, being a constant energy shift as far as θ is concerned, can be neglected. The mixed kinetic term goes to zero: we may expand $g_{ij}(r,\theta)$ about $r=0$ and take functions of θ out of the time integral as they are slowly varying functions of time:

$$\int g_{ij}(r,\theta)\,\dot r^i\dot\theta^j dt = g_{ij}(0,\theta)\,\dot\theta^j\int_0^t\dot r^i dt+\frac{\partial g_{ij}}{\partial r^p}\dot\theta^j\int_0^t r^p\dot r^i dt+O(\hbar^{3/2}\lambda^{-1/4}), \qquad (23)$$

where the derivatives of the metric are evaluated at $r=0$. The first term on the right-hand side is zero, since the integral gives $r^i(t)-r^i(0)=0$ due to the stationary phase condition on the end points. For $p=i$, the integral in the second term is zero for the same reason [the integrand is $d(r^{i\,2}/2)/dt$]. For $p\neq i$ the integral averages to zero, because different directions of the fast variables generically oscillate at different frequencies. The higher-order terms in the expansion vanish in the adiabatic limit [they involve at least two powers of r but only one power of $\dot r$, so scale at least as $(\hbar/\lambda^{1/2})(\hbar^{1/2}\lambda^{1/4})$]. We are thus left with the kinetic term in the slow variables only, with the metric evaluated at the constraint value for r.

Inserting $\mathcal{F}(\theta(\tau),\bar{\theta}(\tau))$ into Eq. (18) gives the reduced density matrix at time t. This factorizes into a part involving θ,θ_0, and $\theta(\tau)$ and a part involving θ',θ_0', and $\bar{\theta}(\tau)$. This implies that the reduced density matrix factorizes: $\langle\theta_f|\rho(t)|\theta_{f'}\rangle = \langle\theta_f|\theta(t)\rangle\langle\theta(\tau)|\theta_{f'}\rangle$, i.e., the final θ state is pure, and so we may describe it in terms of a wave function. Adiabaticity has thus uncoupled the fast and slow degrees of freedom. We have

$$\psi(\theta,t) = \int d\theta \int D\theta(\tau) A(\theta(\tau)) e^{iS/\hbar}\psi(\theta,0), \tag{24}$$

where

$$A(\theta(\tau)) = \prod \left(\frac{\partial^2 \ln\Psi_{GR}}{\partial r^2}\right)_{r=0}^{-1/2} \left(\frac{\partial^2 S_\lambda}{\partial R\,\partial r}\right)_{r=0}^{1/2} \tag{25}$$

$S = S_\lambda$ is the action function for the θ variable on the constrained surface: $S=\int L\,dt$, where the Lagrangian is $L=\frac{1}{2}g_{ij}\dot\theta^i\dot\theta^j - V(\theta)$, with g_{ij} now the metric on the curved space defined by the constraint surface, and the sum is over the slow (θ) variables only.

We may compare this to the expressions discussed in Ali, where one works in the reduced space from the start. Different Feynman kernels are postulated to attempt to account for the curvature of the constrained surface [1,4,8]. There, for an infinitesimal time t,

$$\psi(\theta,t) = \int d\Omega(\theta_0)\bar{G}(\theta,\theta_0)e^{iS/\hbar}\psi(\theta_0,0) \tag{26}$$

$d\Omega(\theta) = \sqrt{g(\theta)}\,d\theta$ is the volume element at θ. Candidates for $\bar{G}(\theta,\theta_0)$ which are often considered in the literature include the identity operator and $[g(\theta)]^{-1/4}D^{1/2}[g(\theta_0)]^{-1/4}$, where g is the determinant of the metric on the curved space, and D is the Van Vleck determinant [$D = \det(-\partial^2 S/\partial\theta\,\partial\theta_0)$]. The different choices give rise to Hamiltonians which differ at order $\hbar^2$ by a certain fraction of $\hbar^2 R$. Ali demonstrated this by choosing locally normal coordinates ξ to evaluate the integrals and considering infinitesimal time, so that the exponent and prefactor can be expanded in ξ. The action exponent is then at lowest order (in ξ) quadratic, and the resulting Gaussian integrals are readily performed. Only the even-order terms in the expansion of the prefactor about the initial value θ contribute. The $t\to 0$ limit is taken and an effective Hamiltonian can be extracted from the resulting differential equation. The expansion of the potential exponent and the initial wave function give the Hamiltonian $-\hbar^2\nabla^2/2m + V$, and it is the quadratic term in the expansion of $\sqrt{g(\xi)}\bar{G}(\xi)$ that gives rise to the $\hbar^2 R$ discrepancies in the effective Hamiltonian. (Higher-order terms give corrections at higher order in $\hbar$.)

The key point is that we may apply the same manipulations to our Eq. (24), where $A(\theta(\tau))$ plays the role of the prefactor $\sqrt{g(\theta)}\bar{G}(\theta)$. Transforming to locally normal coordinates in which there are no linear terms in the action exponent, and expanding $A(\theta(\tau))$ about θ leads to finite $\hbar^2$ corrections in the effective Hamiltonian, as in Ali's approach described above. However, it is important to recognize that our corrections emerge from reducing the full, unambiguous coordinate space evolution down to the reduced curved space by taking the constraint limit, whereas Ali's corrections arise from using a modified Feynman kernel for curved space. We observe that our corrections depend not only on the curvature but also on the constraint potential. These conclusions are in accord with the results of Sec. II, and provide additional insight into the ambiguity and connection with the literature.

IV. CLASSICAL AND SEMICLASSICAL PERSPECTIVE

Finally we provide a third, classical and semiclassical perspective on the ambiguities inherent in quantizing constrained systems. The classical point of view on constraints as limits of strong restoring forces is instructive, and nicely complements the quantum discussion. In classical mechanics, adiabaticity plays an important role. Adiabaticity of classical actions also played an important role in the old quantum theory. Here we will see that the semiclassical approach confirms the inherent order $\hbar^2$ problem of quantizing a constrained system. Again, the plan is to start with the system in the full Cartesian space, transform to curvilinear coordinates and the Laplace-Beltrami kinetic energy operator with no ambiguity, and begin imposing stiff force constants about fixed values of one or more of the coordinates. The result in the limit of infinite restoring forces is constrained dynamics on a Riemannian manifold. Again an ambiguity will arise because we can arrive at identical classical constrained dynamics in ways which differ quantum mechanically.

The idea that classical constraints are the limit of merely stiff degrees of freedom is a natural one, though not often discussed. Arnol'd includes a brief treatment of this in his famous book in a chapter devoted to Lagrangian dynamics on manifolds [9]. Arnol'd states that in the limit $\lambda\to\infty$ the classical dynamics satisfies Lagrange's equations of motion

$$\frac{d}{dt}\frac{\partial L_*}{\partial\dot\theta} = \frac{\partial L_*}{\partial\theta}, \tag{27}$$

where

$$L_*(\dot\theta,\theta) = T|_{\text{[illegible]}} - V|_{\text{[illegible]}}, \tag{28}$$

where T is the kinetic energy and V any nonconstraint potential energy of the full system. However, there is an important difference for the present purposes: we need to consider very large energies stored in the constrained coordinates, corresponding to the quantum zero point energy climbing to arbitrarily high values as $\lambda\to\infty$. This we can do, however, using the theorem on the adiabaticity of classical actions under slow variation of a parameter.

The issues which confront the classical approach to constraints in the high-energy constraint limit are (1) energy stored in the fast variables generally varies as a function of the slow variables, even though actions are constant, thus raising the specter of large energy exchanges with the slow degrees of freedom; (2) the possibility that the slow coordinates are chaotic; and (3) the possibility that the constraint coordinates can exchange energy among themselves, perhaps chaotically.

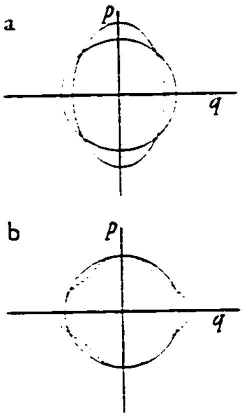

FIG. 2. (a) Area-preserving (adiabatic) change of Hamiltonian parameters generally changes the energy, as indicated by the increase in $|p|$ at $q=0$, where the potential $V=0$. (b) *Some* slow deformations of the Hamiltonian do leave the energy unchanged.

A. One dimension

In the simple case of one-dimensional motion with an adiabatic change of one or more parameters, the variation of the action decreases exponentially as the rate of variation of the parameters decreases [11]. However, as the phase space-diagram in Fig. 2(a) shows, the energy generally changes significantly as the parameters change, as measured by the contemporary value of the Hamiltonian. For example, in the case of a one dimensional harmonic oscillator, suppose we slowly adjust the frequency $\omega(t)=\lambda(t)\omega_0$ toward higher values, beginning with some energy E_0 in the oscillator:

$$H=\tfrac{1}{2}p^2+\tfrac{1}{2}\lambda(t)\omega_0^2q^2. \tag{29}$$

Since the action is constant, the area of the ellipse enclosed by the trajectory is constant, but this means that at $q=0$ the momentum must increase. However at $q=0$, $H=p^2/2$, so the energy increases as $\omega(t)$ increases adiabatically. Specifically, with $\omega\propto\sqrt{\lambda}$, we have $p\propto\lambda^{1/4}$ and $E\propto\lambda^{1/2}$

Now suppose we have only one constraint coordinate r. The situation is depicted in Fig. 1. The slow θ coordinates act as adiabatic parameters. Whatever their motion, in the limit of large, fixed λ the action of the r motion is preserved during the course of the θ motion. Clearly if we are to avoid any of the large zero-point energy of the r coordinates finding its way into the θ coordinates, we must restrict the confining potential $V(r;\theta_1,\theta_2,\ldots)$ to vary with $\theta_1,\theta_2,\ldots$ in a way that maintains fixed energy for fixed action. This condition does not fix the potential uniquely, but is possible for a wide class of potentials, for example satisfying

$$E_\lambda(I)=\lambda^{1/2}(c_1I+c_2I^2+\cdots)\equiv\lambda^{1/2}\epsilon(I), \tag{30}$$

with

$$\epsilon(\hbar/2)=\epsilon_0 \tag{31}$$

independent of λ. The action I is defined, as usual, as

$$I=\frac{1}{2\pi}\oint p_r(E,\lambda)dr. \tag{32}$$

An example showing two potentials (or rather their phase-space contours at identical actions and energies) satisfying this requirement is shown in Fig. 2(b). The area enclosed by the dashed and solid contours is the same and the momentum at $q=0$ (where we assume $V=0$ for both potentials) is also identical, showing the energy is the same for the two potentials at that action. Any potential satisfying Eqs. (30) and (31) at fixed values of the θ coordinates is an allowed constraint potential at that point in θ space; the independence of Eqs. (30) and (31) under changes in the θ coordinates must then be arranged to ensure energy remaining fixed in the r variable.

The *semiclassical* estimate of the energy in the r coordinate is thus independent of the θ coordinates, since that energy is just given by the classical energy at action $I=\hbar/2$; this is what we set constant by definition. However, it is not the semiclassical energy we want, but rather the *exact quantum* energy. Now the key fact is that *the exact and semiclassical energy differ in order* $\hbar^2$. This follows from the derivation of the WKB energy equation, which is an expansion in $\hbar$. Thus, the freedom to choose among potentials which lead to identical classical constrained motion as $\lambda\to\infty$ leads unavoidably to a quantum ambiguity at order $\hbar^2$, in agreement with the discussion in the previous two sections. This is another confirmation of the view forwarded there, and is the main result of this section.

B. Chaos in $\{\theta\}$ variables

The issue of chaos in the $\{\theta\}$ variables is easily disposed of: it makes no difference, since in the limit $\lambda\to\infty$ the frequency of the r variable is far from reach of the slow θ coordinates, which just act as slow parameter changes on the r variable motion. The fact that the changes of the θ coordinates are not quasiperiodic in the chaotic case is of no consequence to the adiabaticity of the r coordinates.

C. Resonance or chaos in $\{r\}$ variables

Interaction between several r variables can be avoided by independent control of as many λ parameters as there are r coordinates. With this control we can force the frequency ratios $\omega_i/\omega_{i-1}\to 0$ even as each $\omega_i\to\infty$. By this ruse we avoid any low-order resonance leading to energy transfer between the r variables. The concern that high-order resonances must always exist is softened by the fact that even if the external control parameters (θ variables) are effectively fixed and the high-order resonance is allowed to act, the energy exchange (resonance width) is expected to be exponentially small in the winding number (frequency ratio) for smooth potentials, as it depends on Fourier coefficients of the order of the winding number. In effect, good actions are maintained in the r variables as $\lambda\to\infty$

In the opposite extreme of full chaos in the r variables, we appeal to Liouville's theorem applied to the invariance of the total phase space volume enclosed by the energy surface in the r motion in the limit that the θ variables are slow enough to be considered to be adiabatically separate external parameters. In addition, we need Hertz's theorem, which states that in an ergodic system the energy shell maps onto another energy shell in the adiabatic limit of changing parameters [12,13]. We may write $E=E_{\{\theta\}}(V)$, where V is the phase-space volume. As long as the constraint potentials are tuned to preserve this energy as a function of the θ variables, i.e., $E_{\{\theta\}}(V)=E_{\{\theta'\}}(V)$ for all $\{\theta'\}$ and fixed V, there will again be no forces on them from the constraints. Having arranged the potentials in this way, there remains the question of the semiclassical energy for the chaotic dynamics. This can be given by periodic orbit theory [14]. Somewhat paradoxically, periodic orbit theory has been shown to give excellent results for low-energy eigenvalues in a number of systems, breaking down at higher energies. We need the lowest (zero point) energy, which at least formally has an error of order $\hbar^2$, so once again we reach the same conclusion about the order $\hbar^2$ ambiguity in the quantization procedure.

V. CONCLUSION

We have shown from three different points of view that the ambiguities which arise in the quantization of a constrained system are physical in nature, and cannot be resolved by finding the "right" mathematical formalism. Considering the constrained surface as a reduced subspace of a larger system, we have found that terms of order $\hbar^2$ inevitably arise in the effective description. These terms depend on the details of the forcing potential as much as on the intrinsic geometry of the constrained surface, but there is no ambiguity in the classical or even semiclassical dynamics. Thus we obtain a large set of equally valid "quantizations" of the same classical system, each corresponding to a particular constraining process. In any physical situation, one such constraining process is the correct one, and the ambiguities disappear. In the absence of detailed knowledge about the nature of the constraints, additional "quantization conditions" must be selected before one can speak of quantizing any classical dynamics on a curved space.

Our discussion has been cast in terms of holonomic constraints (which can be written in terms of the vanishing of one or more functions of the coordinates), but the idea of reaching rigid constraints via a limiting process also applies to nonholonomic constraints, which can be couched only in terms of nonintegrable differentials.

ACKNOWLEDGMENTS

This research was supported by the National Science Foundation under Grant No. CHE-9321260, and through ITAMP at the Harvard-Smithsonian Center for Astrophysics. We thank Michael Efroimsky and Sidney Coleman for helpful comments.

---

[1] L. S. Schulman, *Techniques and Applications of Path Integration* (Wiley, New York, 1981).

[2] P. A. M. Dirac, *Lectures on Quantum Mechanics* (Academic, New York, 1967).

[3] M. C. Gutzwiller, *Chaos in Classical and Quantum Mechanics* (Springer-Verlag, New York, 1990).

[4] M. K. Ali, Can. J. Phys. 74, 255 (1996).

[5] K. S. Cheng, J. Math. Phys. (N.Y.) 13, 1723 (1972).

[6] B. S. Dewitt, Phys. Rev. 85, 653 (1952); Rev. Mod. Phys. 29, 377 (1957).

[7] I. A. Batalin, E. S. Fradkin, and T. E. Fradkina, Nucl. Phys. B332, 723 (1990); I. A. Batalin and E. S. Fradkin, *ibid.* 326, 701 (1989); L. D. Faddeev, Teor. Mat. Fiz. 1, 3 (1969) [Theor. Math. Phys. 1, 1 (1970)]; J. Sniatycki, *Geometric Quantization and Quantum Mechanics* (Springer, New York, 1980); T. Kimura, Prog. Theor. Phys. 46, 1261 (1971); R. C. T. da Costa, Phys. Rev. A 23, 1982 (1981); N. T. De Oliveira and R. Lobo, Nuovo Cimento B 71, 196 (1982); J. E. Avron, A. Raveh, and B. Zur, Rev. Mod. Phys. 60, 873 (1988); N. G. van Kampen and J. J. Lodder, Am. J. Phys. 52, 419 (1984).

[8] R. Feynman and A. Hibbs, *Quantum Mechanics and Path Integrals* (McGraw-Hill, New York, 1965).

[9] V. I. Arnol'd, *Mathematical Methods of Classical Mechanics* (Springer-Verlag, New York, 1978).

[10] C. Lanczos, *The Variational Principles of Mechanics* (Dover, New York, 1986).

[11] L. Landau, *Mechanics* (Pergamon, Oxford, 1976).

[12] P. Hertz, Ann. Phys. (Leipzig) 33, 225 (1910); 33, 537 (1910).

[13] W. P. Reinhardt, Prog. Theor. Phys. Suppl. 179, 121 (1994).

[14] D. Wintgen, A. Burgers, K. Richter, and G. Tanner, Prog. Theor. Phys. Suppl. 116, 121 (1994).

IMAGE EVALUATION TEST TARGET (QA-3)

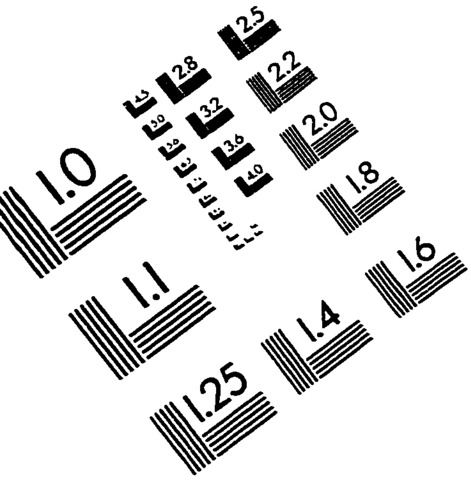

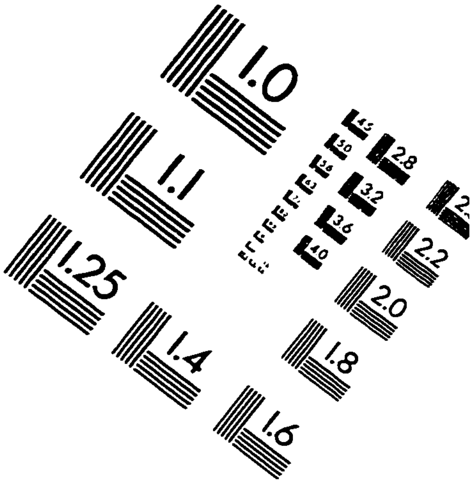

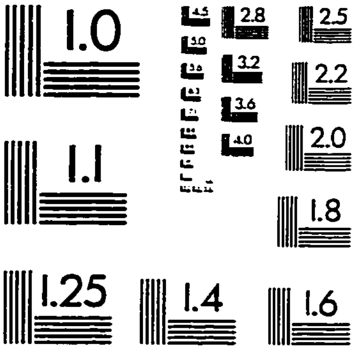

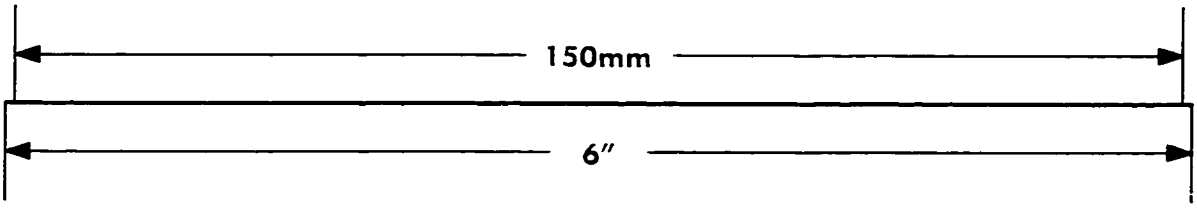

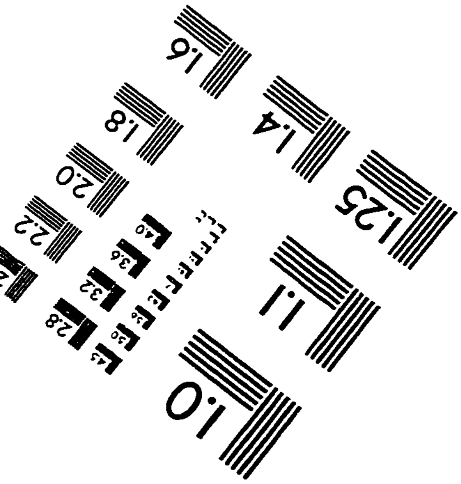

APPLIED IMAGE . Inc
1653 East Main Street
Rochester, NY 14609 USA
Phone: 716/482-0300
Fax: 716/288-5989